UTS UNIVERSITY OF TECHNOLOGY SYDNEY

Mechanical characterisation of Wood-PLA composite materials fabricated by fused deposition modelling under water conditioning

by Weilong Xu

Thesis submitted in fulfilment of the requirements for the degree of

Master of Engineering (Research)

under the supervision of

Principal Supervisor: Doctor Jianguang Fang
Co-Supervisor: Doctor Ali Entezari

University of Technology Sydney
Faculty of Engineering and Information Technology

October 2025

CERTIFICATE OF ORIGINAL AUTHORSHIP

I, Weilong Xu declare that this thesis, is submitted in fulfilment of the requirements for the award of Master of Engineering (Research), in the School of Civil and Environmental Engineering (Faculty of Engineering and Information Technology, FEIT) at the University of Technology Sydney. This thesis is wholly my own work unless otherwise referenced or acknowledged. In addition, I certify that all information sources and literature used are indicated in the thesis. This document has not been submitted for qualifications at any other academic institution.

This research was supported by an Australian Government Research Training Program (RTP) Scholarship doi.org/10.82133/C42F-K220.

Signature:

Production Note:
Signature removed prior to publication.

Date: 27 October 2025

ACKNOWLEDGEMENTS

I would like to express my deepest gratitude to my principal supervisor, Dr. Jianguang Fang, for his unwavering support, invaluable guidance, and expert advice throughout this research. His insight and encouragement were pivotal to the completion of this thesis. I am also deeply grateful to my co-supervisor, Dr. Ali Entezari, for his continuous support, thoughtful feedback, and guidance throughout my academic journey.

A special thank you to my colleague, Meiyu Li, whose technical expertise, constant support, and collaboration have been immensely helpful during my research. I am also thankful to Yanan Xu for their significant contributions and assistance during the course of my work.

I would like to extend my gratitude to the entire research group for their contributions and collaborative spirit: Meiyu Li, Di Zhang, Yang Jiang, Chuwei Chen, Saber Chahardoli, and Sepideh Aghajani. Working alongside such talented individuals has been both inspiring and rewarding.

Furthermore, I would like to thank the staff and technicians at the university for their support, particularly Dr. Larissa Koroleva, Dr. Jinsong Cao, Peter Brown, and Benjamin Smith. Their assistance has greatly facilitated my work and the completion of this research.

Finally, I would like to express my sincere appreciation to my family and friends for their love, patience, and encouragement throughout my academic journey. Their unwavering belief in me has been my greatest motivation.

List of Publications

Journal Article (Published)

[1] **Xu, W.**, Li, M., Xu, Y., Entezari, A., & Fang, J. (2025). Mechanical characterisation of Fused-Deposition-Modelling printed wood-Polylactic-Acid composites under water conditioning. ***Polymer Composites*** (Chapter 3 and Chapter 4).

Journal Article (To be submitted)

[2] **Xu, W.**, Li, M., Xu, Y., Entezari, A., & Fang, J. (2025). Influence of wood fibre content on the mechanical properties of FDM-printed wood-PLA composites after water absorption (Chapter 5).

Table of Contents

List of Figures

List of Tables

List of Abbreviations

ABS	Acrylonitrile Butadiene Styrene
AM	Additive Manufacturing
ASTM	American Society for Testing and Materials
CMC	Carboxymethyl Cellulose
CT	Computed Tomography
DIC	Digital Image Correlation
DDGS	Dried Distillers Grains with Solubles
EPDM-g-MAH	Ethylene Propylene Diene Monomer grafted with Maleic Anhydride
ESO	Epoxidised Soybean Oil
FDM	Fused Deposition Modelling
FTIR	Fourier Transform Infrared Spectroscopy
L-PA	Low-temperature Polyamide
LENS	Laser Engineered Net Shaping
LOM	Laminated Object Manufacturing
MAPP	Maleated polypropylene
PA	Polyamide
PETG	Polyethylene Terephthalate Glycol
PEEK	Polyether Ether Ketone

PEG	Polyethylene Glycol
PLA	Polylactic Acid
POE-gMA	Polyolefin Elastomer grafted with Maleic Anhydride
PP	Polypropylene
SCB	Sugarcane Bagasse
SEM	Scanning Electron Microscopy
SENB	Single-Edge Notched Bending
SLA	Stereolithography
SLS	Selective Laser Sintering
TPMS	Triply Periodic Minimal Surface
TPU	Thermoplastic Polyurethane
TPS	Thermoplastic Potato Starch
UAM	Ultrasonic Additive Manufacturing
wt%	Weight Percent

Abstract

Natural fibre-reinforced composites have garnered growing interest for their biodegradability and sustainability in additive manufacturing, particularly in Fused Deposition Modelling (FDM). However, current research lacks systematic understanding of how natural fibre content influences mechanical performance and how moisture absorption affects structural integrity in humid conditions. To fill these gaps, this thesis investigated the following:

Firstly, this thesis examined the mechanical performance of commercially available pure PLA (Polylactic Acid) and wood-PLA filaments fabricated via FDM in their original state (without any special conditioning). Tensile and SENB (single-edge notched bending) were evaluated to assess differences in strength, stiffness, and energy absorption. The results demonstrated that wood fibre reinforcement led to reduced tensile strength but enhanced energy absorption, due to altered fracture mechanisms. This stage provided a performance baseline and insight into how fibre inclusion influences failure behaviour.

Secondly, this thesis evaluated the tensile and fracture properties of wood-PLA and pure PLA composites fabricated via FDM under water-immersed conditions, followed by a redrying process to assess the potential for property recovery. The study revealed distinct differences in mechanical behaviour between the two materials, particularly in response to moisture uptake. Variations in strength, stiffness, and energy absorption were analysed to better understand each material's sensitivity to environmental exposure. The findings clarified the reversible nature of moisture-induced plasticisation and provided a foundation for evaluating the long-term reliability of natural fibre composites in humid service environments.

Thirdly, the thesis developed custom wood-PLA composite filaments with various wood fibre contents through melt-extrusion blending. These tailored materials were used to fabricate tensile specimens via FDM, enabling a systematic investigation of how

fibre concentration influences mechanical performance in both dry and moisture-conditioned states. The study revealed that fibre content significantly affects the trade-off between strength and energy absorption, offering practical guidance for optimising composite formulations. Furthermore, the degree of water-induced plasticisation and the extent of property recovery upon drying were found to correlate with fibre concentration, providing deeper insights into the microstructural mechanisms underlying performance variation. This work supports the development of environmentally sustainable FDM composites for broader engineering applications.

Chapter 1. Introduction

1.1. Background

Additive manufacturing (AM) technology, or 3D printing, was initially developed in the 1980s [1], adding material layer by layer may create items from a geometric representation, offering a precise and expressive way to create highly complex structures and substituting the laborious mould-making procedure[1]. Following the turn of the twenty-first century, this technology began finding applications in several industries, such as aviation [2], jewellery [3], medical science [4], automobile manufacturing [5] and food production [6]. In recent years, 3D printing technology has gained widespread adoption, enabling individuals and families to integrate it into everyday routines. This innovation allows consumers to manufacture items that traditional manufacturing processes cannot produce [7]. Currently, 3D printing technology encompasses various methods, including material extrusion (e.g., FDM), material jetting, vat photo polymerisation (e.g., Stereolithography, or SLA), powder bed fusion (e.g., Selective Laser Sintering, or SLS), directed energy deposition (e.g., Laser Engineered Net Shaping, or LENS), binder jetting, and sheet lamination (e.g., Laminated Object Manufacturing, or LOM, and Ultrasonic Additive Manufacturing, or UAM), in which FDM is one of the most early established method, offering the broadest range of applications and the best economic benefits [1].

In contemporary FDM printing technology, a wide variety of materials are supported, with polymer-based materials being the most commonly used, including PLA [8], ABS (Acrylonitrile Butadiene Styrene) [9], PETG (Polyethylene Terephthalate Glycol) [10], TPU (Thermoplastic Polyurethane) [11], and others. Among the diverse range of materials, fibre-polymer composites have increasingly gained attention in recent years. These materials leverage the advantages of both fibres and polymers [12],

allowing for enhanced performance (including their biocompatibility, lightweight, durability, and aesthetic superiority [13]) compared to single-material systems and offering broader applications [14, 15]. Currently, the commonly used and widely available fibres in FDM include carbon fibre [16], glass fibre [17], and aramid fibres [18]. These fibres offer distinct properties with specific advantages, making them suitable for a wide range of applications.

Besides the above-mentioned conventional fibres, natural or bio-based fibres have recently emerged as promising materials for composite applications. Natural fibres are frequently combined with polymers such as PLA [19], TPU [20], and PA (Polyamide) [21] to produce filaments in FDM, exhibiting several advantages, including their easy availability from natural sources, biodegradability, and lower carbon emissions [15, 22]. These environmentally friendly features have made them attractive for applications in packaging, automotive parts, construction components, and consumer goods [23, 24]. Among the various natural fibres, such as flax [25], hemp [26], and bamboo [27], wood fibre has emerged as one of the most widely used reinforcements due to its ready availability, low cost, and ease of integration with thermoplastics [28].

Wood fibre composites, particularly those based on PLA, have seen growing use in additive manufacturing technologies, especially in FDM. However, the incorporation of wood fibres introduces complexity in terms of moisture sensitivity and mechanical variability [28, 29]. These factors raise important questions about the structural performance and environmental durability of such materials. In this context, the present study aims to systematically investigate the mechanical behaviour of wood-PLA composites, considering both material composition and environmental exposure, thereby contributing to the optimisation and broader application of bio-based materials in functional and structural contexts.

This study contributes to the current understanding of natural fibre-reinforced composites in additive manufacturing by providing a systematic investigation of the mechanical behaviour of FDM-printed wood-PLA under water conditioning. Unlike

previous studies that mainly focused on the original characterisation, this work examines the effects of water absorption and redrying on the tensile and fracture properties and compares the behaviour of wood-PLA composites with different wood fibre contents, revealing the reversible plasticisation induced by moisture uptake. The findings offer new insights into the environmental durability of wood-PLA composites and their potential for practical applications in moisture-varying environments.

1.2. Research scopes

In response to the three research gaps identified in this field, this study proposes three research objectives to address the current challenges.

1. Although wood-PLA composites are widely used in FDM applications, limited studies have directly compared their mechanical properties with those of pure PLA under consistent processing and testing conditions. To address this, the first objective is to establish a mechanical baseline by experimentally comparing the tensile and fracture behaviour of commercially available pure PLA and wood-PLA filaments in their original printed state. This comparison aims to clarify the impact of wood fibre inclusion on energy absorption and failure mechanisms.

2. The environmental sensitivity of natural fibre composites, particularly their response to moisture, remains insufficiently characterised. Most studies have not systematically explored how water immersion and subsequent drying affect mechanical properties such as strength, stiffness, and toughness. Therefore, the second objective is to investigate the reversible plasticising effects of water on PLA and wood-PLA composites. The study will assess moisture-induced degradation and recovery to support their use in humidity-variable service environments.

3. While fibre content is known to influence composite performance, existing research lacks detailed analysis of intermediate wood fibre concentrations. Therefore, the third objective is to produce and assess a series of custom wood-PLA filaments with

controlled fibre loadings. This stage will examine the impact of fibre content on tensile performance, water absorption, and redrying behaviour, with the goal of identifying an optimal composition that balances mechanical resilience and moisture resistance.

1.3. Thesis organisation

The thesis is structured into six chapters. This chapter provides an overview of the research background, objectives, and scope of the study.

Chapter 2 presents a literature review for this thesis. It begins by reviewing prior research focused on the incorporation of various types of fibres into FDM-printed composite materials. This includes investigations involving conventional reinforcements such as carbon and glass fibres, as well as more recent attention directed towards wood and other natural fibres. Emphasis is placed on the growing interest in bio-based alternatives due to their sustainability and compatibility with additive manufacturing. The chapter then examines studies that have assessed the mechanical performance of fibre-reinforced composites under humid or moisture-exposed environments, highlighting how environmental conditions can significantly influence structural integrity. Finally, it summarises key research concerning the practical applications of fibre-reinforced FDM composites, particularly in structural components, where both mechanical strength and material adaptability are critical considerations.

Chapter 3 presents the first part of the experimental study, investigating the mechanical performance of FDM-printed PLA and wood-PLA composites in their original, unconditioned state. Two commercially available filaments, pure PLA and a wood-PLA composite containing 40% wood fibre by volume, were used to fabricate the specimens. Mechanical characterisation was performed using tensile and SENB tests. The results showed that, compared to pure PLA, the wood-PLA composite exhibited lower tensile strength and stiffness, but a significantly higher energy absorption capacity. This chapter establishes a baseline for understanding how the incorporation of wood

fibre affects the fracture behaviour and toughness of the material.

Chapter 4 presents the second part of the study examining how water immersion and subsequent redrying influence the mechanical behaviour of the same PLA and wood-PLA composites. Following controlled water conditioning, both tensile and SENB tests were repeated to assess the effects of moisture uptake and recovery. The results revealed that water immersion led to a noticeable decrease in strength and stiffness, while simultaneously enhancing the energy absorption and elongation at break, particularly in wood-PLA composites. These changes were largely reversed after redrying, confirming the plasticising effect of water as a reversible process. This chapter highlights the environmental sensitivity of natural fibre composites and their potential for use in moisture-variable conditions.

Chapter 5 presents the third part of the study, in which custom filaments with varying wood fibre contents were successfully manufactured and evaluated. The fabrication process used the same two commercially sourced base filaments (pure PLA and 40% wood-PLA). After mechanical grinding, the materials were blended in controlled proportions and re-extruded using a filament extruder to produce printable filaments containing 5%, 10%, 15%, and 20% wood fibre by volume. Printing trials confirmed the printability of all formulations using FDM. The study then examined and compared the tensile performance, water absorption characteristics, and post-immersion mechanical changes of these materials, along with their recovery following redrying. Notably, the filament with 15% wood fibre content demonstrated the highest toughness, achieving the optimal balance between strength and ductility. This investigation provided a more detailed understanding of how wood fibre content influences mechanical behaviour, and the identification of the 15% formulation as the most effective further supports its potential for broader application in sustainable manufacturing.

Chapter 6 summarises the key findings of the present thesis and highlights the promising topics of future work.

Chapter 2. Literature review

2.1. Different used fibre composite materials

Carbon and glass fibres are commonly used reinforcement materials known for their significant strengthening effects [30]. In current research within this field, the enhancement mechanisms are primarily focused on the strength of the fibres themselves [31], the length and volume of the fibres [12, 32], as well as the bonding efficiency between the fibres and the matrix [19, 33]. The sophisticated research findings on these two types of fibres have enabled their widespread application across various industries today, including automotive[34-36] and aerospace manufacturing [11, 30]. However, with the growing awareness of environmental issues, carbon and glass fibres have gradually exhibited several disadvantages in their applications, including high carbon emissions [11, 27] during the production lifecycle and their non-biodegradable nature [33]. As a result, there has been a growing interest in finding alternative fibres to replace them. Bio-based fibres, as materials that can be directly obtained from nature [28] and are biodegradable [37], have emerged as the most suitable alternatives. Therefore, as shown in the above comparison, bio-based fibre composites possess significant research value as an emerging material. Additionally, by summarising the reinforcement mechanisms of carbon and glass fibres, insights can be provided for analysing the strengthening mechanisms of bio-based fibres.

Additive manufacturing encompasses various printing techniques, including FDM, SLS, SLA and LOM. Each of these methods possesses distinct advantages and limitations, making them suitable for different application requirements. Moreover, these techniques are capable of processing a wide range of fibre composite materials, such as glass fibre, carbon fibre, and wood fibre, depending on the intended functionality and structural needs [38, 39]. For the use of these printing methods in wood-fibre composites, FDM has received the most extensive research due to its

advantages, such as low cost and high efficiency [28], and compared to SLA and SLS, FDM can support larger fibre particle sizes [39].

This section will review several studies focusing on the mechanical properties of FDM composites reinforced with various types of fibres, including carbon, glass, and bio-based fibres. The characteristics of each type of fibre will be presented in each sub-section (2.1.1. and 2.1.2.), notably in Section 2.1.2. Wood and natural fibre-reinforced FDM Filament will highlight a discussion on the properties and advantages of bio-based fibres. In this context, the composites reinforced with wood fibres will be emphasised.

2.1.1. Conventional fibre-reinforced FDM filament

Both carbon fibre and glass fibre are characterised by their high tensile strength and modulus, significantly outperforming the polymer matrix, such as PLA [12, 33, 40], PA [16, 41], PETG [42], ABS [43], PEEK (Polyether Ether Ketone) [31], and PP (Polypropylene) [44]. These properties enable them to effectively share and transfer external loads when embedded in the matrix, thereby reducing stress concentration within the polymer.

Anwer [32], Ferreira et al.[40] and Li et al. [12] each conducted studies on three different sizes of carbon fibre-reinforced PLA composites, focusing on nano-fibres, short fibres, and continuous fibres, respectively.

Anwer [32] investigated mechanical enhancement of nanoscale micro carbon fibres by designing materials with varying mass fractions ranging from 1% to 15%. The results indicated that in the group with a 15% carbon fibre content, Young's modulus was increased by 42%. Ferreira et al. [40] compared short carbon fibre-reinforced PLA and pure PLA and concluded that adding carbon fibre of 15% mass fraction resulted in a 2.2-fold increase in tensile modulus in the direction of printing (0°) and a 1.25-fold increase in the transverse direction (90°) compared to the mechanical properties of pure

PLA. This finding is consistent with the results of several other studies[12, 32, 33]. Li et al. studied the FDM performance of continuous carbon fibre-reinforced PLA [12]. By improving the nozzle design, the research enabled the carbon fibre bundles to be extruded alongside the molten PLA material through the nozzle, facilitating the printing of continuous carbon fibre-reinforced structures (Figure 2.1 (a)). Furthermore, the carbon fibre bundles were pre-treated with a PLA wetting agent, significantly enhancing the adhesion between the carbon fibres and the matrix. The results indicated that this approach increased 13.5% in tensile strength and 164% in flexural strength compared to untreated carbon fibre-reinforced PLA [12].

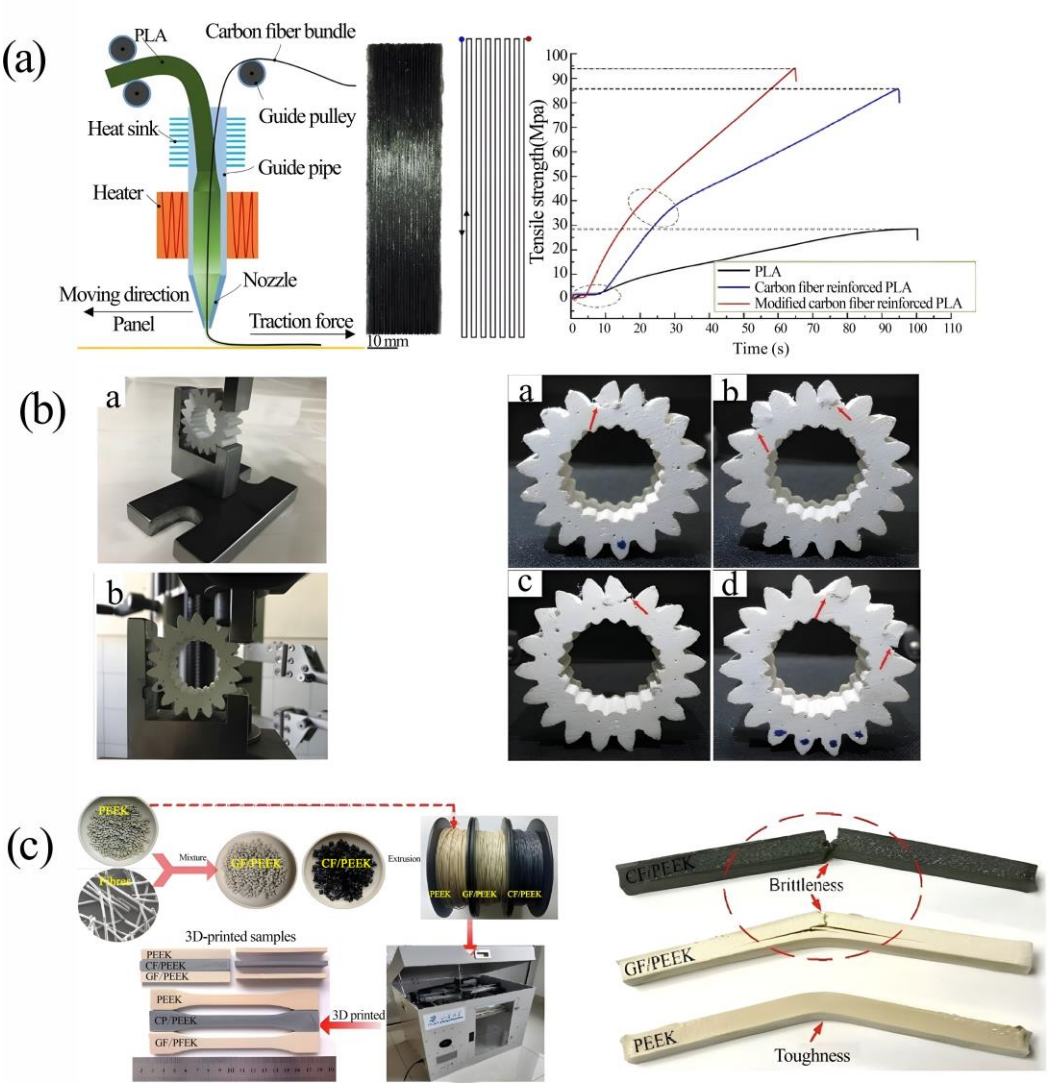

Figure 2.1. Different carbon fibre and glass fibre composites: (a) the continuous carbon fibre reinforced PLA [12], (b) the glass fibre and ABS gears [43], (c) the glass

fibre and carbon fibre with PEEK [31].

There has also been some research on carbon fibre-reinforced nylon, another common material used in FDM. Melenka et al. [41] studied carbon fibre-reinforced nylon FDM structures with varying volume fractions of carbon fibre contents, specifically 4.04%, 8.08%, and 10.1%. The experimental results indicated that as the carbon fibre content increased, the elastic modulus of the nylon structures progressively rose, with values of 1767.2 MPa, 6920.0 MPa, and 9001.2 MPa, respectively[41].

Alarifi [16] investigated the bending properties of the nylon-carbon fibre composite materials using a three-point bending test considering three different printing orientations (0°, 90° and ±45°). It was concluded that adding carbon fibres enhanced the overall elastic behaviour, achieving a significant increase in deflection at the expense of some bending strength. In contrast, the incorporation of glass fibres resulted in a substantial increase in the material's overall stiffness, demonstrating an enhancement in bending performance. The improvement in bending performance can be attributed to the effective stress transfer provided by the interfacial bonding between the nylon matrix and the fibres.

Srinidhi et al. [42] compared the performance variations of PETG with an increased carbon fibre content of 20% by weight while designing different infill patterns during printing, including grid, honeycomb, rectilinear, and cubic configurations. Experimental results indicated that the grid infill pattern exhibited superior performance, which can be attributed to the inherent structural advantages of the grid design. The combination of carbon fibre reinforcement and the unique geometry of the grid infill pattern contributed to improvements of 16.7% in tensile strength, 22% in impact strength, and 10.7% in flexural strength. This improvement is attributed to the carbon fibre content and the subsequent removal of internal stress in these samples [42].

Glass fibre is another widely used material for the production of composites. In the automotive industry, short glass fibre-reinforced polyamides are widely utilised for load-bearing and semi-structural applications, including parts found in engine

compartments [34-36]. Currently, many commercially available filaments incorporating glass fibres are accessible for public use in FDM 3D printing. The extensive use of glass fibres can be attributed to several advantages, including cost-effectiveness, corrosion resistance, excellent structural strength, superior strength-to-weight ratio, high heat distortion temperature, electrical non-conductivity, and the ability to be moulded to precise tolerances [30, 45].

Cao et al. [17] employed some treatment methods to address the disadvantage of poor surface roughness in mixed FDM-manufactured PLA/TPU/short glass fibres composite samples, thereby enhancing the precision of the printed components.

Akhoundi et al. [19] conducted a study focused on improving the mechanical properties of PLA after FDM by incorporating continuous glass fibres. In this study, as the fibre content increased, the tensile strengths of samples with fibre volume contents of 40%, 46%, and 49% were measured at 401 MPa, 446 MPa, and 478 MPa, respectively. Regarding the tensile modulus, the corresponding values were found to be 24.3 GPa, 27.8 GPa, and 29.4 GPa. The reinforcement with continuous glass fibres was demonstrated to be reliable [19].

Bodaghi et al. [43], in their study of glass fibre-reinforced ABS materials, researched the impact of the fibre content and the adhesion between the fibre and the matrix. The study designed and investigated the special gears produced from ABS composites infused with short glass fibres through FDM (Figure 2.1 (b)). The study aimed to gain insights into the impact of glass fibre addition on key parameters such as tooth failure load, tooth bending strength, hardness, weight loss, wear resistance, mechanical wear, and the overall performance of composite gears to explore the potential for real-world applications of the gears. It was found that increasing the glass fibre content from 0% to 5% led to an 11% rise in hardness. The enhancement is linked to the effective distribution and presence of the glass fibres. Furthermore, the strong bonding between the glass fibres and the matrix material facilitated the transfer of applied forces, which helped prevent permeation and resist plastic deformation, thus improving hardness

[46]. However, with further increases in glass fibre content, the hardness began to decrease, likely due to the growing number of voids between the fibres and the matrix. ABS with 5% glass fibre showed optimal performance, with a 44% increase in hardness and 61% better wear resistance compared to pure ABS. This improvement is due to the effective adhesion between the glass fibres and the ABS matrix, which strengthens the gear teeth and improves wear resistance. However, higher fibre content led to voids and clumping, increasing wear-induced weight loss. These findings highlight 5% glass fibre-reinforced ABS as an optimal material for gears with excellent strength and wear resistance [43].

Sodeifian et al. [44] studied a PP composite reinforced with glass fibres for FDM, incorporating POE-gMA (Polyolefin Elastomer grafted with Maleic Anhydride) as an additive to enhance flexibility. Glass fibres increased the strength from 20 MPa to 32 MPa (a 60% improvement) but reduced toughness, with elongation at break dropping from 24% to 7% (a 70% reduction) due to restricted polymer chain mobility [47]. Adding POE-gMA partially restored flexibility, improving elongation at break to 12%, though strength and modulus were slightly compromised.

There have been studies that attempt to compare the performance differences between the two types of fibres, carbon and glass. Wang et al. [31] explored PEEK composites for FDM, incorporating carbon fibres (5 wt%) or glass fibres (5 wt%) respectively (Figure 2.1 (c)). They found that printing parameters significantly influence the mechanical performance of composites and optimal mechanical properties was obtained at 440 °C. Higher temperatures improved melt flow, interlayer adhesion, and reduced porosity [48, 49]. Low printing speeds enhanced extrusion stability, while thinner layers improved bonding and overall performance[50]. Employing thinner layers leads to closely bonded stacks, driven by nozzle extrusion, which enhances overall performance [51]. Glass fibres significantly increased tensile and flexural strengths, indicating strong fibre-matrix anchoring. However, impact resistance declined due to porosity and molecular chain deterioration during filament production [31].

Although carbon and glass fibres have numerous applications, they also present several limitations, such as high carbon emissions [11, 27] during manufacturing and their non-biodegradable ending [33]. To mitigate the environmental impact of these fibres, some studies have explored the use of recycled fibres to investigate the reliability of recycling. Tian et al.[33]. achieved 100% carbon fibre and 73% PLA recovery from recycled 3D-printed materials, improving tensile strength by 20% and flexural strength by 25% due to enhanced fibre-matrix bonding. However, the process consumed 133.7 MJ/kg, suggesting a need for energy-efficient alternatives [33].

As mentioned above, a key limitation of glass and carbon fibre composites lies in their environmental impact and recycling challenges compared to natural fibres [52, 53]. A primary concern is the ecological footprint: manufacturing can consume significant energy and emit harmful chemicals [11, 27]. Additionally, the resin matrix that holds the fibres together complicates the recycling of glass fibre composites at the end of their useful life [54]. This creates difficulties in disposing of carbon and glass fibre products, which frequently end up in landfills and are resistant to decomposition [55]. The concerns related to environmental issues, present a significant obstacle to the development of traditional fibre in this field. These challenges have also driven the industry to focus on identifying alternative fibres that are more environmentally suitable.

2.1.2. Wood and natural fibre-reinforced FDM Filament

Some studies on FDM have utilised natural fibres to produce composite filaments, representing advancements in environmental sustainability and enhancements of mechanical performance. In the current research, commonly used biopolymers for the production of FDM filaments primarily consist of natural fibres, including bast fibres (such as jute, flax, hemp, and ramie), leaf fibres (such as those derived from pineapple and banana), seed fibres (such as cotton), husk fibres (from walnut, almond, coconut, peanut, and hazelnut), as well as stem and reed fibres (including bamboo and sugarcane),

and wood fibres [56-61]. Wood fibres, due to their high cellulose content and ease of natural availability, are widely utilised in the research of polymer blends. This section will review several studies on natural fibre composites , including research on the impact of wood fibre content on mechanical properties [20, 62, 63], the influence of printing parameters on mechanical performance [64, 65], and the printability of wood fibre composites [66]. Additionally, other types of natural fibre composites will also be discussed [13, 67-73].

Kariz et al. [62] investigated the performance of wood fibres and PLA composites in FDM. This study designed six samples with varying wood fibre contents, specifically comparing changes at levels of 0%, 10%, 20%, 30%, 40%, and 50% by weight (Figure 2.2 (a)). The most evident finding was a decrease in the overall density of the materials. Samples with a wood fibre content of 10% and 20% exhibited a density reduction of 17%, while those with wood fibre content ranging from 30% to 50% showed a 24% decrease in density. This reduction contributes to the search for weight-optimised materials in civil engineering applications. Tensile strength (Figure 2.2 (a)) exhibited a slight increase at low wood fibre contents; specifically, the tensile strength of the filaments increased from 55 MPa to 57 MPa with a 10% addition of wood fibres. However, as the wood fibre content increased, the tensile strength declined consistently, dropping to 49 MPa at 30% and further to 30 MPa at 50%[62]. The elastic modulus (Figure 2.2 (a)) exhibited a trend of increasing and then decreasing with the increase of the wood fibre content. It rose from 3.27 GPa at 0% to 3.94 GPa at 20%, after which the value began to decline, reaching 3 GPa at 50% wood fibre content. At lower wood fibre contents, a slight increase in the elastic modulus and tensile strength was observed; however, these values decreased with higher loading levels. The wood particles can provide a reinforcing effect at low wood fibre content. Conversely, the polymer may not fully encapsulate the particles at elevated loading levels, leading to poor adhesion and limited load transfer.

Yang and Yeh [64] investigated the influence of FDM printing parameters on the performance of wood fibres and PLA composite materials. As the printing speed

increases, the colour of the final product's surface progressively darkens while its density gradually decreases. As printing speed increases, 3D-printed wood fibre/PLA composite parts show a decrease in compressive qualities. In particular, increasing the printing speed from 30 to 70 mm/s resulted in a considerable decrease in the modulus and compressive strength of the FDM-printed items by 14.6% and 34.3%, respectively. At greater printing rates, the surrounding layers' bonding strength weakens, so the compressive properties decrease. By employing SEM (Scanning Electron Microscopy), several conclusions regarding surface morphology were drawn: Higher printing speeds result in an uneven surface of the wood-plastic composite part, with a narrower width of printed layers and more frequent pull-outs of wood fibres on the fracture surface of the tensile samples [64].

Duigou et al. [65] also investigated the impact of printing parameters on the performance of wood fibre-reinforced PLA. In this study, the primary parameters were the printing orientation (0° and 90°) and the line width of the print. Changes in printing width (100%, 200%, and 300%) caused significant variations in the mechanical properties of 0° and 90° printed samples. The 0°-printed samples exhibited increased ductility with the rise in printing width; however, the tensile strength gradually decreased. Specifically, the tensile strength of the bio-composites at 100% and 300% printing widths decreased by 30% and 50%, respectively, while the tensile modulus decreased by 50% and 65%. The decline in performance can be attributed to the increased porosity but lowers the cohesion of the material, resulting from the wider printing line widths. This study found that as the printing width increased from 100% to 200% and 300%, the porosity increased from 14.7% to 15.5% and 21.8%, respectively (Using the SEM and CT (Computed Tomography)). Such an increase in porosity also enhanced water absorption. Compared to samples produced through compression, increasing the printing width from 100% to 300% resulted in a 5- to 10-fold increase in water absorption (will be introduced in the next part) [65].

Kariz et al. [62] stated that the performance of printed components is impacted when

wood content is added to the 3D-printed PLA material. The wood's structural filling function and inconsistencies in the printing material, caused by nozzle clogging, led to varying diameters in wood-PLA filaments. These variations reduced the material amount in the printed samples and caused inadequate layer fusion, which in turn lowered mechanical properties. With increased wood content, bending performance declined, though the effects were not statistically significant under these moist conditions. The samples' moisture content increased with higher wood content in all climate conditions. Samples with higher wood content also showed greater length expansion due to hygroscopicity [62].

Tao et al. [66] used the laboratory-made mean particle size of 14 μm Aspen wood flour and a desktop-class plastic extruder to fabricate the wood fibre/PLA composite filaments with 5% wood powder by weight. The study discovered that the fracture surface of pure PLA filaments was smooth and flat by comparing the SEM pictures of the fracture surfaces of the two materials: wood fibre composites and pure PLA filaments. In contrast, the addition of wood fibre caused the composite fracture surface to become rough, with visible gaps between the PLA and wood fibre interface in certain areas. It suggests that the interfacial bonding between PLA and wood fibre is inadequate, which led to the results of this experiment: the tensile strength decreased by 20% with the addition of 5% wood powder. wood fibre and PLA should have less interfacial adhesion since wood fibre has a polar (hydrophilic) surface and PLA has a non-polar (hydrophobic) surface [67, 74]. The results revealed that the addition of wood fibres led to poor interfacial bonding between the wood fibres and PLA, resulting in an increased occurrence of pores. The bad adhesion, in turn, contributed to a decrease in tensile strength and an enhancement in water absorption. Such characteristics are not entirely disadvantageous; they present potential applications as well [65, 66].

Several studies have also investigated the characteristics of wood fibre composites with other polymers, such as TPU [20]. Bi et al. [20] investigated the performance of TPU and wood fibre composites by preparing five different wood fibre content levels:

10 wt%, 20 wt%, 30 wt%, 40 wt%, and 50 wt% (Figure 2.2 (b)). The results indicated that as the wood fibre content increased, the elongation at break of the samples gradually decreased from 500% to 50%, while the tensile strength initially decreased from 28 MPa to 16 MPa and then increased to 21 MPa (Figure 2.2 (b)). The composite exhibited the lowest tensile strength at a wood fibre content of 20 wt%. Subsequently, additives, such as EPDM-g-MAH (Ethylene Propylene Diene Monomer grafted with Maleic Anhydride), were introduced to enhance the flexibility of the TPU/wood fibre composites and improve interfacial adhesion. The study confirmed that EPDM-g-MAH enhanced the interfacial adhesion between TPU and wood fibre. The EPDM-g-MAH modified TPU/wood fibre composites displayed the highest storage modulus, loss modulus, and viscosity, with an approximately 100.14% increase in the elongation at the break of the wood fibre/TPU composites [20]. Such high flexibility differentiates wood fibre-reinforced TPU from conventional brittle 3D printing materials available in the market, providing significant application potential. For example, the study [20] attempted to print a phone case that demonstrated excellent flexibility, capable of absorbing energy during falls and offering protection for the device, thereby meeting current market demands. The study by Diestel and Krause [75] reached similar conclusions, indicating that the tensile strength of TPU decreased with increasing wood flour content (from 0% to 35% decreased from 16 MPa to 12 MPa) and then increased again with further additions of wood flour, reaching up to 70%.

Pandey et al. [63] utilised a co-rotating twin-screw micro extruder to produce PLA, TPU, and wood flour composites. By keeping the wood flour content constant at 10 wt%, the study varied the amounts of TPU and PLA to design multiple samples, with TPU content set at 10 wt%, 20 wt%, 30 wt%, and 50 wt%. As the TPU content increased, the elongation at break consistently improved, while the tensile strength and modulus decreased. This is attributed to the fact that TPU provides flexibility and elasticity to the blend [20], resulting in reduced tensile strength and modulus while enhancing the elongation at break. The research also manufactured the composite add

with wood fibres (composites with three contents: PLA, TPU and wood fibres) Compared to composites filled with wood flour, the impact strength or toughness of the blends with no wood fillers was slightly higher, particularly at higher TPU content (50 wt%). At lower percentages of TPU, there was no significant difference in impact strength after being filled with extra wood fibbers. Because the wood fibres particles were well distributed throughout the mixture, hydrogen bonding between the wood flour and the PLA/TPU mixture improved interfacial adhesion [62]. The mechanical characteristics of the composites were enhanced as a result of this better interfacial adhesion. Such advancements open up potential applications in various industries, including automotive, packaging, and furniture [63].

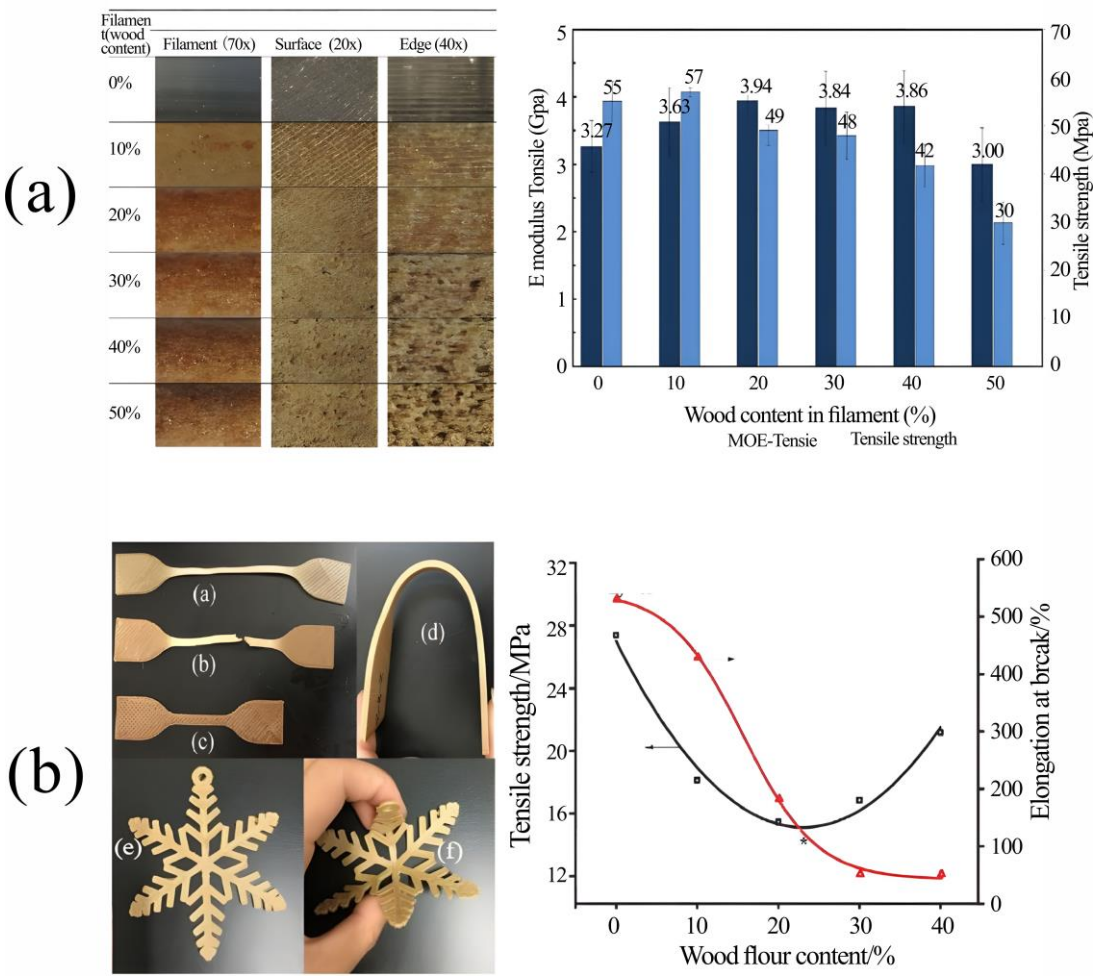

Figure 2.2. The wood fibre composites: (a) the wood fibre PLA and its

mechanical properties with different content [62], (b) wood fibre TPU has superb elasticity and mechanical properties with different content [20].

In recent years, there has been a surge of research that not only focuses on the performance of wood fibre-based composite materials in FDM but also explores the use of other bio-based materials in conjunction with polymers to create composites [15]. In current research, such natural fillers primarily originate from various plants and fine aggregates derived from the grinding of different types of stones [73]. The primary reason for the adoption of various plant-based composites is their rich content of cellulose, hemicellulose, and lignin [76]. These components enhance the performance of the original polymer while also minimising environmental impact, as these natural materials are readily biodegradable [13].

Haryńska et al. [67] designed a composite filament based on PLA mixed with TPS (thermoplastic potato starch) and investigated its mechanical properties in comparison to commercial PLA filaments (Figure 2.3 (a)). In the study, the PLA/TPS filament had a TPS composition of 40% by weight, with potato starch comprising 65.7%, glycerine 33.3%, and epoxidised soybean oil 1%. This formulation results in high potato starch content. Compared to commercial PLA printed outputs, the hydrophilicity and sensitivity to hydrolytic degradation were significantly improved, enhancing composability. Furthermore, this study demonstrated that PLA/TPS filaments exhibit printability comparable to the commercial counterparts, making them suitable for personalised anatomical models and complex porous structures in FDM. The study showed the Young's modulus of PLA/TPS was in the range of 1.6−1.7 GPa, the tensile strength was around 15−16 MPa, and the elongation at break was at 1.8−3.0%. Other studies [77] have found that using injected-moulded (continuous) test samples, the addition of TPS to pure PLA increases elongation at the break while reducing tensile strength. Furthermore, when compared to pure PLA, no significant increase in the ductility of PLA/TPS samples was observed. This can be attributed to poor interlayer

adhesion within the PLA/TPS composite.

In a different study, Liu et al. [68] used a chemical treatment technique to extract cellulose fibres from leftover SCB (sugarcane bagasse) and prepare PLA composite materials that could be used in FDM. The SCB contains large amounts of cellulose (45.7 wt%), hemicellulose (24.2 wt%) and lignin (21.8 wt%). Incorporating SCB into PLA reduces both the tensile and flexural strengths of the 3D-printed samples but increases the flexural modulus. Notably, the tensile strength reaches the optimum when the SCB content is at 6 wt%, while the flexural modulus decreases with increasing SCB content. Furthermore, SCB exhibits sufficiently high thermal decomposition temperatures to meet the requirements for the melt extrusion processing of PLA composites. Additionally, the SCB fibres can promote the crystallisation of PLA. SEM analysis revealed that, in addition to the 'inter-strand voids' inherent to FDM, the fracture surface morphology of the 3D-printed samples also exhibited 'internal voids' and 'interlayer voids' [78]. Moreover, the same optimal SCB content (6%) can be achieved via 'cross' and 'parallel' printing techniques, yielding the best mechanical performance. However, the mechanical characteristics of the 3D-printed samples are severely harmed by the rise in porosity brought on by a large filler fraction [68].

Costa et al. [69] conducted research on ABS reinforced with pine cone residues, focusing on the thermal stability of the composite material and the feasibility for use in FDM. The pine ABS serves as an alternative for reducing solid waste and enhances the concept of green composites. Prior to mixing, all fibres were bleached using a hydrogen peroxide solution, which was shown to enhance the thermal stability of the composites compared to unbleached fibres. Subsequent FTIR (Fourier Transform Infrared Spectroscopy) analysis at the microscopic level revealed that the addition of bleached fibres to ABS resulted in a uniform distribution embedded throughout the cross-section of the filament. It indicates that the fibres are hydrogen-bonded to the ABS, leading to an increase in filament density. Finally, the study attempted to extrude filaments using a 3D printing pen, which exhibited good performance in terms of appearance, shape, and

stability. It demonstrates the potential applicability in FDM. The use of ABS reinforced with pine cone fibres reduces raw material costs compared to pure ABS and provides a second life to natural materials through recycling [69].

Bajwa et al. [70] investigated a bio-based composite using PLA reinforced with DDGS (Distillers Dried Grains with Solubles) (Figure 2.3 (b)). The study involved three different composites, each incorporating one of three distinct plasticisers: ESO (Epoxidised Soybean Oil), PEG (Polyethylene Glycol), and glycerol. Following this, the study assessed the tensile properties, demonstrating that the PLA-DDGS composite plasticised with ESO showed a greater elongation at break than both pure PLA and PLA-DDGS blends that were plasticised with glycerol and PEG. In comparison to pure PLA samples, the PLA-DDGS blend with 10% ESO showed a 6% increase in storage modulus, whereas the addition of 12.5% ESO led to a 27% reduction in storage modulus. For the 3D printed samples plasticised with PEG and glycerol, the storage modulus decreased by 32% and 89%, respectively. The results indicate that ESO is the most effective plasticiser for enhancing the elongation at the break of PLA composites. Overall, this study demonstrates the feasibility of designing PLA-based filaments for 3D printing using 10-15% DDGS filler and ESO as a plasticiser [70].

Marton et al. [13] utilised solid waste from recycled palm residues (Australian royal palm) and ABS to create a bio-based composite polymer for use in FDM. Filaments with different palm fibre contents (5%, 10%, 15%, and 20% by weight) were produced using a thermodynamic mixer for processing, followed by a mini extruder to process various fibre loadings (Figure 2.3 (c)). The original ABS exhibited no porosity, whereas the filament composites displayed a porous structure with pore sizes smaller than 50 μm due to the presence of fibres and the higher fibre loadings. It could be explained by the way the fibres and matrix interact at the interface, placing restrictions on the matrix as a result of the fibres. The finding was validated by FTIR analysis, which showed a rise in hydrogen bonding coefficients. According to the findings, adding fibres could have a positive impact on the environment, especially in the areas of land usage and ozone

depletion. It is because the filament composites used less polymer resin, and there was less waste from Australian royal palms, which are frequently mishandled and have a detrimental impact on ecosystems. Finally, the study successfully extruded filaments using a 3D printing pen, which demonstrated good performance in terms of appearance, shape, and stability, confirming the feasibility of this material [13].

Taborda-Ríos et al. [71] conducted a study on bamboo fibre-reinforced PLA, utilising a commercially available PLA that contains 20% bamboo fibre. The experiment compared three filling patterns during printing: (a) grid, (b) cubic, and (c) zigzag, as well as other printing parameters, including layer thickness and infill density. The experiment found that, regardless of changes in printing parameters, the tensile test results for bamboo fibre-reinforced PLA were lower than those for pure PLA. Both tensile strength, elastic modulus, and energy absorption decreased. These reductions are attributed to the lack of adhesion between the PLA matrix and the bamboo fibres, allowing the fibres to separate [62, 68]. This failure may be related to the presence of bubbles, cracks, and localised deformations. Furthermore, due to the different filling patterns, the internal fibre orientations do not fully align with the direction of applied stress (fibres align with the nozzle movement), thereby reducing the capacity to absorb energy [71].

Long et al. [72] also studied bamboo fibre composites, designing a blend of bamboo fibre, PLA, and PP. The experiment demonstrated that as the bamboo fibre content increased, the tensile strength and elongation at the composite break decreased. Specifically, the tensile strength dropped from 38 MPa to 27 MPa as bamboo fibre content increased from 0% to 30%, while the elongation at break decreased from 17% to 10%. The reasons for the declines are similar to those analysed in previous studies, attributed to insufficient bonding between the matrix and the fibres[68, 71, 79]. Therefore, this research further explores the use of chemical modification to overcome this deficiency. MAPP (Maleated Polypropylene) was added to the bamboo fibre composite, improving the mechanical properties of the PP/PLA composites by enhancing the interfacial adhesion between the bamboo fibres and the polymer matrix. MAPP

significantly increased the compatibility between the fibres and the matrix, enhanced thermal stability, and accelerated the crystallisation rate of PP/PLA, resulting in better mechanical performance. Experimental results showed that the tensile strength of the previously underperforming 30% bamboo fibre composite increased from 29 MPa to a maximum of 33.5 MPa, while the elongation at break improved from 10% to 14.5%. Modifying the material to address the microscopic defects has expanded the potential applications of the composite [72].

In addition to natural-based materials for FDM composite production, recent studies have explored the use of various rock powders, including basalt fibre [80]. Hua et al. [73] designed and produced flexible plastic called L-PA (low-temperature polyamide) filaments, containing 15% by-weight basalt fibre, which offers the advantages of sustainability and recyclability. The experiment utilised the Taguchi L9 orthogonal array method to compare the effects of printing parameters (printing temperature, printing speed, and layer height) on the performance of the material. The results concluded that printing temperature had the most significant impact, while printing speed had the least effect. When basalt fibre is added to L-PA, it improves the tensile modulus, tensile strength, and energy absorption per unit volume without compromising ductility in comparison to pure L-PA. These enhancements reached increases of up to 176.6%, 142.0%, and 172.2%, respectively, relative to the pure L-PA. Microscopic structural analyses reveal that the fibres serve as reinforcing agents within the L-PA matrix. The effective adhesion both within individual layers and between successive layers is a primary reason for the improved mechanical properties of the FDM-printed composite samples. Incorporating a small quantity of basalt fibres improves the material's overall properties, thereby expanding the potential applications of FDM-based 3D printing in sustainable and recyclable fibre-reinforced flexible thermoplastic composites [73].

In summary, this section reviews various studies on fibre-reinforced composites in FDM, focusing on wood and natural fibres. It represents a novel research direction, as

carbon and glass fibres have been widely utilised in the industry for a considerable time. However, natural fibres still require further investigation. Most existing research addresses the challenge of inadequate adhesion at the interface between the fibres and the matrix, which frequently leads to issues within fibre composites and hinders their mechanical performance and applicability. Some studies have attempted to resolve this issue through additives, while others have explored various physical post-processing methods. Therefore, future research should aim to explore more economical, practical, efficient, and reliable approaches to enhance the bonding between fibres and the matrix, ultimately achieving improved performance of natural fibres.

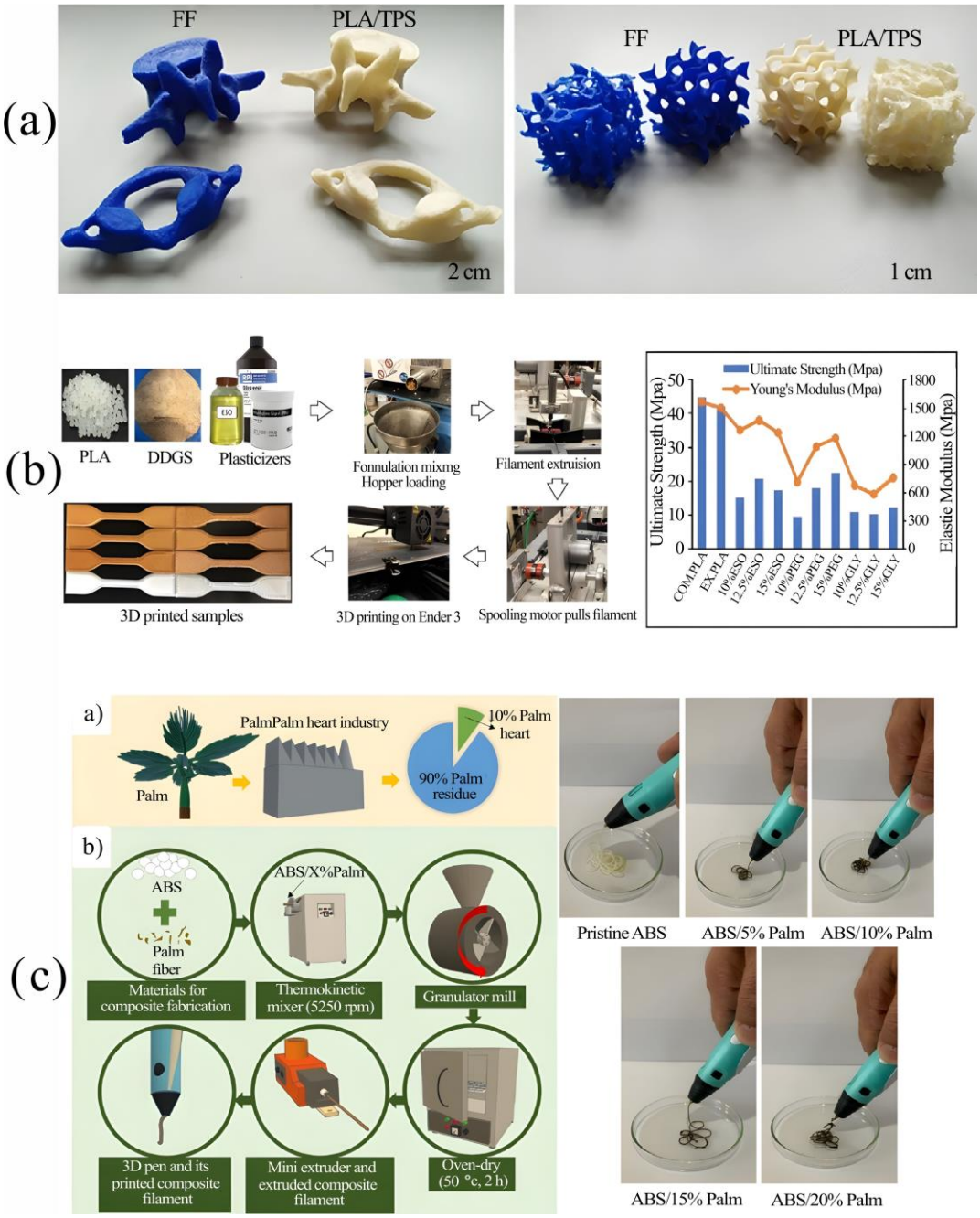

Figure 2.3. The novel natural fibre composites: (a) the complicated structures are made from potato fibre composite [67], (b) the DDGS fibre PLA [70], (c) the ABS is made of palm fibres and uses a 3D printing pen for extrusion [13].

2.2. Water and moisture effect on the FDM fibre composites

The introduction of fibres creates new voids within the initially dense polymer matrix [13, 68, 72], which can affect the mechanical properties of the final product by

influencing the bonding between the fibres and the matrix. Similarly, the voids facilitate water ingress, making it essential to study the impact of moisture on the performance of the fibre composites. In practical applications, many scenarios involve high humidity levels, leading to potential challenges [14]. The following section will present several studies examining the performance of different fibre composites (carbon, glass and natural fibre) under water immersion or in humid environments.

2.2.1. Conventional fibre-reinforced FDM filament

Ergene et al. [81] focused on carbon fibre-reinforced PLA structures' corrosion resistance and wear performance in a seawater environment. They compared FDM structures with filling densities of 20%, 60%, and 100%, which enhanced the composite's interaction with seawater. As the filling density increased (while keeping the immersion time in seawater constant), the volume loss values decreased[65]. This indicates that a higher filling density is more effective in combating seawater corrosion [82]. On the other hand, with the addition of carbon fibre, it was observed that at lower filling densities, the volume loss was greater. However, as the filling density increased, seawater corrosion resistance can be achieved by simultaneously increasing both the filling density and the carbon fibre content, thereby broadening the application potential[81].

Di Pompeo et al. [21] investigated the effects of drying on short carbon fibre and PA FDM composites. Their results showed that drying out the residual moisture improved tensile performance: the ultimate tensile strength increased from 127 MPa to 138 MPa, and Young's modulus rose from 13.5 GPa to 14.1 GPa, representing increases of 9% and 4%, respectively (Figure 2.4 (a)). The study highlighted that moisture impairs the interfacial stress transfer between carbon fibres and the PA matrix, reducing material performance. Additionally, drying enhanced the maximum strain and load capacity under buckling conditions [78]. These findings demonstrate that water’s impact is reversible, and performance can be restored by complete drying [41, 78]. Future studies should explore a wider range of materials and loading conditions [21].

Zhang [83] arrived at comparable conclusions in his study of short carbon fibre-reinforced PA composites, highlighting the critical role of interfacial properties between the fibres and the matrix in determining tensile strength, damage mechanisms, and failure characteristics. Specifically, the findings of this research revealed significant damage and a more pronounced reduction in tensile strength of the PA composites due to water absorption [72].

Guo et al. [84] studied continuous carbon fibre-reinforced nylon composites produced by FDM. The study focused on significant changes in tensile properties under hydrothermal conditions. The aim was to simulate the materials in high humidity and high-temperature conditions, typical of aerospace applications. The results showed a strong correlation between water absorption and both filling density and layer thickness, with layer thickness having the greatest impact [65]. As the layer thickness increased from 0.3 mm to 0.6 mm, the water absorption rate decreased from 70% to 30%. By comparing various parameter combinations, the optimal combination for the best performance was found to be a layup angle of 0°, a nozzle temperature of 260 °C, a fibre filling density of 80%, and a layer thickness of 0.6 mm [84].

Similar to Guo et al. [84], Zhang [83] also investigated continuous carbon fibre-reinforced PA, finding that its strength decreased minimally after water immersion compared to short carbon fibre composites. It is due to the fact that tensile performance of continuous carbon fibre-reinforced composites primarily depends on the fibres themselves rather than the bonding between the fibres and the matrix, making them less sensitive to moisture absorption.

Currently, there is research in research field about the fibre composite that focuses on the performance of glass fibre-reinforced composites in water immersion or humid environments. This section will introduce several studies on glass fibre composites, focusing on the effects of moisture absorption. These studies include both pre-moisture (moisture inherently present within the material) [85] and post-moisture (moisture introduced from the surrounding environment after manufacturing) [86] conditions.

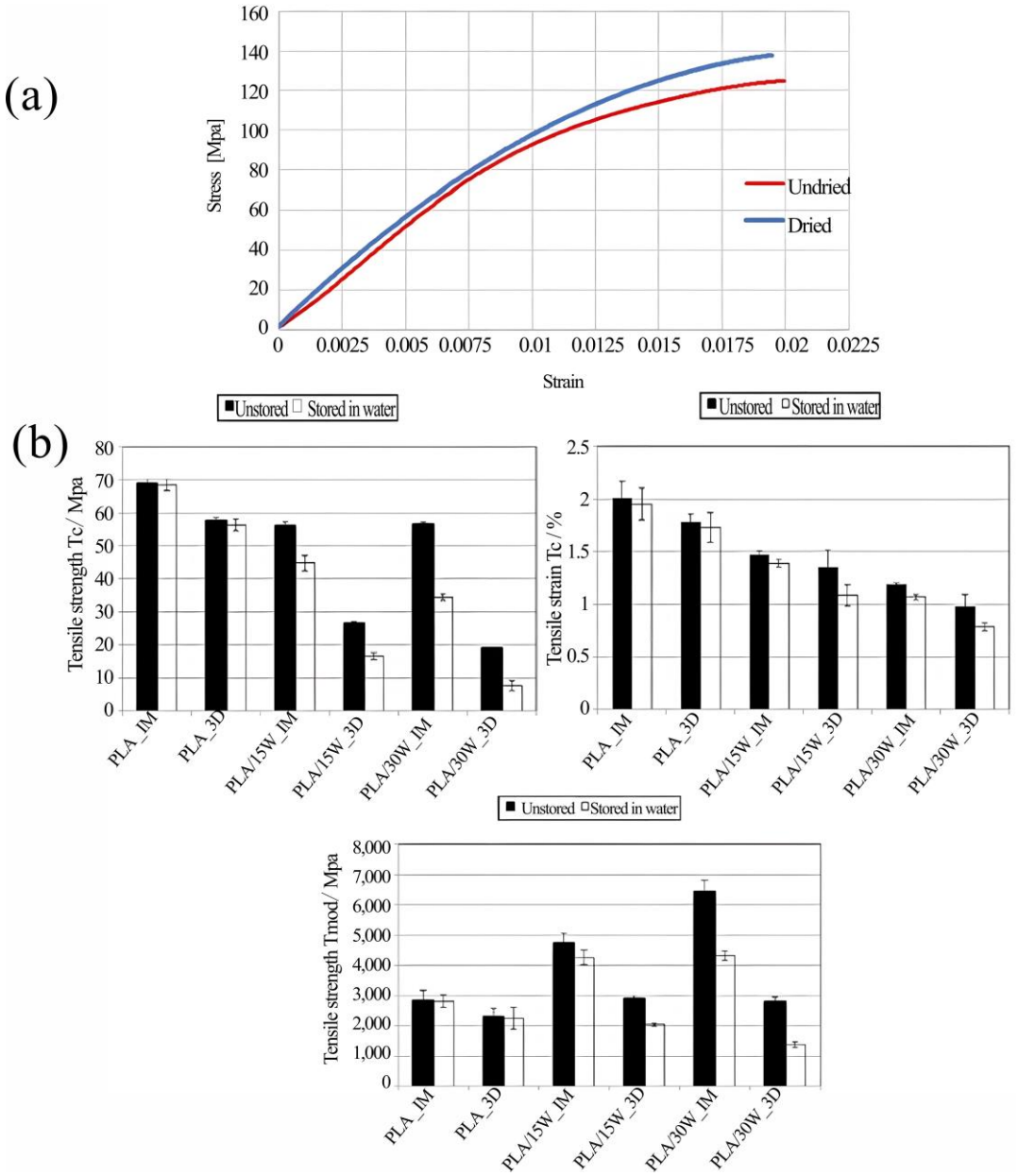

Figure 2.4. The effect of the water absorption on the mechanical properties of the fibre composites: (a) the carbon fibre PA performance after drying [21], (b) the PLA wood was stored in water, and the mechanical test results [78].

Hassan et al. [85] investigated the pre-moisture of the glass fibre composite. The authors investigated PA materials with three different volume fractions of glass fibre (4%, 8%, and 12%) to test the mechanical properties under three moisture conditions: dry, 50% relative humidity, and wet. From the tensile test, compared to PA without glass

fibre, the tensile modulus and tensile strength significantly increase with the addition of glass fibre, while tensile strain decreases [85]. As the humidity of the exposed environment increases, the samples' strength and modulus decrease, along with an increase in final strain. The authors attribute the observed changes of the mechanical properties under humid conditions to the plasticising effect of water [87, 88], as the polymer swells when exposed to water, resulting in alterations to its size, shape, stiffness, and permeability [85]. The authors explain the increase in strain as a result of the lubricating effect of water molecules [89]. When water molecules enter the system, they reduce the hydrogen bonding and dipole-dipole interactions originally present between the fibre and matrix, instead forming interactions with the water molecules [90]. This change facilitates lubrication between the polymer chains. As the humidity of the environment increases, this lubricating effect becomes more pronounced. It is important to note that fibres in the composite make the material's response to water more pronounced compared to pure polymer. It is because water has a greater impact on the interactions between the fibres and the matrix, which are typically the weakest points in the material [85].

Hadi et al. [86] investigated glass fibre-reinforced PA FDM composites, and included an examination of the influence of moisture content on mechanical performance. The study also focuses primarily on various printing parameters aimed at minimising the effect on the mechanical properties of the samples from the moisture. They concluded similar findings to those presented in the previous study, noting that lower initial moisture content corresponds to higher tensile strength in the samples[21]. One of the most significant problems that arises from moisture in 3D printing (including FDM) is the formation of bubbles during the extrusion of a filament that contains moisture [62]. These bubbles are caused by trapped water (moisture) in the plastic, which expands and vaporises at temperatures above 100 °C, creating a series of bubbles in the filament. The bubbles' creation of voids in the heated filament strand causes a number of problems in FDM [86]. After the addition of glass fibre, the negative effects

associated with this issue become more pronounced, as the pre-existing poor contact between the matrix and the fibres is exacerbated [72].

The above studies comprehensively demonstrate that both pre-moisture and post-printing moisture have significant adverse effects on conventional fibre-reinforced (carbon and glass fibre) composites. Therefore, it is essential to avoid these moisture issues in applications to ensure the structural stability and safety of the materials.

2.2.2. Wood and natural fibre

Currently, research on natural fibres in composites primarily focuses on various types, such as wood fibres [20, 28]. These natural fibres are rich in cellulose, which enhances the hydrophilicity and water absorption of the composite [91]. Consequently, the performance changes observed after immersion in water are more pronounced in these natural fibre composites compared to those made with other types of fibres [78]. This section will review several research studies investigating the effects of water absorption on natural fibre composites. These studies focus on composites made from various fibres, including wood fibre [65, 78, 92], potato starch fibre [67], palm fibre [13], and cellulose pulp fibre [91, 93].

The study by Duigou et al. [65], investigated the effects of printing width on water absorption and subsequent changes in the properties of wood fibre-reinforced PLA, and the results were also compared with those of samples produced using compression moulding. Additionally, in this research, Duigou et al. developed a method that utilised water to induce deformation in the material. By using the SEM and micro-CT, this study found that as the printing width increased from 100% to 200% and 300%, the porosity increased from 14.7% to 15.5% and 21.8%, respectively. Such an increase in porosity led to an increased water absorption ability. Also, increasing the printing width from 100% to 300% resulted in a 5- to 10-fold increase in water absorption. After absorbing moisture, there was a significant decline in tensile properties. Socked samples lose 10% and 30% of

their stiffness and strength, respectively, in comparison to dry samples. Compared with the compressed sample, FDM-printed samples exhibited a more pronounced decline in tensile properties (strength and modulus) after saturation as the printing width increased. The high expansion rate of wood bio-composites reflects the anisotropic hydro-mechanical properties. The study leveraged the anisotropic characteristics to design a method for achieving hygromorphism [94, 95]. By studying bio-inspiration paradigms in nature, such as phenomena like seed dispersal in pine cones, the study achieved a dual-layer printed structure by customising the printing orientation (0° and 90° across multiple layers) while maintaining similar components of the wood bio-composite to prevent delamination between layers (Figure 2.5 (a) and (b)) [65]. After absorbing water, the bio-composite layers began to actuate, demonstrating autonomous bending. Dynamic hydromorphic bio-composites offer self-shaping actuation (Figure 2.5 (a) and (b)), a novel capability for bio-composites, in contrast to static bio-composites, which are designed to provide stiffness and strength [65].

Consistent with the results of Duigou et al. [65], Kamau-Devers et al. [92] found that the incorporation of wood fibre contributes to enhancing the water absorption capacity of PLA. After soaking for 400 hours at room temperature (25 °C), the water absorption of pure PLA was less than 1%. The water absorption value is directly proportional to the wood fibre content, with the sample containing 30% wood fibre exhibiting a water absorption rate of 10% [92]. The significant enhancement in water absorption capacity can be attributed to two main factors. First, Ayrilmis et al. [96] demonstrated that pores within the material provide the entire sample with the capacity to retain water. The pores originate from the interactions between the fibres and the matrix, as well as from the gaps between the strands during the printing process [96]. Another explanation lies in the chemical properties of wood fibres, which contain significant amounts of cellulose, hemicellulose, and lignin. Cellulose exhibits pronounced hydrophilicity compared to PLA, which is hydrophobic. This contrast contributes to the overall enhancement of the sample's water absorption capacity [23, 67, 97].

Ecker et al. [78] conducted a study comparing the mechanical property changes of pure PLA and various amounts of wood fibres after water absorption [78]. Besides, the research examined the performance differences resulting from two manufacturing methods: FDM and injection moulding [98, 99]. The study demonstrated that after seven days of immersion, the water's effect reduced the samples' stiffness, regardless of the presence of wood fibres. Furthermore, the decline in stiffness was more pronounced with the increasing wood fibre content (Figure 2.4 (b)).

Additionally, samples produced using injection moulding exhibited a smaller decrease in stiffness compared to those manufactured through FDM. The injection moulding process utilises the deformation rate induced by high pressure and a rapid cooling process, resulting in a more compact microstructure throughout the sample [100, 101]. The compactness reduces the impact of water absorption. In contrast, the FDM technique tends to create larger voids, leading to a greater susceptibility to the effects of water. The reduction in performance after water absorption is a significant barrier to the material's application, as prolonged exposure to extreme weather and humidity, ranging from one week to one month, can severely affect its mechanical properties in practical use [78, 102].

Haryńska et al. [67] discussed the performance of their independently designed potato-PLA composite in FDM within their research. In this study, the PLA/TPS filament was utilised to examine the water absorption effect. Through water contact angle experiments, the hydrophilicity of the PLA/TPS composite was demonstrated. At 0° (printing direction), the contact angle for PLA/TPS was 6°, while that for PLA was 75.77°. At 90°, the contact angle for PLA/TPS was 81.54 °, compared to 111.46° for PLA. In tensile testing, standard PLA exhibited significant differences in performance across different printing directions and methods (0° and 90°, as well as XY and ZX printing) [67].

Marton et al. [13] utilised solid waste from recycled palm residues (Australian royal palm) and ABS to create a bio-based composite polymer for use in FDM [13]. Filaments

with different palm fibre contents (5%, 10%, 15%, and 20% by weight) were produced using a thermodynamic mixer for processing, followed by a mini extruder to process various fibre loadings. The water absorption properties at various fibre compositions were investigated in this study. The findings showed that water absorption increased with time. Furthermore, it was discovered that the inclusion of fibres raised the rate of water absorption of the reinforced composite materials. This increase can be attributed to the presence of voids between the fibres and the matrix [13].

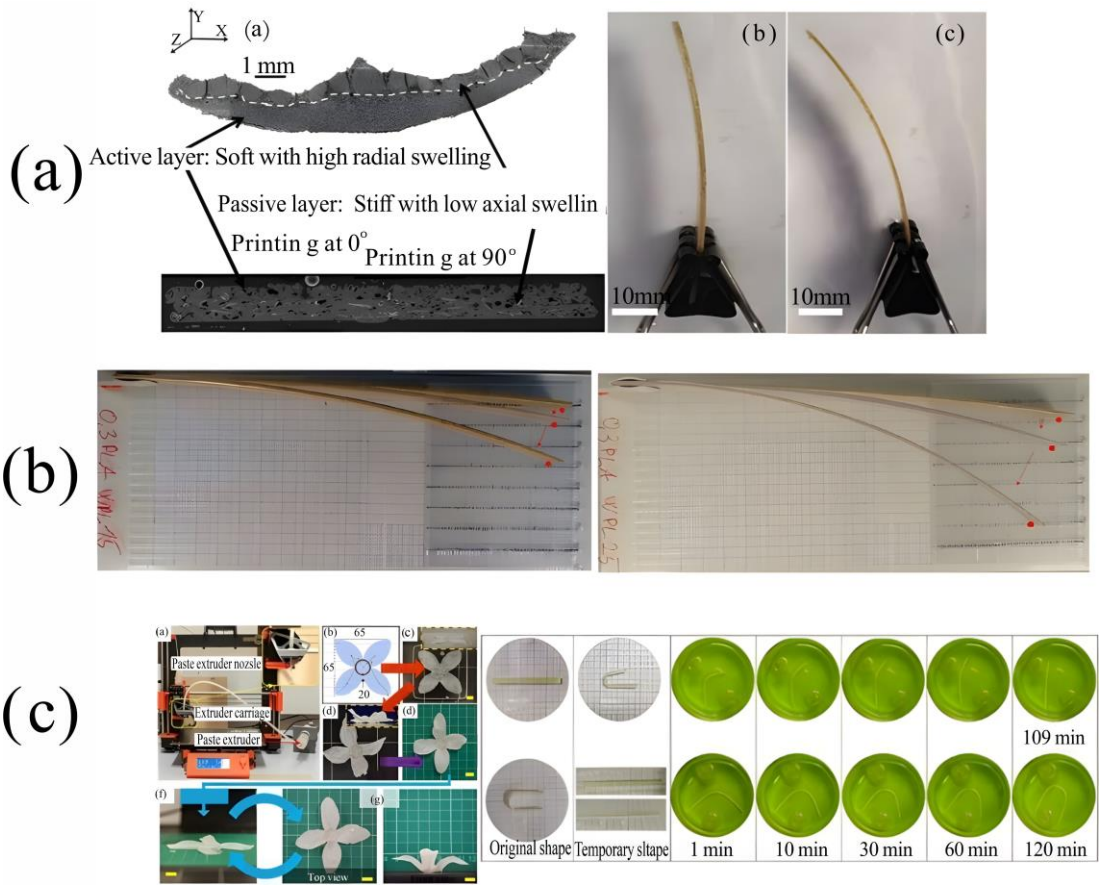

Figure 2.5. The research about the effect of moisture on the natural fibre composites: (a) and (b) dual-layer printed structure with wood fibres for actuation functionality [65], (c) water actuation shape changes printing practices with cellulose content [91].

Due to the previously mentioned results, natural fibre composites feature a higher water absorption ability [13]; many researchers have predicted, attempted, and utilised natural fibre composites to explore the potential for water actuation shape changes [65,

103]. Water actuation shape changes allow structures to change and morph over water immersion while exhibiting self-repair and self-assembly capabilities [104]. This intelligent feature enables the technology to be utilised across various advanced fields, including aerospace [2] and medical science [15, 58]. Water actuation shape changes technology is mainly compatible with shape memory polymers. The mechanism of this technology enables the structure to absorb water and swelling to change the overall volume of the structure. Then, the shape can be changed by the internal mechanics [104]. This method has been frequently researched in this realm due to its simple concept and the stimuli (water) that can be controlled readily. The primary considerations in designing water actuation shape changes are swelling anisotropy and the design of printing materials with different swelling characteristics in various directions in a water environment [65]. From the concept, the target materials for this technique must have a good performance in water absorbency. Cellulose has some advantages, such as its biodegradability and existence in nature, enabling cellulose to be a typical material for water actuation shape changes.

Mulakkal [91] conducted a novel practice. A sustainable and cost-effective ink (cellulosic pulp hydrogel composite ink) was developed with a high total cellulose content and good dispersion of cellulose fibres within the hydrogel matrix. The cellulose pulp fibre was mixed with CMC (carboxymethyl cellulose). Montmorillonite was added to give the ink good extrusion properties and storage stability. The practice results show that the flower's petals made from special ink can be opened and closed (Figure 2.5 (c)) during hydration and dehydration processes [91]. However, further research is required to show that the ink can be extruded smoothly without congestion.

Gladman et al. [93] conducted research to find out the microscopic principles of the shape memory effect of cellulose-based material, ensuring the direction of cellulose fibres is identical to the printing direction. After soaking in a moist environment, the swelling rate is higher in the printing direction. The research shows that the water-driven shape memory effect presents anisotropy properties, which can be applied to achieve

better shape memory performance and lower manufacturing costs for future designs [93]. In water actuation shape changes, the high-water absorption characteristics of cellulose enable originally hydrophobic polymers to acquire hydrophilicity, thus facilitating the possibility of water actuation shape changes.

2.3. Complex structures manufactured by FDM and their applications

Some studies employ complex structures to achieve improved performance and broader application prospects [105]. Wood-PLA composites, being bio-based and sustainable, are gaining attention in the field of energy absorption [106-108] due to their good mechanical properties and environmental advantages [11]. The development of complex energy-absorbing structures using wood-PLA composites could open up new possibilities for their use in lightweight, impact-resistant applications [109], particularly in industries such as automotive and construction. When designing complex energy-absorbing structures, it is essential to consider several key factors, including materials, components, optimisation, and deformation[108]. Among the key factors for designing energy-absorbing structures, material selection plays a significant role in determining the performance of the structure. Bio-based composites, with their combination of natural fibers and polymer matrix, offer excellent opportunities for energy absorption, especially in lightweight designs where sustainability is a priority [26]. Based on these factors, common complex energy-absorbing structures studied in current research include lattice structures [105], foam structures [110], and graded material structures [111]. Among them, research on lattice structures is the most extensive [112]. Furthermore, depending on the different components within the lattice, lattice structures can be further divided into numerous subcategories, including honeycomb structures [5], re-entrant honeycomb structures [53], various TPMS (Triply Periodic Minimal Surface) structures [113], and others. Wood-PLA composites have been used in some studies to fabricate energy-absorbing lattice structures, such as honeycomb and TPMS designs

[26]. Their lightweight, bio-based properties make them ideal candidates for improving the energy absorption capacity of these structures, especially in applications requiring both mechanical strength and environmental sustainability [28].

In this section, the three common types of lattice structures (honeycomb (2.3.1), re-entrant honeycomb (2.3.2), and TPMS (2.3.3)) will be introduced. The studies selected for review all utilise fibre composites as materials, including carbon fibres, glass fibres, and natural fibres.

2.3.1. Honeycomb structure

The hexagonal honeycomb structure has been widely utilised in sandwich construction across aerospace, naval, and packaging sectors since 1940 [114]. This structure is an effective shock absorber in applications like air-dropped containers and crashed vehicle bodies [5]. Its diverse applications stem from its capacity to convert impact energy into energy associated with plastic deformation. The energy absorption characteristics are influenced by the material used, cell wall thickness, and geometric configuration [5]. This section will review several research studies on using fibre composites in honeycomb structures and their applications.

Dou et al. [115] investigated the compression performance of hexagonal honeycomb structures made from continuous carbon fibre-reinforced PLA fabricated via FDM. They compared the compression performance with similar structures made from pure PLA and aluminium alloy, considering two loading directions: X1 (horizontal) and X2 (vertical) (Figure 2.6). The experiments demonstrated that the hexagonal honeycomb structure reinforced with continuous carbon fibres exhibited a significant advantage in the X1 direction compared to the other two materials, showing energy absorption improvements of 186.58% and 596.84% over pure PLA and aluminium alloy, respectively. The in-plane compression altered the deformation characteristics of the structure, transforming it from brittle and fragile to standard elastoplastic behaviour [12],

resulting in a smoother and more stable stress-strain curve(Figure 2.6). These changes are attributed to the continuous carbon fibres inhibiting the further propagation of cracks in the matrix under compression [84], with the fibres providing internal tensile forces that keep the soon-to-fragment sections tightly connected. It illustrates that continuous carbon fibres can enhance the reliability of structural applications by enabling excellent energy absorption and that the performance of such structures can be further improved by optimising the bonding between the fibres and the matrix [115].

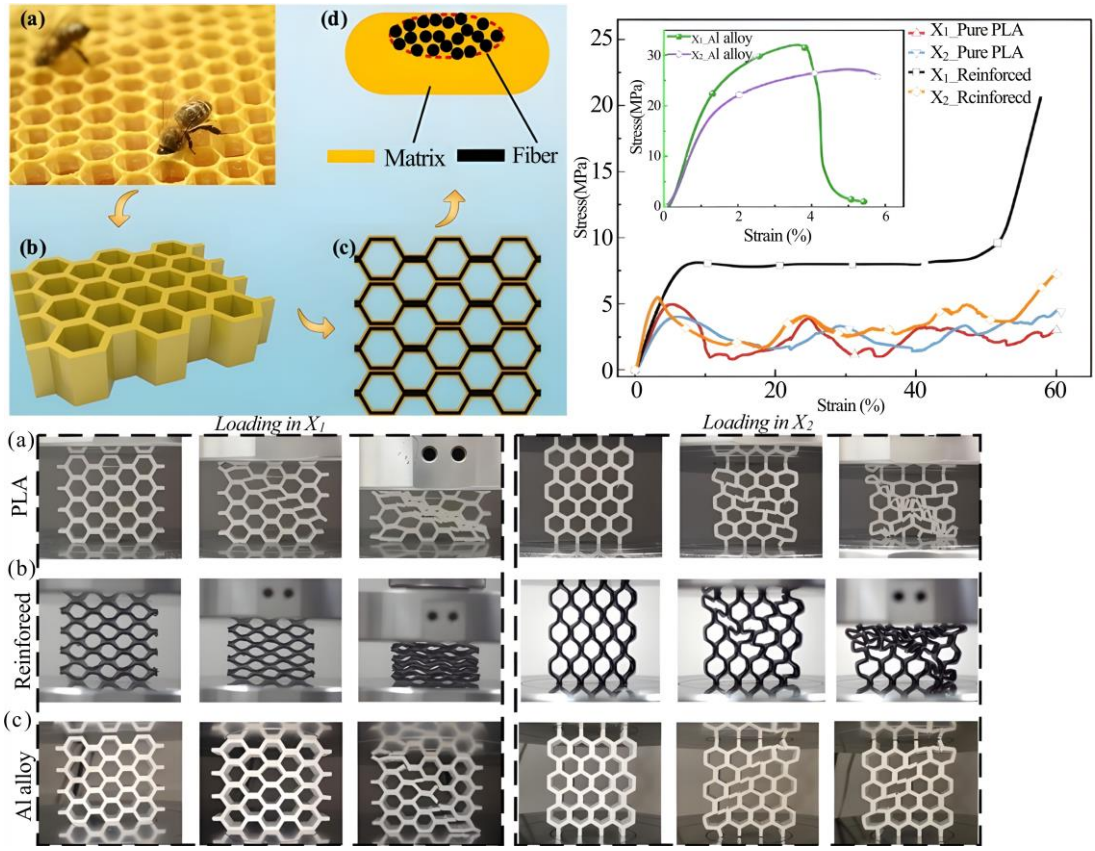

Figure 2.6. The carbon fibre-reinforced PLA honeycomb structure [115].

Cheng et al. [116] also investigated the continuous carbon fibre-reinforced PLA hexagonal honeycomb structures. After compression testing and deformation, they used heating to achieve the shape-memory effect. In the experiment, the constant carbon fibres served two functions: on the one hand, they enhanced the mechanical performance of the structures; on the other hand, they facilitated heating (Figure 2.7 (a)). By connecting both

sides of the honeycomb structure to the positive and negative terminals of a power source, the conductivity of the carbon fibres created an electric circuit, allowing the entire structure to be uniformly heated through Joule heating. Firstly, the honeycomb structure reinforced with carbon fibres exhibited significantly higher energy absorption capacity and stiffness than the conventional structure, regardless of the loading direction. This confirms the first function of the carbon fibres. After compressing until a fixed strain of 0.2 and unloading, electric heating was applied to restore the sample. It was observed that after the first heating, the strength and recovery reached 87% of the original value. Finally, the authors suggested that due to the insufficient memory properties of PLA, future research should explore the use of entirely new materials, such as TPU, to achieve improved shape memory effects [116].

Antony et al. [26] utilised hemp PLA materials with a content of 20%-25% hemp fibres to fabricate hexagonal honeycomb structures, incorporating flat panels on both the top and bottom to create a sandwich structure (Figure 2.7 (b)). The structures are applicable in fields such as automotive and aerospace applications, highlighting the potential of these composites in reducing plastic content while maintaining mechanical performance [11]. Using hemp/PLA honeycomb structures offers several advantages, including their superior compressive strength compared to other materials [117]. Specifically, they surpass the compressive strength of hemp/PP honeycomb (6.51 MPa), aluminium core (9.37 MPa), and stainless-steel core (2.41 MPa). This design achieves better recyclability, renewability, and biodegradability of the materials without compromising mechanical strength, promoting sustainable development [26].

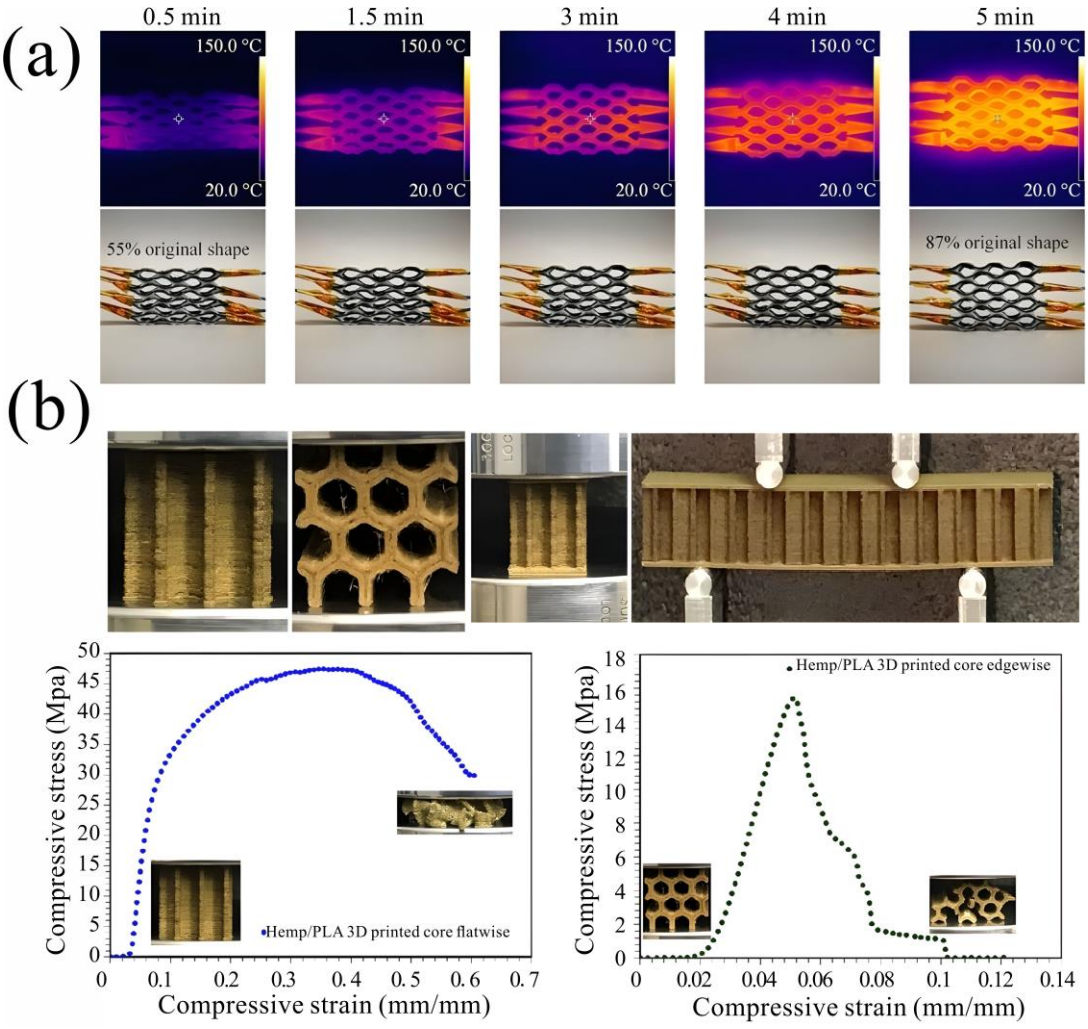

Figure 2.7. The honeycomb structure and its applications: (a) the shape memory test uses carbon fibre as the heating source [116], (b) the hemp PLA composite honeycomb structure [26].

2.3.2. Re-entrant honeycomb auxetic structure

The re-entrant honeycomb auxetic structure is characterised by a negative Poisson's ratio [118]. When compressed perpendicular to its axis, the structure contracts while it expands under perpendicular tensile forces. The innovative design of the re-entrant honeycomb auxetic structure was initially developed by Lakes in 1987. It exhibits remarkable qualities in terms of shear stiffness [119], resistance to indentation, fracture

toughness, energy absorption, and distinctive acoustic properties [118]. These attributes allow the structure to absorb energy during compression and impact effectively. Its applications include energy-absorbing and sound-dampening frameworks, as well as structural reinforcements. For this innovative structural design, using fibre-reinforced composites can yield improved performance and demonstrate various mechanical advantages, enhancing its potential for broader applications [120]. This section will review several research studies on using fibre composites in re-entrant honeycomb structures and their applications.

W. Liu et al. [121] focused on comparing the re-entrant honeycomb auxetic structure with the hexagonal honeycomb regarding compression and crushing performance. Early densification enabled the re-entrant honeycomb auxetic structure to absorb more energy [122]. The re-entrant structure exhibits higher peak stress to resist equivalent impact energy in the experiment data. When subjected to the same initial velocity, the re-entrant honeycomb requires less crushing strain or time to halt the impact plate than the hexagonal honeycomb. Moreover, both structures show similar sensitivity to the relative density gradient in the direction of impact [121].

Quan et al. [109] utilised continuous carbon fibre-reinforced PLA to fabricate a re-entrant honeycomb auxetic structure via FDM. Compression tests demonstrated that the re-entrant honeycomb auxetic structure exhibited significantly greater compressive stiffness and energy absorption compared to pure PLA while only resulting in a 6% increase in mass. Using a 5×3-unit cell configuration, the final structure measures 96.8 mm in length, 50 mm in width, and 79.34 mm in height. In loading orientations 1 and 2 (Figure 2.8), the continuous carbon fibre-reinforced PLA exhibited stiffness increases of 98.7% and 86.3%, respectively, with total energy absorption improvements of 87% and 100%. These significant enhancements can be attributed to the continuous fibres effectively inhibiting crack propagation within the matrix [12], thereby preventing pillar failure and overall structural collapse. In contrast, the pure PLA structure experienced premature pillar failure, resulting in a sudden drop in load-bearing capacity. The authors

note that there is still room for improvement in this approach; by increasing fibre content and reducing printing defects, further enhancements in mechanical performance can be achieved [109].

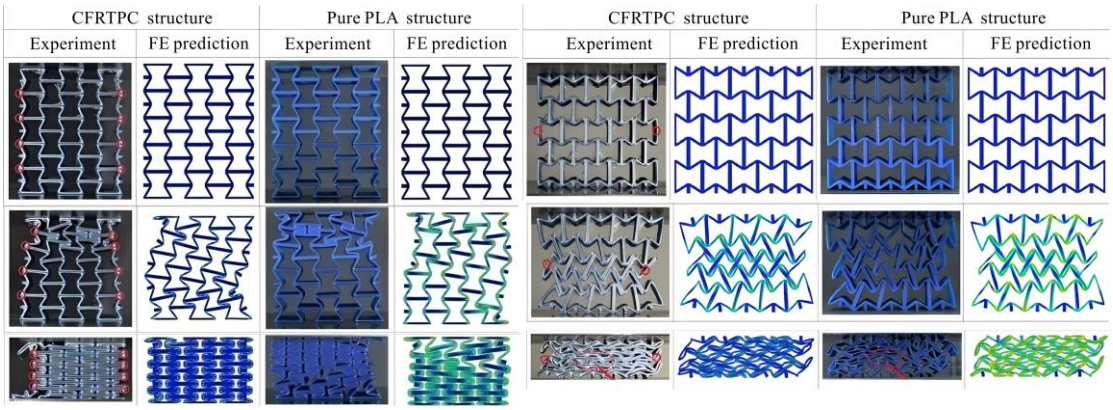

Figure 2.8. The carbon fibre PLA re-entrant honeycomb structure with two directions [109].

Essassi et al. [123] employed a flax (bio-based) fibre and PLA composite to fabricate a re-entrant honeycomb auxetic structure, utilising a sandwich design to enclose the upper and lower surfaces fully. The stress ratio's influence on the samples' fatigue performance was determined through cyclic bending tests. The experiment included a variable concerning the printing density of the core material sandwiched in the middle. The findings indicate that core density significantly impacts the fatigue performances of sandwich composites [124]. In detail, sandwiches with the lowest core densities have the most extended fatigue lives and can support a lower maximum load [26]. Therefore, selecting the appropriate core density based on the actual application scenario is crucial, as it involves a trade-off between fatigue life and maximum strength [123].

Taherkhani et al. [125] capitalised on the advantages of the re-entrant honeycomb auxetic structures, characterised by its negative Poisson's ratio and strong energy absorption capabilities, in conjunction with the benefits of carbon fibre reinforcement, to design a flexible and stretchable strain sensor. The structures can be applied in various fields, including robot design and healthcare monitoring [11, 126]. Flexible substrates

were designed using the re-entrant auxetic structure to increase the stretchability and improve the sensitivity of the flexible, stretchable strain sensor. It enhances stretchability by 98% and sensitivity by 24 times more than the conventional sensors; these sensors have high sensitivity at even low strain and can be used for lower strain conditions like vocal cord dysfunctions, wrist pulses, and earth vibrations [125].

2.3.3. TPMS

TPMS are mathematically defined structures with zero mean curvature in three dimensions and large surface areas [124, 127]. TPMS structures provide desirable advantages for the application, including being structurally lightweight, providing impact protection, and good thermal conductivity [124]. However, the complex geometry makes TPMS challenging to fabricate using traditional techniques such as mould manufacturing [128]. There are various types of TPMS structures, among which the Gyroid, Primitive, and Diamond (Figure 2.9 (a)) forms are commonly studied [129]. These structures exhibit distinct shapes.

The structure of TPMS can be applied across various fields, with its most significant application being in the medical domain [130]. It primarily serves as a fundamental structure for artificial bones and tissues [131], crucial in this area. Additionally, TPMS can be applied in aerospace and automotive manufacturing, where its primary function is to provide impact absorption and protect internal structures and components [132]. Numerous studies utilise fibre-reinforced composites to manufacture TPMS, employing techniques such as SLA, SLS [133], and FDM. Among all these fibre composites related to TPMS research, carbon fibre-reinforced composites are the most widely used [128, 129]. This section will review several research studies on using different fibre composites in TPMS structures and their applications.

Saleh et al. [129] utilised PLA infused with 15% short carbon fibres to fabricate various TPMS samples (Gyroid, Primitive and Diamond) through FDM. The study mainly investigated the effects of carbon fibre incorporation, unit cell type, size effects,

and relative density on the compressive performance of the TPMS structures. The results revealed that among the three-unit cell structures, the Schwarz-Diamond (d for Diamond) configuration exhibited the best energy absorption capacity and compressive strength, and the Primitive configuration performed the worst (Figure 2.9 (b)). This is attributed to its larger surface area and improved material distribution, which enhances wall contact and minimises voids between the walls [134, 135]. Relative density has a significant impact on the mechanical properties of TPMS structures. An increase in relative density results in enhanced compressive strength and modulus. This effect can be observed across TPMS topologies, including Gyroid, Primitive, and Diamond (Figure 2.9 (b)). Higher relative density indicates that the walls within the structure become thicker, which implies that more material is used during the FDM process. This results in an overall increase in the structural resistance, thereby enhancing the mechanical properties. Additionally, incorporating carbon fibres in all three structures demonstrated increased compressive strength, compressive modulus, and energy absorption compared to pure PLA. Moreover, this enhancement is particularly pronounced in structures with high relative density [129].

Lazar et al. [128] investigated glass fibre and PA composites, fabricating TPMS structures through FDM. Also, it compared the effects of relative density, unit cell type, and fibre incorporation on the compressive performance of TPMS structures and the impact of loading direction. Consistent with previous research [129], the findings indicate that the Schwarz-Diamond (d) unit cell structure exhibits the best performance [129]. As relative density increases, the overall performance of the structure was significantly improved. Additionally, altering the loading direction can change the mechanical properties, primarily affecting the failure mode. All structures experienced a progressive layer-by-layer collapse mode of deformation under axial compression as opposed to shear bands and catastrophic failure, resulting in smoother curves and increased energy absorption. Adding glass fibres to reinforced composites significantly increases the final structures' strength and stiffness but at the expense of the ductility

[85, 86]. Short fibre alignment greatly increases modulus and strength in the alignment direction and produces direction-dependent material characteristics [136]. Furthermore, short glass fibre reinforcements' notable heat conductivity encourages polymer diffusion and reduces porosity, which enhances interfacial bonding and prevents fibre breakage and matrix cracking [128].

Mandava et al. [137] utilised a composite called PAPC, composed of cellulose fibres, PA, and polyolefin, to fabricate TPMS structures suitable for simulating bone scaffolds through FDM. PAPC is a medical-grade, biocompatible polymer composite commonly used in research related to artificial bones and tissues. It offers numerous advantages, including enhanced mechanical and impact properties [113, 124], due to its combination of polyamide's flexibility and polycarbonate's high strength. Additionally, this material possesses thermal stability, chemical resistance, and low weight, making it one of the most widely used medical materials in this field [131]. Compressive tests were conducted to assess their performance. The compressive tests concluded that the diamond structure remains the most effective configuration compared with all the other types TPMS structures. The authors attributed this to the fact that the Schwarz-Diamond (d) structure, under the same printing parameters, achieves a higher deposited mass than other structures, enhancing its compressive performance. In contrast, the compressive performance of the other TPMS structures (Gyroid and Primitive), decreases as their deposited mass declines. This study validated the feasibility of creating artificial bone tissue using TPMS structures and FDM, setting the stage for developing complex composite bone scaffolds with customisable medical and functional characteristics [137].

Many studies have also explored the effects of various natural fibres on TPMS structures. Veeman et al. [138] utilised a composite of wood fibres and PLA to fabricate Gyroid TPMS structures through FDM, adding a 2.5 mm thick wall around the structure (Figure 2.9 (c)). They conducted compressive tests on the resulting structures. The study employed the Taguchi method [139] to compare the effects of various printing

parameters on the performance of the Gyroid structure, including raster angle, layer thickness, and wall thickness. The results indicated that a raster angle of 45°, a layer thickness of 0.1 mm, and a wall thickness of 0.8 mm yielded the best compressive strength and could absorb more energy. Although the wood fibre-PLA TPMS cannot be used for medical applications, this study also demonstrated the potential for other applications of this material and structure. For instance, it proved that FDM can be utilised to print such complex structures, which could be applied in furniture design or the production of art pieces [138].

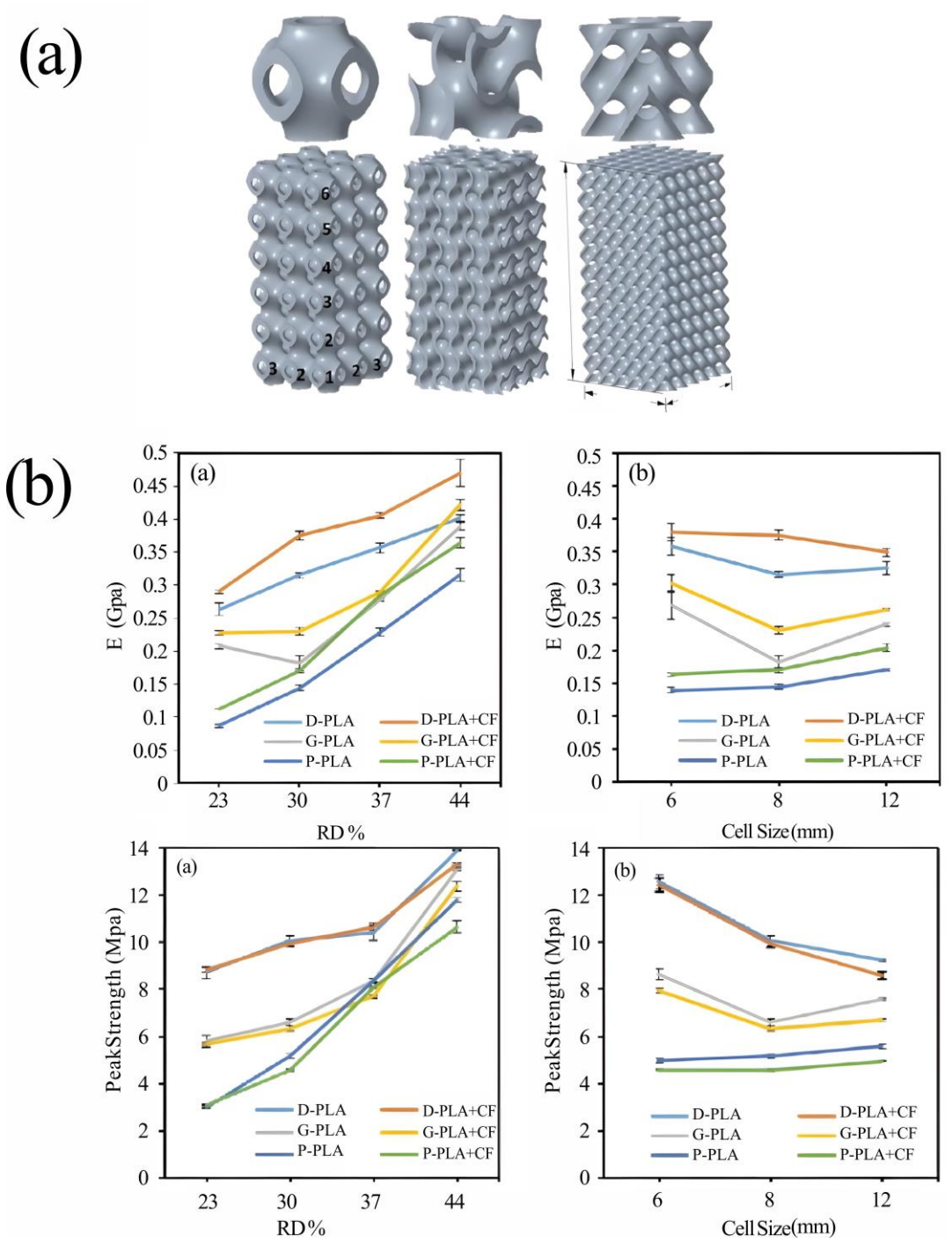

Figure 2.9. The research about the TPMS structures with different kinds of fibre composites: (a) different types of TPMS [129], (b) the influence of different types of TPMS and their RD%, cell size [129], and (c) Gyriod structure with wood-PLA [138].

2.4. Research gaps

Based on the previous literature review, there is a foundational understanding of fibre composites in FDM. However, several research gaps remain that need to be addressed. The three main gaps can be summarised as follows:

1. Although extensive studies have examined carbon- and glass-fibre composites, research on wood-fibre-reinforced composites, especially those produced by FDM, remains limited. Most existing works have concentrated on filament formulation and printability rather than the mechanical and fracture behaviour of printed parts.

2. Previous studies have mainly explored the water absorption behaviour of wood-fibre composites in terms of moisture uptake and dimensional change. However, the degradation mechanisms associated with water exposure—such as plasticisation, interfacial debonding, and reversibility upon redrying—are not yet fully understood.

3. While natural-fibre-reinforced composites have been widely studied, the progressive effects of different fibre loading levels on the mechanical performance (e.g., strength, ductility, and energy absorption) of FDM-printed wood-PLA composites have not been systematically characterised.

2.5. Research objectives

To address the research gaps identified in Section 2.4, this thesis has been structured into three main experimental stages, each corresponding to one of the outlined gaps.

To address **Gap 1**, a foundational understanding of the mechanical properties of wood fibre-reinforced PLA was developed by comparing the tensile and fracture behaviour of two commercially available FDM filaments: pure PLA and wood-PLA. This comparative analysis aimed to clarify the baseline mechanical differences introduced by incorporating wood fibres and to assess the practical feasibility of substituting traditional fibres in additive manufacturing. The findings are presented in

Chapter 3.

For **Gap 2**, the study examined how water immersion and subsequent drying affect the mechanical properties of both PLA and wood-PLA. Mechanical testing was conducted before and after water exposure, followed by a redrying phase, to determine whether the observed degradation is reversible. This research provided insight into the role of moisture in changing the mechanical properties and evaluated the reliability of wood-fibre composites under humid environmental conditions. This stage of research is detailed in **Chapter 4**.

To respond to **Gap 3**, the influence of different wood fibre contents (ranging from 0% to 20%) on mechanical performance was systematically investigated. The study examined how fibre content affects tensile strength, ductility, and energy absorption, as well as how these properties respond to water immersion and drying. This helped identify optimal formulations with improved performance. The results of this investigation are presented in **Chapter 5**.

Together, these three chapters form a cohesive framework that addresses the previously identified knowledge gaps and advances the understanding of wood fibre composites in additive manufacturing.

Chapter 3. Mechanical properties of PLA and wood-PLA composites fabricated via FDM

3.1. Introduction

In recent years, additive manufacturing, also known as 3D printing, has progressively found applications in an increasing number of fields, due to its ability to reduces the human labour, material consumption, and time required throughout the production process, thereby enhancing overall efficiency [140]. Among the various types of 3D printing technologies, FDM has attracted growing attention in the scientific community due to its early development, advanced state of refinement, high prevalence, and wide range of applications [141-144]. It has found broad applications in industries such as automotive, aerospace, construction materials, and medical devices [4, 24, 145].

Fibre-polymer composites have gained significant attention in FDM applications owing to their improved strength-to-weight ratio and durability compared to single-material systems [14, 15, 146]. Currently, the fibres commonly used in FDM include carbon fibre [12, 32, 33, 147, 148], glass fibre [17, 34], and aramid fibres [18]. These fibres have distinct properties that provide specific advantages, making them suitable for various applications across various fields.

Natural or bio-based fibres have emerged in recent years as new materials suitable for composites, frequently combined with polymers such as PLA, TPU, and PA to produce filaments for FDM [20, 62, 64, 66, 149]. Compared to traditional materials like carbon fibre, these bio-based fibres offer several advantages, including easy availability from natural sources, biodegradability, and lower carbon emissions [15, 22, 150]. Recent studies have begun to focus on the mechanical properties of natural fibre composites and how the other factors affect their mechanical properties, including the effects of varying fibre content [62], printing parameters [64], and the impact of additives on the optimisation of their internal structure and properties [20]. Some studies have also

focused on utilising recycled raw materials to produce natural fibres, thereby enhancing their sustainability benefits. This includes the use of materials such as flax [25], potato starch [67], grains [70], and recycled palm residues [13], which are blended with various types of polymers to create FDM-compatible filaments. Additionally, the high cellulose content in natural fibres contributes to the material's significant water absorption properties [13, 65, 67, 92], leading to more pronounced changes in properties upon exposure to moisture.

Wood-PLA composites represent a unique class of natural fibre composites that simultaneously exhibit biodegradability [151, 152]. They have become one of the most widely adopted natural fibre-reinforced materials for FDM applications [28]. Understanding the mechanical behaviour of wood-PLA is essential for expanding its practical applications in load-bearing and structural contexts [26]. However, its inherent heterogeneity and fibre-matrix interactions may significantly alter its mechanical performance [78]. Therefore, examining how wood-PLA behaves under mechanical loading, particularly in terms of strength and energy absorption ability, is critical for determining its feasibility.

This chapter compares the mechanical behaviour of two commercially available filaments: a pure PLA and a wood-PLA composite. All specimens were printed and tested in their original state (without any special conditioning) shortly after fabrication. Mechanical characterisation including both tensile and SENB tests were conducted, aiming to assess strength, stiffness, and energy absorption. Section 3.2 outlines the materials and methods used, including the fabrication process, mechanical testing, and post-test analysis. Section 3.3 presents and compares the experimental results for the two materials, and Section 3.4 concludes with a summary of key findings and observations.

3.2. Methods and materials

3.2.1. Materials and samples preparation

Two commercial filaments are involved in this research project:

1) The pure PLA, called PLA EF 3D850, with a diameter of 2.85 mm, was purchased from commercial supplier (Nanovia, France). The density of the filament is 1.24 g/cm^3, and the recommended extrusion temperature is between 190 °C and 230 °C;

2) The wood-PLA composite filament, containing 40 % pine wood fibre by volume and with a diameter of 2.85 mm, was purchased from the same supplier. The density of the filament is 1.13 g/cm^3, the recommended extrusion temperature is between 210 °C to 230 °C.

In this study, tensile samples and SENB samples were fabricated and tested using PLA and wood-PLA materials. Ultimaker S5 FDM printer (Ultimaker, Netherlands) was used to printing these two materials following the printing configurations listed in Table 3.1. The preparation process of samples is illustrated in Figure 3.1. Tensile samples were Type IV, conforming to ASTM D638 specifications, with a thickness of 1.6 mm [153]. To fabricate tensile samples with unidirectional filament, a hollow square tube with dimensions of 160 mm × 160 mm × 60 mm and a thickness of 1.6 mm was printed. The hollow tube was printed by using a concentric infill pattern to ensure that the structure was fully symmetric on all sides. Type IV dog-bone tensile samples were cut from each side of the hollow tube using the laser cutter (Thunder, Australia) [126]. In this way, the smooth transition in sample dimensions helps to minimise stress concentration in the fillet radius area, addressing the issue typically observed in directly printed samples [154, 155].

Table 3.1. FDM printing parameters

Printing parameters	Configurations
Layer height	0.2 mm
Line width	0.8 mm
Printing temperature	210 ℃
Building temperature	28 ℃
Bed temperature	65 ℃
Printing speed	35 mm/s
Fill pattern (tensile)	Concentric
Fill pattern (bending)	Line

For SENB samples, the dimensions, especially the length of notch, vary across standards due to differences in material of interest and the test objectives. Given that 3D printing is a relatively novel technique compared to traditional manufacturing techniques, standardised guidelines specifically addressing the mechanical testing of FDM printed materials have not yet been established. Current testing practices rely on existing standards for conventional manufacturing method [156]. Hence, SENB samples with different notch lengths, in accordance with two standards, i.e., ASTM D5045 standard and ASTM E1820, were utilised to investigate the fracture behaviour under bending [157-160]. Since the notch length may affect stress distribution at the crack tip and influence crack propagation, samples with notch lengths of 4 mm and 10 mm were prepared. The total length of SENB samples was 90 mm, with a thickness of 10 mm and a height of 20 mm (Figure 3.1). During the printing, a linear infill pattern was adopted for the SENB samples to ensure structural uniformity and reduce anisotropy in the crack propagation direction. This configuration facilitates a more stable crack path during testing, thereby improving the reliability of fracture behaviour analysis.

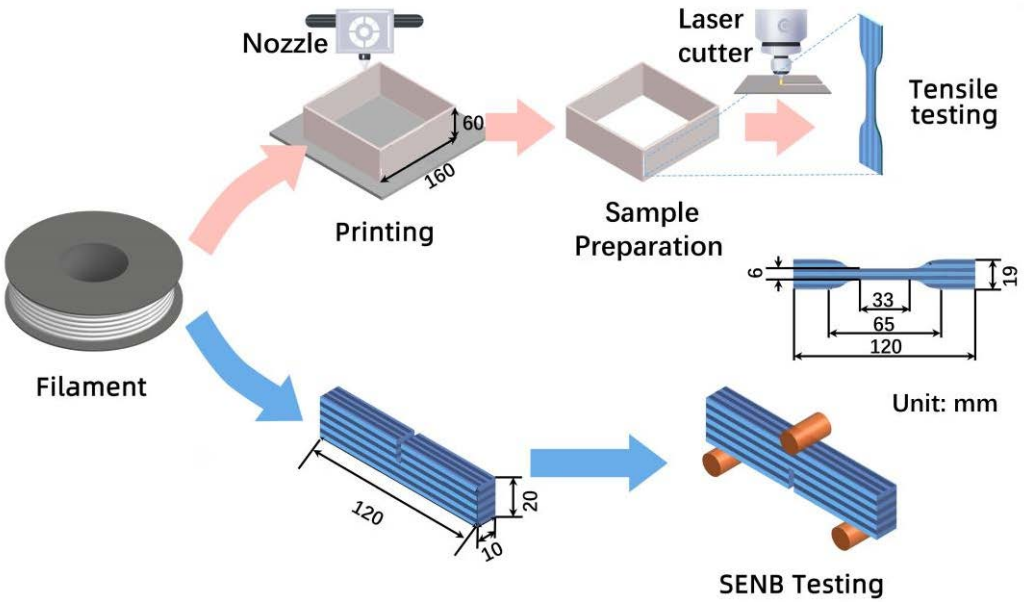

Figure 3.1. The sample preparation processes.

3.2.2. Mechanical testing and post analysis

Tensile and SENB tests were performed on samples of PLA and wood-PLA samples using a universal testing machine (AGX-50kN, Shimadzu, Japan). The tensile tests were conducted at a constant loading speed of 2 mm/min, while the SENB test was performed at 4 mm/min. The SENB test was considered complete when the applied load dropped to 10 N. During the tests, DIC (Digital Image Correlation) system was also employed to capture images and calculate strain data. Additionally, DIC images were used to generate local strain contours, providing a more detailed analysis. To ensure accurate recognition by DIC software, a sufficient amount of speckle was required on the surface of samples. Therefore, all samples were painted to create identifiable speckle patterns.

Stress-strain curves were obtained from tensile tests, and key mechanical parameters, including ultimate tensile strength, Young's modulus, elongation at break, and strain energy density, were evaluated. The Young's modulus was determined from the slope of the linear region of the stress–strain curve (strain range 0.5–1%), which represents the elastic response while minimising initial loading errors and avoiding

nonlinearity near the yield point. The strain energy density (Ψ, J/m³) is defined as the amount of energy absorbed per unit volume during the tensile test and is calculated using:

$$\Psi = \int_0^{\varepsilon_{max}} \sigma d\varepsilon \,, \tag{3. 1}$$

where σ is the stress, ε is the strain, and ε_{max} is the elongation at break.

In the SENB tests, energy absorption and peak force were analysed, with energy absorption determined by the area under the force-displacement curve. The local strain was calculated using DIC images to investigate the crack initiation and propagation.

3.3. Results and discussion

3.3.1. Mechanical properties of PLA and wood-PLA without water immersion

This section presents the mechanical behaviours of PLA and wood-PLA in the control group, including tensile and SENB testing results, as well as the corresponding fracture characteristics. Additionally, the printing quality of these two materials was compared to demonstrate the influence of wood fibre addition.

3.3.1.1. Print quality

Figure 3.2 (a) shows a SENB specimen with the red frame marking the region for surface observation. The PLA surface exhibited a relatively smooth and uniform layer-by-layer pattern (Figure 3.2 (b)). In contrast, the wood-PLA sample (Figure 3.2 (c)) displayed a rough and uneven surface with noticeable stringing defects, characterised by small filaments left on the surface. The incorporation of solid wood fibre particles introduces disturbances to the melt flow field, primarily due to the disparity in flowability between the molten PLA and the non-melting fibres [161]. These disturbances, combined with the rigidity and pronounced polarity of the wood particles,

further disrupt the continuity of the polymer melt phase, thereby promoting surface roughness [162]. Moreover, the potential non-uniform distribution of wood fibres can lead to spatial viscosity variations, giving rise to transient flow instabilities, pulsed extrusion behaviour [163] and stringing defects [162]. Figure 3.2 (d) shows the images of the surface characterization of wood-PLA captured using the optical microscope. The distribution of the wood fibres and several of their characteristics (highlighted with red dashed lines) are clearly visible, and the stringing defect is also indicated in the image.

The deviations in mass and thickness are summarised in Table 3.2. The nominal mass of the samples was determined by multiplying the STL-designed volume of samples by the filament density, while the nominal thickness corresponded to the STL-designed thickness. Both PLA and wood-PLA samples exhibited higher actual masses and thickness than their nominal values, indicating potential over-extrusion during printing. The deviations in the thicknesses for both materials are comparable, which is around 0.30 mm (3%), indicating good dimensional accuracy.

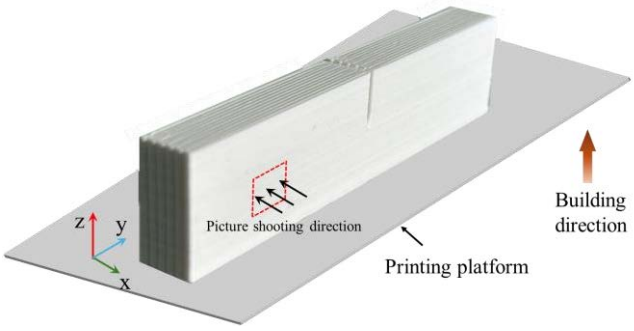

(a)

(b)

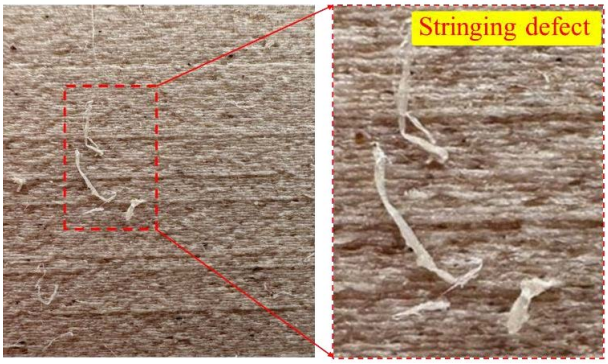

(c)

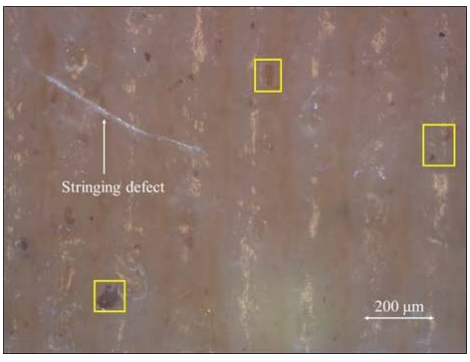

(d)

Figure 3.2. (a) Schematic of the SENB specimen with the red frame indicating the observed region, (b) the surface of PLA and (c) wood-PLA SENB specimen, and (d) surface morphology of wood-PLA SENB specimen under an optical microscope.

Table 3.2. Deviation in mass and dimension between the printed and designed sample

Sample	Mass (g)			Thickness (mm)		
	Nominal	Actual	Deviation (%)	Nominal	Actual	Deviation (%)
PLA	22.04	22.74 (0.29)	3.2	10	10.32 (0.11)	3.2
Wood-PLA	20.08	21.37 (0.18)	6.4	10	10.24 (0.08)	2.4

Note: Data were derived from 30 SENB samples, with standard deviation shown in parentheses.

3.3.1.2. Tensile properties of PLA and wood-PLA

Compared to pure PLA material, wood-PLA exhibited reduced ultimate tensile strength and Young's modulus. As presented in Table 3.3, PLA had an ultimate tensile strength of 54.6 MPa, whereas wood-PLA demonstrated a significantly lower value of 23.4 MPa, corresponding to a 57% reduction. The Young's modulus of wood-PLA was 1495 MPa, approximately 52.7% of that of PLA (3050 MPa). However, wood-PLA showed a higher elongation at break than PLA, reaching 4.7%, compared with 2.7% for PLA.

The stress-strain curves in Figure 3.3 (A) show that wood-PLA exhibited a plastic deformation stage (from point II to III) after reaching its ultimate tensile strength, whereas PLA underwent brittle failure with no significant post-yield deformation. The strain distribution in Figure 3.3 (B) reveals that PLA fractured immediately upon the formation of localised strain concentration in the gauge area. In contrast, wood-PLA displayed a more uniform deformation at the same strain value (point II) and a broad

plastic deformation range before breakage (point III), as shown in Figure 3.3 (C). Due to the plastic deformation in wood-PLA, the strain energy density (see Eq. (3. 1) of wood-PLA reached 8.91×10^{-7} J/m^3, which is 1.41 times greater than that of the PLA sample. These findings are consistent with other studies on wood fibre-PLA and biofibre-reinforced PLA composites. Lage-Rivera et al. observed that increasing fibre content led to a progressive decrease in tensile strength [164], while the elongation at break increased, reaching its maximum at a fibre content of 15%. Siddiqui et al., [165] and Mazur et al., [166] reported the reduction of Young's modulus of wood-PLA. Similarly, Yu et al. confirmed these observations in their work [167].

The higher strain energy density observed in wood–PLA composites may be attributed to several synergistic mechanisms. Interfacial debonding between the wood fibres and the PLA matrix, followed by fibre pull-out, serves as an effective energy dissipation process. In addition, the introduction of wood particles results in a heterogeneous internal structure that disrupts crack propagation paths, increases the effective crack path length, and reduces local stress concentrations. These combined effects delay the onset of catastrophic failure, enabling the material to accommodate greater deformation prior to fracture.

The reduction in the ultimate tensile strength and Young's modulus results from the introduction of the wood fibre. According to Tao's research [66], wood fibre has a polar (hydrophilic) surface, whereas PLA has a non-polar (hydrophobic)surface. The disparity between the polar and non-polar surfaces prevents the formation of a strong interfacial bond [168]. During the tensile test, the pull-out effects are often observed in on the wood-PLA samples in previous studies [64]. Besides, many researchers have found that short fibre reinforcement can reduce the tensile strength of polymer, as these fibres cannot effectively bear tensile loads the way continuous molecular chains do [19, 20].

In addition to the interfacial challenges caused by the wood fibres, thermomechanical degradation of the PLA matrix during melt processing can also play a significant role in reducing the mechanical performance of wood-PLA composites [169].

During compounding and extrusion, repeated heating and shearing may induce chain scissions in the PLA, leading to decreased molecular weight, which in turn compromises the thermal stability and mechanical integrity of the material [170]. These degradative changes are often accompanied by an increase in crystallinity, as shorter polymer chains reorganize more easily [171].

Table 3.3. The tensile results of PLA and wood-PLA

Parameters	PLA	wood-PLA
Ultimate tensile strength (MPa)	54.6 (2.44)	23.4 (1.0)
Elongation at break (%)	2.0 (0.2)	4.7 (1.0)
Young's modulus (MPa)	3074 (170)	1568 (102)
Strain energy density (10^{-7} ×J/m^3)	6.39 (0.9)	8.91 (1.8)

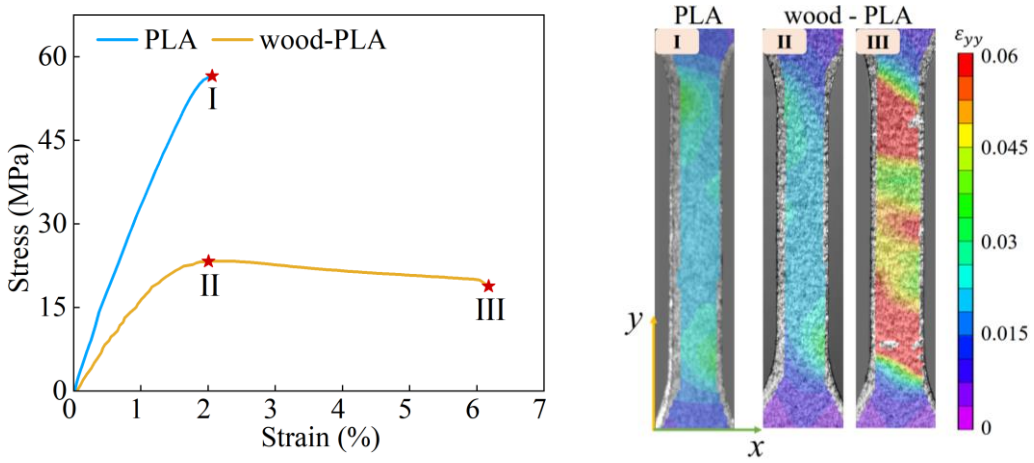

(a) (b)

Figure 3.3. The tensile results of PLA and wood-PLA samples in the control group: (a) stress-strain curves, (b) ε_{yy} strain contour of the PLA and wood-PLA samples at critical displacement (Marked on red stars in (a)).

3.3.2. SENB test of PLA and wood-PLA

3.3.2.1. Fracture pattern

Figure 3.4 exhibits the crack initiation and propagation of PLA and wood-PLA samples during SENB tests. The contour diagrams illustrate the evolution of the ε_{xx}

strain during the loading processes. For the PLA sample, crack initiation occurred at the notch tip, followed by an increasingly pronounced crack propagation as the applied displacement increased. The observed strain distribution indicates that stress was concentrated around the notch tip, resulting in brittle fracture characteristics with a straight, upward crack propagation. Notably, samples with a 4 mm notch length exhibited more pronounced cracking under the same applied displacement due to the larger maximum stress at the crack tip. The maximum flexural stress in SENB samples is approximately calculated in Appendix using a simplified three-point bending model. It shows that the maximum flexural stress decreases as the notch length increases in the notch length under the same deflection.

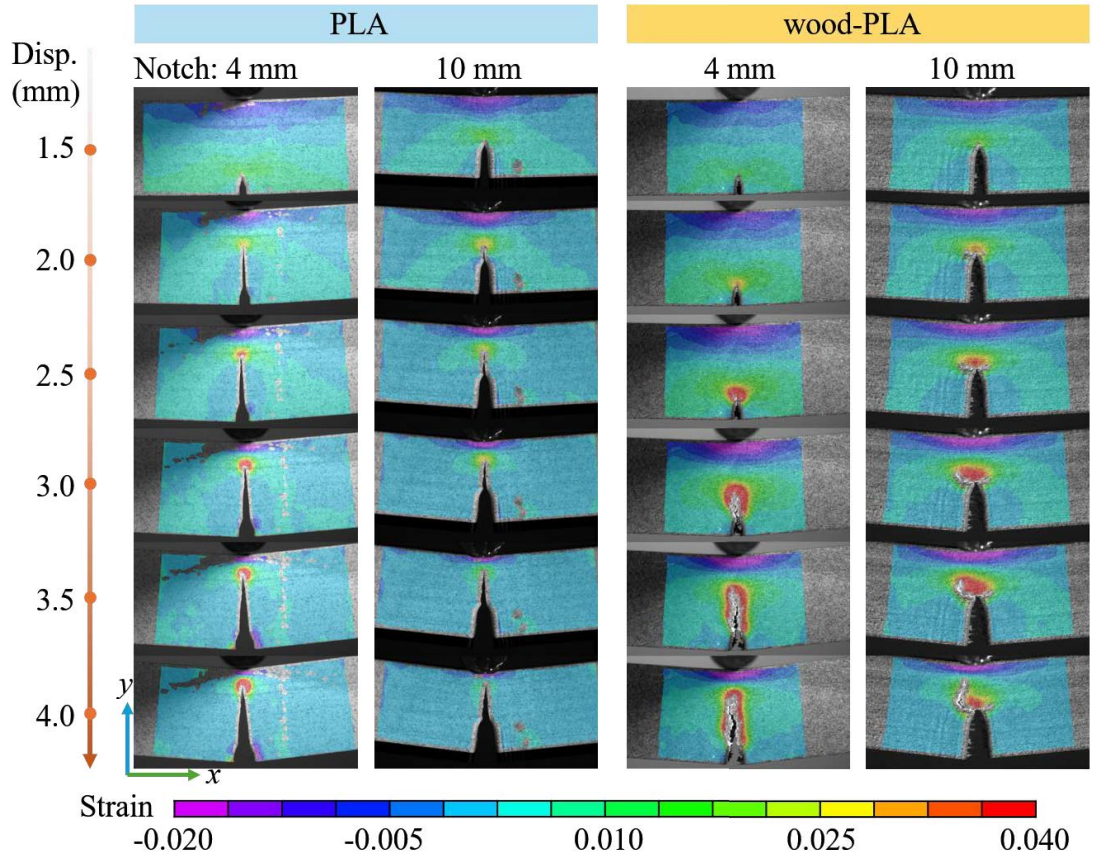

Figure 3.4. The ε_{xx} contour diagram of PLA and wood-PLA SENB samples with 4 mm and 10 mm notch length during the loading process.

Due to the introduction of wood fibres, wood-PLA samples exhibited a different

crack evolution pattern, which was impacted by the notch length. The presence of wood fibres led to more distributed plastic strain accumulation around the crack tip as highlighted in the red areas (Figure 3.4), which was consistent with the observation in Section 3.3.1.2 that wood-PLA exhibited more plastic deformation before break. The sample with a 4 mm notch exhibited slight zigzag crack pattern with the propagation primarily in the vertical direction. In contrast, the 10 mm notched wood-PLA sample showed horizontal crack propagation before the applied displacement reached 3 mm. This behaviour was attributed to the lower maximum flexural stress at the notch tip compared to the 4 mm notched sample, which inhibited the initial upward crack propagation. Instead, the strain mismatch between the elongated region above the notch tip and the undeformed material below led to interlayer shear debonding, causing the crack to propagate horizontally at first. After the applied displacement exceeded 3 mm, the crack changed its direction and developed vertically upwards due to the tensile stress.

3.3.2.2. Force-displacement curve

Figure 3.5 (a) presents force-displacement curves obtained from SENB samples with notch length of 4 mm and 10 mm. PLA samples exhibited a higher initial peak force, followed by a sharp drop in load, characteristic of brittle fracture. In contrast, wood-PLA samples displayed a lower peak force but a more gradual force decline, corresponding to the ductile fracture mode in Figure 3.4.

For the 4 mm notched samples (Figure 3.5 (b)), wood-PLA exhibited a larger displacement at crack onset compared to PLA, measuring 2.3 mm. For the 10 mm notched samples, the wood-PLA sample initially developed a horizontal crack at a displacement of 2.1 mm, followed by vertical crack propagation beginning at 3.2 mm. During the debonding phase from 2.1 mm to 3.2 mm, no significant force reduction was

observed in wood-PLA.

Figure 3.5 (c) shows that wood-PLA samples exhibited higher energy absorption compared to PLA. The energy absorption of wood-PLA was 2.90 J for the 4 mm notched samples and 2.13 J for the 10 mm notched samples, while the corresponding values for PLA counterparts were 2.05 J and 1.53 J, respectively.

In Figure 3.5 (d), PLA exhibited significantly higher peak force of 1.53 kN with the 4 mm notch, which decreased to 1.23 kN with the 10 mm notch. In contrast, the peak force for wood-PLA samples was only 0.75 kN and 0.59 kN for the 4 mm and 10 mm notched samples, respectively, confirming the lower strength of wood-PLA.

Hence, despite its lower strength, wood-PLA exhibited superior energy absorption capability and ductile fracture characteristics, preventing sudden failure under loading.

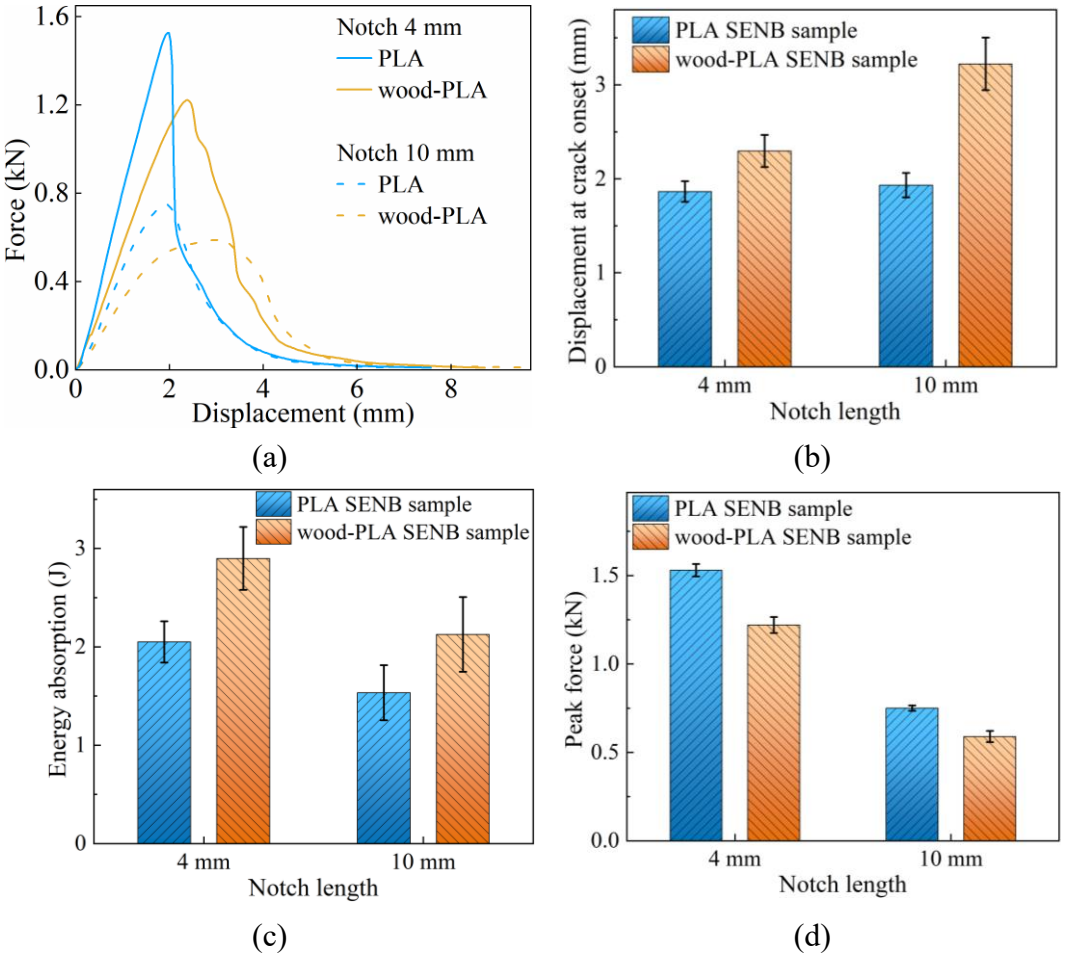

Figure 3.5. Results of SENB samples in control group: (a) force-displacement curves, (b) displace at crack onset, (c) energy absorption and (d) peak force. The displacement at crack onset of wood-PLA with a 10 mm notch corresponds to the

vertical crack onset.

3.3.2.3. Discussion on the SENB test

The distinct fracture pattern observed in wood-PLA samples during SENB testing can be attributed to the introduction of wood fibres. The zigzag fracture pattern of the wood-PLA is primarily associated with crack bridging [161], where individual wood fibres interact with the advancing crack front, delaying its growth in the process [159, 172]. As the crack attempts to propagate, some fibres act as bridges across the crack surfaces, temporarily holding the material together and resisting separation [173]. This phenomenon increases resistance to fracture initiation and promotes a more gradual failure process.

Consequently, the zigzag fracture pattern and complex crack path of the wood-PLA extended the duration of the fracture process and spread [112, 160]. As a result, the energy required to complete the fracture, represented by the area under the force-displacement curve, significantly increased [159]. Based on the finding of superior energy absorption, wood-PLA composites may be well suited for applications requiring impact resistance or energy dissipation [14], such as protective packaging [23], where gradual failure and higher toughness are advantageous.

3.4. Summary

This study investigated the mechanical performance of two commercially available FDM filaments: pure PLA and a wood-PLA (40% wood fibre content) composite. Tensile and SENB tests were performed to evaluate differences in strength, stiffness, and energy absorption under consistent fabrication and testing conditions. The objective was to assess how the incorporation of natural wood fibres influences the mechanical behaviour of PLA-based materials in their original state.

The results revealed that the addition of wood fibres led to a noticeable reduction in

tensile strength and elastic modulus compared to pure PLA. However, wood-PLA demonstrated a significant improvement in energy absorption capacity across both testing methods. SENB results showed that wood-PLA underwent a more gradual and extended fracture process, attributed to crack-bridging mechanisms introduced by the wood fibres. These mechanisms contributed to a zigzag crack path and increased deformation, enhancing the material's overall toughness.

The findings highlight the role of natural fibres in altering failure behaviour and improving fracture energy in 3D-printed composites. The comparison provides a clear baseline for understanding performance trade-offs between stiffness and toughness. This insight is essential for guiding the application of bio-based FDM materials in structural components where controlled deformation and energy dissipation are desirable. However, considering the variability of environmental conditions in practical applications, it becomes crucial to investigate the influence of moisture exposure on mechanical properties. This vital point will be systematically addressed in Chapter 4.

Chapter 4. Mechanical characterisation of FDM-printed wood-PLA composites under water conditioning

4.1. Introduction

FDM is one of the most widely used additive manufacturing technologies due to its low cost, geometric flexibility, and material efficiency [142-144]. Its compatibility with fibre-reinforced thermoplastics has led to increasing interest in the use of bio-based fillers to improve environmental sustainability [15]. Among various reinforcement options, natural fibres have gained significant attention for their biodegradability and renewable sourcing [22, 150]. In particular, wood fibres have become a popular choice for combining with PLA, resulting in commercially available filaments that offer a balance between processability and environmental performance [28]. These wood-PLA composites have been adopted in a range of applications, including aesthetic components, design prototypes, and low-load structural elements [4, 24, 145]. As their use becomes more widespread, especially in contexts where environmental exposure is likely, it is essential to investigate how such materials respond to changing conditions to ensure their mechanical reliability and long-term functionality.

However, a critical challenge in utilizing wood-PLA composites is their inevitable moisture absorption in real-world environments [174]. The highly hydrophilic nature of wood fibres makes wood-PLA composites significantly more susceptible to swelling or softening [67, 175]. These moisture-induced changes pose serious concerns for applications requiring environmental durability, such as outdoor decorative elements, biodegradable packaging, and functional prototypes [20, 176, 177], which are often exposed to humid environments, temperature fluctuations, or direct water contact during their service life [178].

Numerous studies have investigated the effects of water absorption on wood-PLA composites. Ainin et al. found that wood-PLA shows significant strength loss due to the

swelling and structural distortion upon immersion [179], while Ecker et al. reported more severe degradation in FDM-printed samples compared to injection-moulded ones [78]. Oliver-Ortega et al. showed that PLA composites reinforced with bleached softwood fibres still exhibited moisture sensitivity due to the hydrophilic nature of the fibres [180]. Ayrilmis and his colleagues revealed that increasing wood content and layer thickness leads to higher porosity, thus reducing strength and increasing water uptake [181, 182]. Several reviews have explained these effects through fibre swelling, diffusion, and interfacial debonding [183]. Martínez-Sánchez et al. highlighted the role of printing parameters in controlling moisture adsorption [162], and Zandvliet et al. noted that even for interior applications [184], PLA-based composites face dimensional instability from water exposure. Surface property studies also show compromised wettability and bonding performance as wood content increases. Numerous studies have investigated the effects of water absorption on wood-PLA composites. Ainin et al. found that wood-PLA shows significant strength loss due to the swelling and structural distortion upon immersion [179], while Ecker et al. reported more severe degradation in FDM-printed samples compared to injection-moulded ones [78]. Oliver-Ortega et al. showed that PLA composites reinforced with bleached softwood fibres still exhibited moisture sensitivity due to the hydrophilic nature of the fibres [180]. Ayrilmis and his colleagues revealed that increasing wood content and layer thickness leads to higher porosity, thus reducing strength and increasing water uptake [181, 182]. Several reviews have explained these effects through fibre swelling, diffusion, and interfacial debonding [183]. Martínez-Sánchez et al. highlighted the role of printing parameters in controlling moisture adsorption [162], and Zandvliet et al. noted that even for interior applications [184], PLA-based composites face dimensional instability from water exposure. Surface property studies also show compromised wettability and bonding performance as wood content increases.

Despite these findings, few studies have addressed the recovery of mechanical performance after re-drying, or directly compared PLA and wood-PLA under the same

aging and drying conditions. Mechanical evaluations are often limited to tensile or bending tests, lacking fracture-based insights.

Compared to the study presented in Chapter 3, this chapter investigates the mechanical performance of wood-PLA composites fabricated via FDM, with particular focus on their behaviour after water absorption and subsequent redrying. Comprehensive mechanical testing was conducted to assess the material's response to moisture exposure and its potential for property recovery upon redrying. Section 4.2 outlines the materials and methods employed. Section 4.3 presents and discusses the results, focusing on the mechanical effects of water absorption and redrying. Section 4.4 summarises the key findings of this study.

4.2. Methods and materials

This study focuses on evaluating and comparing the mechanical performance of wood-PLA and pure PLA after water immersion. The materials used, a commercially available wood-PLA filament containing 40% wood fibre by volume and PLA EF 3D850, are the same as those utilised in Chapter 3. Further details regarding these materials are provided in Section 3.2.

Mechanical characterisation in this chapter is conducted through tensile testing and SENB tests. The specimen dimensions and fabrication processes used for both test types are identical to those outlined in Chapter 3.

Additionally, the testing procedures and post-analysis methods applied in this chapter closely follow those previously established (Section 3.2), ensuring consistency and comparability across experimental conditions.

In this study, the effects of water absorption on the tensile and bending properties of PLA and wood-PLA materials were investigated. The experimental workflow is depicted in Figure 4.1. Based on the water treatment procedures, the samples were categorised into three groups: (1) the control group, consisting of samples that were not

subjected to water immersion; (2) the wet group, comprising samples immersed in water for varying durations; and (3) the redried group, which included samples subjected to water immersion followed by a controlled drying process.

The water absorption tests were performed in accordance with ASTM D570-22 [185], with soaking water maintained at a constant room temperature of 25 °C. The immersion duration was set at 3, 7, 10 and 15 days, with weight gain recorded after each period. Surface water was wiped dry with a paper towel before weighing. The water absorption rate M_t (%) was determined by:

$$M_t = \frac{W_w - W_d}{W_d} \times 100 \quad (4.1)$$

where W_d and W_w are the weights of dry (before immersion) and wet (after immersion) samples.

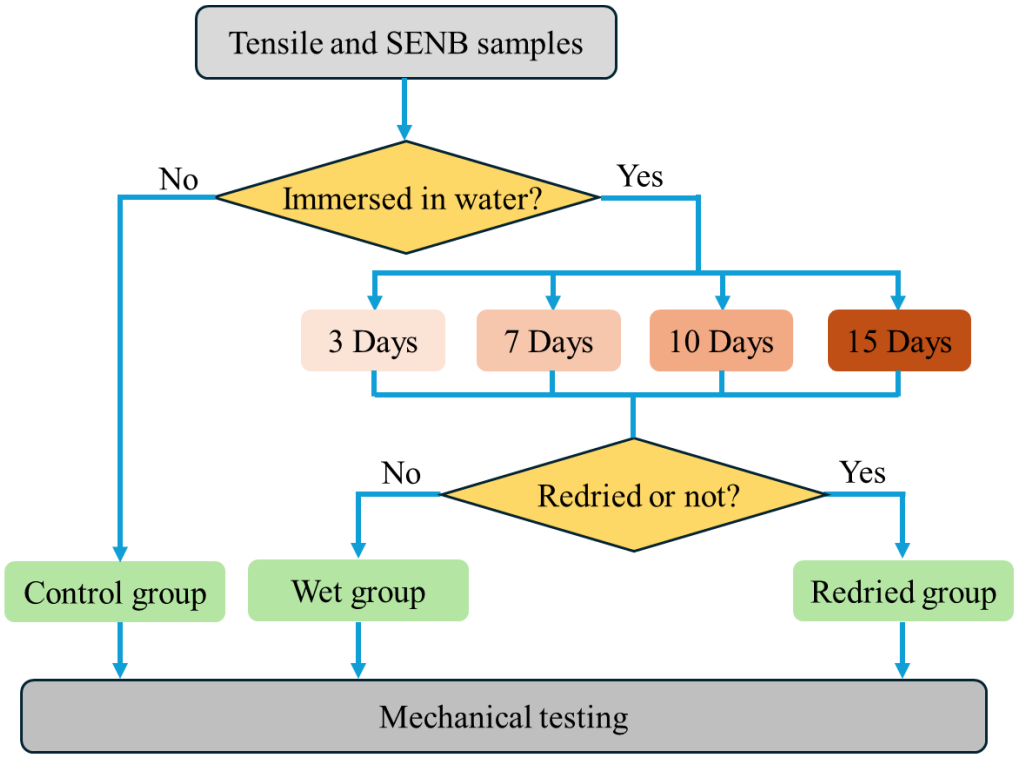

Figure 4.1. Experimental workflow

The drying process for the redried group was conducted using a vacuum desiccator containing silica gel at the bottom to facilitate moisture absorption. The desiccator was maintained under vacuum at a constant room temperature of 25 °C to ensure efficient

moisture removal. Each sample was dried for at least three days, after which it was weighed to verify whether its weight had returned to the initial value prior to water exposure.

To investigate the interactions between chemical bonds and the forces between polymer chains within the material, Fourier-Transform Infrared spectroscopy (FTIR) technology was employed to examine the distribution characteristics of specific functional groups, particularly hydroxyl groups [186]. FTIR spectra were recorded using a Thermo Scientific Nicolet 6700 FTIR spectrometer (Thermo Fisher Scientific, Waltham, Massachusetts, USA) equipped with an Attenuated Total Reflectance (ATR) accessory. The spectra were collected in the wavenumber range of 4000–400 cm^{-1} with a resolution of 4 cm^{-1}. A total of 32 scans were performed for each sample, and background spectra were recorded before each measurement. The samples, which were 1.6 mm thick with dimensions of 1 × 1 cm, were prepared using FDM printing. Both PLA and wood-PLA samples were scanned after complete drying treatment or after immersion in water for 15 days. The samples were directly placed on the ATR crystal for measurement. The spectra were analysed using OMNIC software (OMNIC 9.0, Thermo Fisher Scientific, Waltham, Massachusetts, USA).

Thermal analysis was conducted using a simultaneous thermal analyser (STA 449 F1 Jupiter, Netzsch, Germany) to characterize both thermal stability and thermal transitions of the materials. Material samples were extracted from tensile specimens in the virgin group and from those in the wet group after 15 days of immersion. The material samples of approximately 6.0 to 9.0 mg were placed in aluminium crucibles with pierced lids. In an inert nitrogen atmosphere, these crucibles were heated to 600 ℃ at a rate of 10 ℃ /min. The measurements provided the glass transition temperature (Tg) from the DSC signal, as well as thermogravimetric (TG) curves and derivative thermogravimetry (DTG) reflecting the mass loss as a function of temperature.

4.3. Results and discussion

4.3.1. Water absorption ability

The wood-PLA tensile samples exhibit a significantly higher water absorption rate compared to the pure PLA samples. Figure 4.2 (A) exhibits that after soaking for 3 days, the water absorption rate of wood-PLA reached 5.24%, which was 12.8 times higher than that of PLA (0.41%). Thereafter, the water absorption rate of wood-PLA continued to increase significantly with immersion time, whereas the increase in PLA remained negligible. Notably, after 15 days of immersion, the water absorption rate of the wood-PLA samples rose to 9.81%, which was 21.7 times higher than that of the PLA samples (0.45%). The high water absorption in wood-PLA arises from the hydrophilic nature of wood fibres, where the cellulose composition promotes interactions with water molecules [164]. The ATR-FTIR results [187, 188] in Figure 4.2 (C) shows that the wood-PLA exhibited a pronounced increase in the peak intensity within the wavenumber range of 3000–4000 cm^{-1} (with transmittance reaching approximately 80%) after water immersion, whereas PLA showed no significant change. The pronounced peak in this region indicates an increased presence of hydroxyl groups, which reflects the enhanced formation of hydrogen bonds and the uptake of water molecules within the wood-PLA composites [186].

In SENB samples (Figure 4.2 (b)), PLA maintained consistently low values (around 0.44%) with minimal change over time, aligning with the results observed in the tensile samples. However, the values of wood-PLA were significantly lower than those of their tensile counterparts, despite exhibiting a similar increasing trend over time, with a maximum value of 1.72% at 15 days. The reduction observed in SENB samples was caused by their increased thickness, as well as differences in shape and surface area, which reduced their overall contact efficiency with water. Additionally, the greater thickness likely hindered water penetration into the inner layers, resulting in a lower

absorption rate over the same immersion duration.

Pure PLA exhibits relatively poor hydrophilicity, particularly on the smooth surfaces of PLA materials produced by traditional manufacturing methods [67, 78]. Although using FDM can effectively enhance hydrophilicity by creating surface porosities and uneven, wavy textures that increase contact with water [189], the water absorption of FDM printed PLA remains limited.

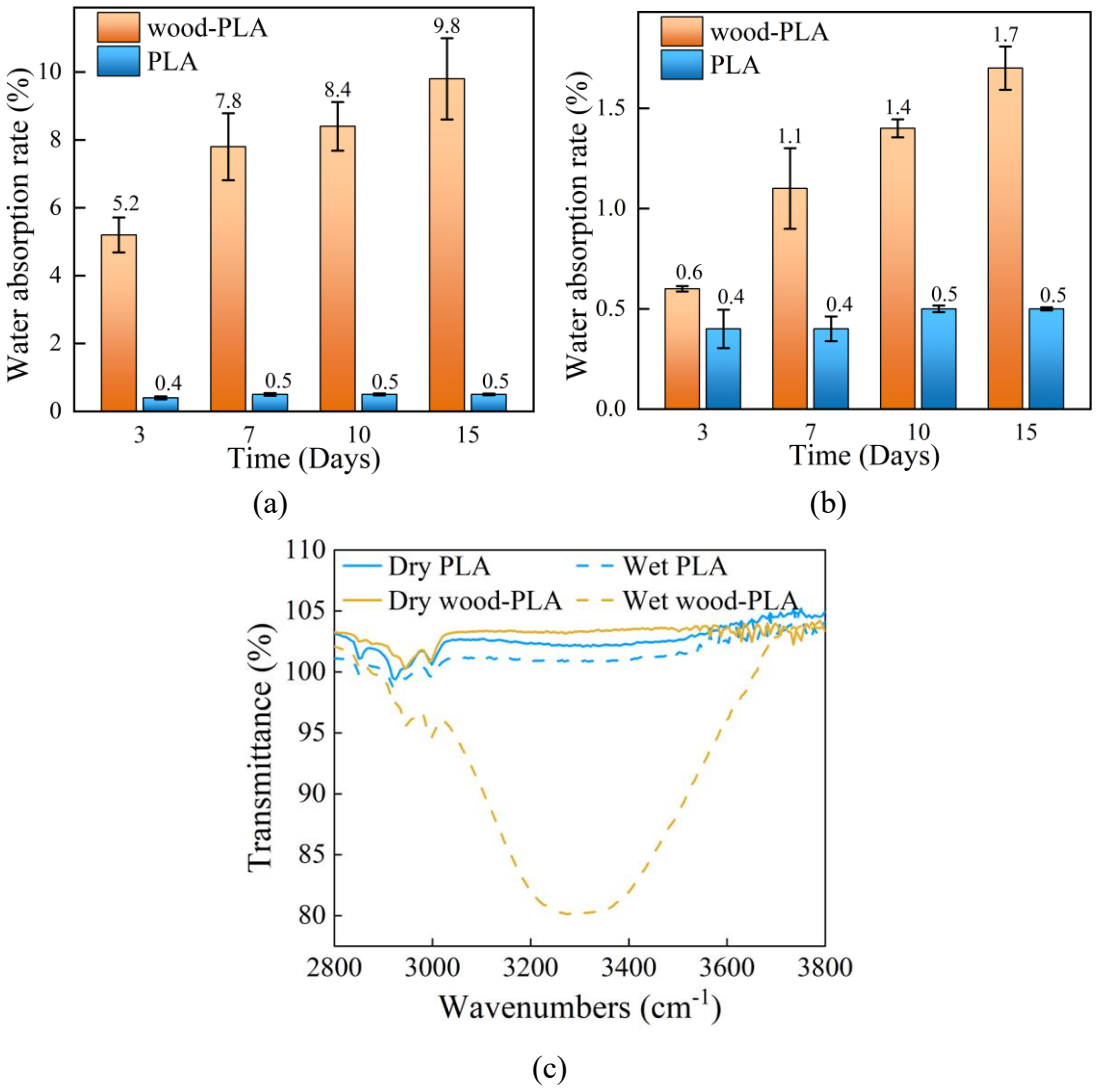

Figure 4.2. (a) The water absorption rates of wood-PLA and PLA tensile samples, (b) SENB samples, and (c) ATR-FTIR spectra of PLA and wood-PLA samples after drying and after 7 days of water immersion.

4.3.2. Effect of water absorption on thermal properties

Figure 4.3 (a) presents the DSC thermograms of PLA and wood-PLA in both dry and wet states. The glass transition temperature (Tg) of dry PLA was measured at 58.8 °C, indicating that water absorption had only a marginal effect on the polymer chain mobility of neat PLA. In contrast, dry wood-PLA exhibited a lower Tg of 57.2 °C, which further decreased to 55.5 °C after moisture absorption. This more pronounced reduction highlights the effect of water absorption on wood particles in wood-PLA, which enhances segmental motion and lowers the glass transition temperature.

The TG results shown in Figure 4.3 (b) reveal that the major weight loss for all samples occurred between 300 and 400 °C, corresponding to the thermal decomposition of the PLA matrix. The wet wood-PLA displayed a slight shift of the TG and DTG curves toward lower temperatures, suggesting the evaporation of absorbed moisture retained by the hydrophilic wood fibres. In contrast, wet PLA showed negligible weight loss in this region due to its much lower water uptake. Importantly, the decomposition profiles of wet and dry samples after 15 days of immersion at room temperature exhibited no notable differences, indicating that no measurable degradation had taken place during this period.

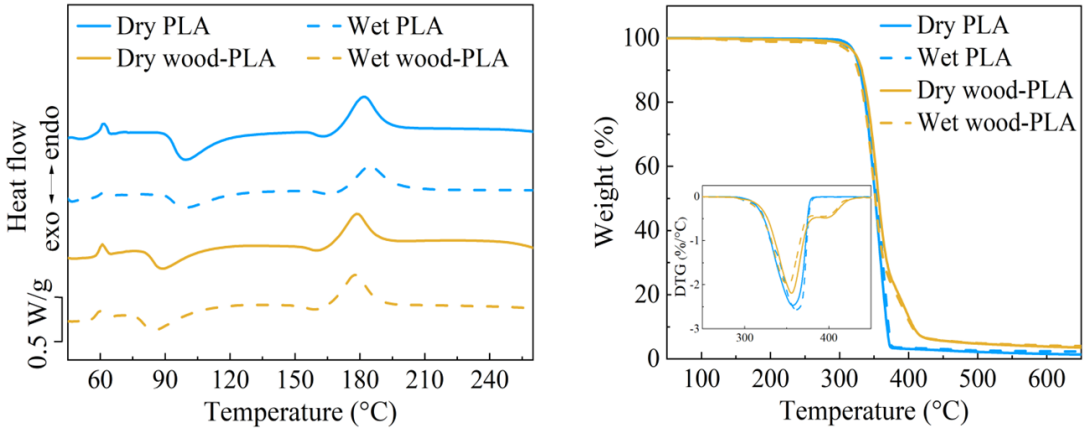

Figure 4.3. Thermal analysis curves from (a) DSC tests and (b) TGA tests.

4.3.3. Tensile properties with water immersion

4.3.3.1. Stress-strain curves

Figure 4.4 presents the tensile stress-strain curves of PLA and wood-PLA after different immersion durations. Additionally, it compares the curves of samples that were re-dried after each immersion stage, providing insights into the effects of water exposure on the mechanical properties of the materials. It can be observed that prolonged immersion led to a decline in tensile strength and stiffness for both materials in the wet group. Wood-PLA exhibited a more pronounced reduction in tensile strength due to its higher hydrophilicity. In the wet group, the elongation at break of wood-PLA increased significantly after 7 days of water exposure. The redried samples showed notable recovery in their tensile stress-strain behaviour, indicating that the observed degradation was primarily physical and reversible, rather than a result of permanent chemical breakdown. Both wet and redried groups exhibited the same deformation and fracture patterns shown in Figure 4.4 (b).

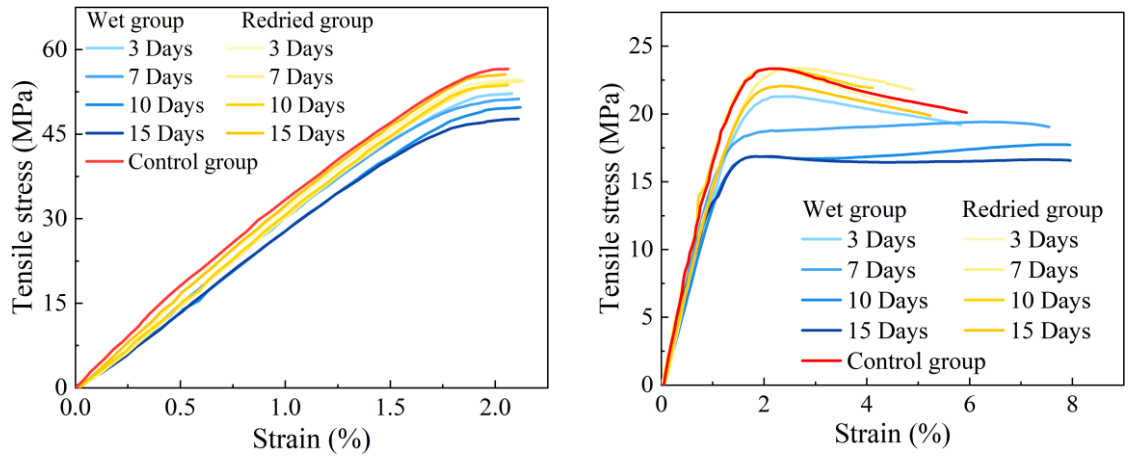

(a) (b)

Figure 4.4. The stress-strain curves of (a) PLA and (b) wood-PLA with different conditions.

4.3.3.2. Mechanical properties

The ultimate tensile strength, elastic modulus, elongation at break and strain energy density were extracted from tensile stress-strain curves and presented in Figure 4.5. The mechanical metrics of control group samples were plotted as dashed lines for comparison. As shown in Figure 4.5 (a), the ultimate tensile strength notably decreased as the water immersion duration increased from 3 to 15 days. The ultimate tensile strength of PLA samples dropped from 54.6 MPa in the control group to 47.8 MPa after 12 days of immersion, demonstrating a 12% reduction. The ultimate tensile strength of wood-PLA samples decreased from 23.4 MPa in the control group to 21.1 MPa after 3 days, further dropping to 18.5 MPa after 15 days, representing a 20% reduction. For both PLA and wood-PLA samples, the most significant decrease in ultimate tensile strength occurred within the first seven days, after which the decline gradually stabilised. By applying the Jonckheere–Terpstra test [190] to the ultimate tensile strength of wood-PLA and PLA after water immersion, both datasets were shown to exhibit a clear monotonic decreasing trend. The one-sided p-values were 0.998 and 0.982, respectively for wood-PLA and PLA, both exceeding the significance threshold of 0.95. After redrying, the tensile strength of both samples returned almost to the control level.

Figure 4.5 (b) shows that in the wet group, Young's modulus of wood-PLA decreased with prolonged immersion, dropping from 1468 MPa in the control group to 1333 MPa after 15 days, corresponding to a 10% reduction. After redrying, the Young's modulus of the samples from each immersion stage returned to its original value. PLA samples exhibited a decrease from 3074 MPa to 2846 MPa after 15 days of water exposure, representing an 8% decrease. The Young's modulus of PLA samples immersed for 3 days fully recovered to its initial value after redrying. However, for other immersion durations, the redried samples exhibited a lower modulus than the initial value. After 15 days of immersion, the Young's modulus of the redried samples was 2863 MPa.

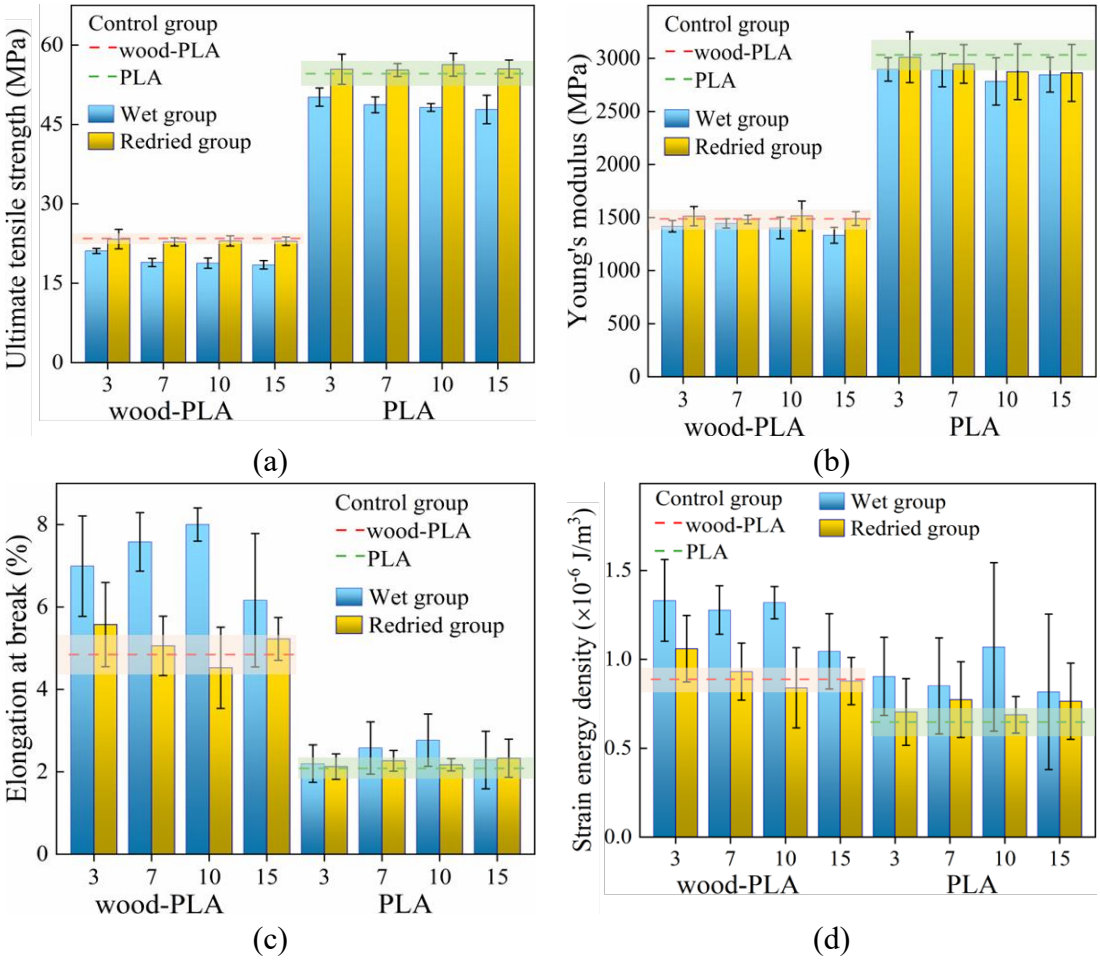

Figure 4.5. Tensile results of wet and redried groups: (a) ultimate tensile strength, (b) Young's modulus, (c) elongation at break, and (d) strain energy density.

Water absorption had a significant influence on elongation at break. As shown in Figure 4.5 (c), with increasing immersion time, both PLA and wood-PLA samples exhibited a notable increase in elongation at break, reaching a peak value at 10 days, followed by a decline by 15 days. Wood-PLA sample had an initial elongation at break of 4.8% in the control group, reaching a peak of 8.0% after 10 days, representing a 66% increase. For PLA, the value started at 2.1% and peaked at 2.8% after 10 days. After redrying, elongation at break of wood-PLA samples decreased compared to the wet group but remained higher than control group, possibly due to residual moisture trapped within the wood fibres. The p-values were 0.026 and 0.037, respectively for wood-PLA and PLA, both below the significance threshold of 0.05. After redrying, elongation at break of wood-PLA samples decreased compared to the wet group but remained higher

than control group, possibly due to residual moisture trapped within the wood fibres. However, the elongation of PLA returned close to the control level after redrying, suggesting a fully reversible effect in PLA.

Primarily due to the increase of elongation at break, both wood-PLA and PLA samples exhibited an increased energy absorption after water immersion as shown in Figure 4.5 (d). Initially, the strain energy density of wood-PLA and PLA was 8.91×10^{-7} J/m³ and 6.39×10^{-7} J/m³, respectively. After 10 days of immersion, the strain energy density of the wood-PLA and PLA samples peaked at 1.32×10^{-6} J/m³ and 8.46×10^{-7} J/m³, and with the maximum increase rate 48% and 32% respectively. Then, the values for both materials decreased to 9.78×10^{-7} J/m³ for wood-PLA and 6.87×10^{-7} J/m³ for PLA, though both remained higher than their initial values. Hence, both wood-PLA and PLA demonstrated a noticeable increase in their energy absorption capacities within a short period (up to 15 days) of water absorption. After redrying, both samples showed a decline in strain energy density, with their values closely aligning with that of control group, indicating that the energy absorption capacity was reversible during the water soaking and redrying treatment processes.

Similar observations have been reported in previous studies on wood-PLA and other biofibre-reinforced PLA composites after water immersion. For instance, Ecker et al. [78] found that immersion in water led to a noticeable reduction in tensile strength particularly in composites containing higher hydrophilic fibre content. Ayrilmis et al. [181] similarly reported that water uptake caused pronounced reduction in tensile strength in wood-PLA. Ali et al. [191] emphasized the significant increase in elongation at break and toughness of flax/PLA composites.

The observed changes in mechanical properties can be attributed to water-induced plasticisation [192]. Water functions as an external plasticiser by reducing intermolecular interactions and enhancing chain mobility [193]. Although both PLA and wood-PLA underwent this process, the effect was more pronounced in wood-PLA owing to its hydroxyl-rich constituents (i.e., cellulose and hemicellulose) and higher

porosity, which facilitated water uptake and hydrogen bond formation, as discussed in Section 4.3.1. FTIR analysis corroborated this mechanism, showing intensified absorption in 3000 – 4000 cm^{-1} regions after immersion, indicative of increased hydroxyl groups and hydrogen bonding.

4.3.4. SENB test results with water immersion

Figure 4.6 (a) and (c) show the force-displacement curves for wood-PLA with 4 mm and 10 mm notches, respectively. Unlike the tensile results, water absorption has a negligible impact on the peak force of SENB samples. Compared to the curves of the redried samples, the wet samples consistently exhibited a slower force decline stage with higher force levels after the peak force. In contrast, Figure 4.6 (e) presented that for PLA with a 4 mm notch, regardless of the immersion time or whether the sample was redried, the curves were tightly clustered with very minimal differences. The deformation and fracture patterns remain consistent with the control group as presented in Chapter 3 (Figure 3.4 and Figure 3.5), regardless of the water immersion.

As shown in Figure 4.6 (b) and (d), wood-PLA samples with 4 mm notch exhibited an initial energy absorption of 2.89 J in the control group, which increased to 3.326 J after 15 days of water immersion. Similarly, wood-PLA samples with 10 mm notch had a slight lower energy absorption of 2.12 J but increased to 2.89 J by 15 days. Both types of wood-PLA samples exhibited a significant increase in energy absorption: the 4 mm notch sample showed a growth rate of 15%, while the 10 mm notch sample demonstrated an even more pronounced increase of 36%. The increase in energy absorption was primarily reflected in the descending phase of the force-displacement curves. As mentioned earlier, compared to the redried samples, the wet samples consistently exhibited a more gradual force decline while maintaining higher force levels after reaching the peak force. Consequently, the area beneath the curves for the wet samples was larger, resulting in greater energy absorption. After redrying, both samples exhibited a reduction in energy absorption, with the values returning to their

original level as indicated by control group.

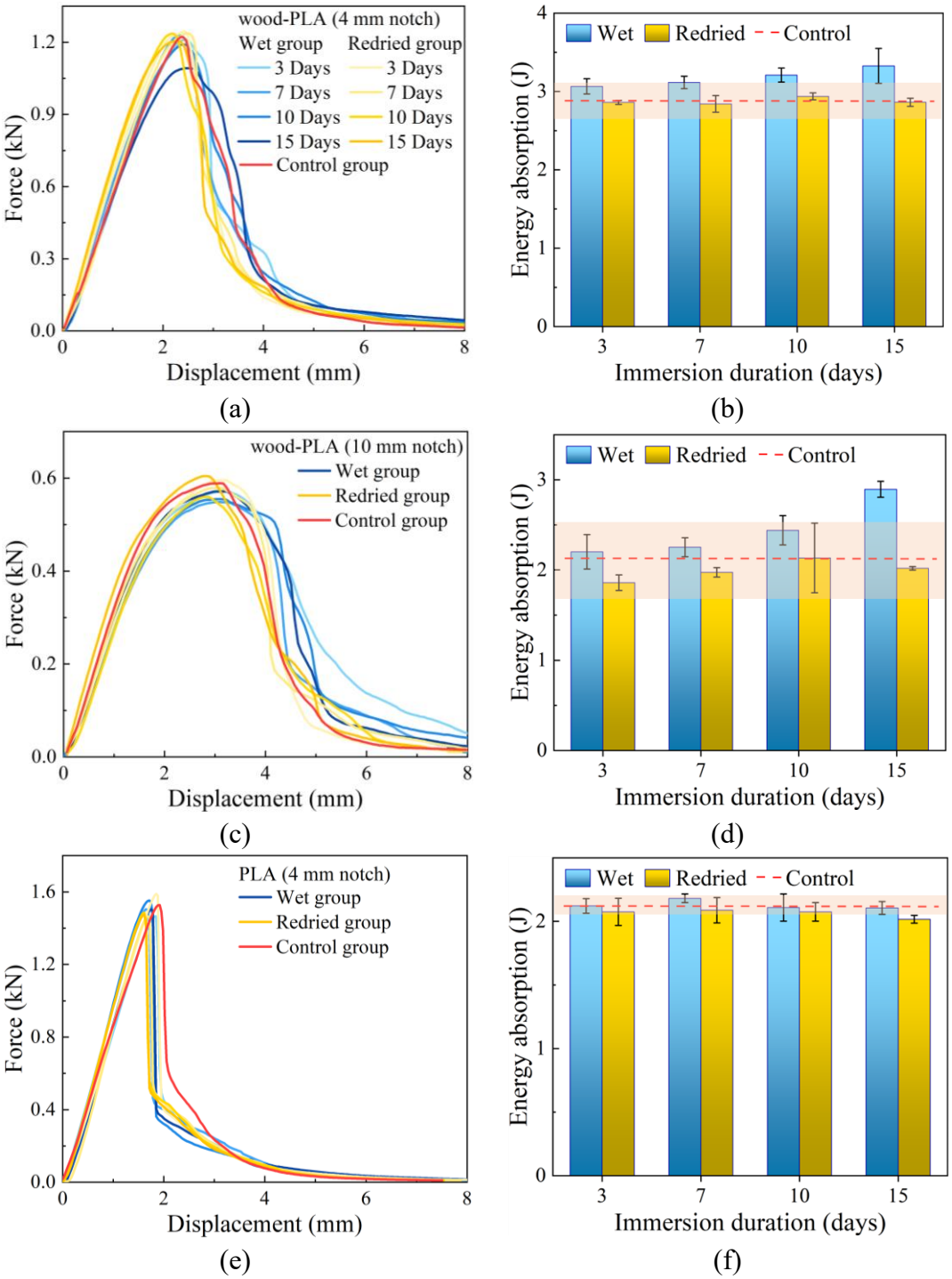

Figure 4.6. The force-displacement curve and energy absorption of the SENB sample with different conditions: (a) and (b) wood-PLA with 4 mm notch, (c) and (d) wood-PLA with 10 mm notch, (e) and (f) PLA with 4 mm notch.

In contrast, the pure PLA samples showed minimal changes in energy absorption after water immersion as demonstrated in Figure 4.6 (f). The energy values remained

stable around 2.1 J, with only slight fluctuations observed. The subtle changes observed in the PLA SENB test can be attributed to the structural characteristics of the SENB testing method. Unlike the dog bone samples used in the tensile test, the SENB configuration exhibited reduced contact efficiency with the surrounding water. The increased thickness of the sample hindered water penetration (mentioned in Figure 4.2 (b) before), limiting the water absorption effect on the material [67, 92, 194]. This reduction in water absorption was noted in both PLA and wood-PLA samples. Additionally, the minimal variation in energy absorption observed for PLA in the SENB test, compared to wood-PLA, can be explained by the inherent material differences. PLA is less sensitive to water exposure than wood-PLA, which incorporates wood fibres.

4.3.5. Discussion on mechanisms and implications

The changes in mechanical properties of PLA and wood-PLA samples can be attributed to plasticisation effects [192]. Water can play a role in plasticisation by acting as the external plasticiser [89, 195, 196], where external plasticisers alter the intermolecular forces between the molecules in the material [193, 197-199]. During the water immersion, both PLA and wood-PLA experienced plasticisation, but wood-PLA exhibited a more pronounced effect under the same water immersion conditions. This is because of the differences in their internal chemical structures, which enable wood-PLA to form more hydrogen bonds with water molecules [23]. The main components of wood-PLA, cellulose and hemicellulose, possess abundant hydroxyl groups in their chemical structure, which allow water, as a plasticiser, to freely form hydrogen bonds with each carbonyl oxygen atom in the matrix once it enters [76, 97]. In this process, the interactions between different chains decrease, but the flexibility of each chain increases, thereby plasticising the overall structure to a higher degree. Besides, the great plasticisation in wood-PLA is also attributed to its porosity, as discussed in Section 4.3.1. The material's porous nature substantially improved water absorption, facilitating

enhanced interaction between the water molecules and the internal structure, thereby leading to a more pronounced plasticisation effect.

The irreversible effects of water immersion on wood-PLA material within a short duration have significant implications for their practical applications:

1. Environmental sensitivity: The hydrophilic nature of wood fibres leads to moisture uptake in humid conditions, compromising the composite's mechanical strength. This necessitates careful consideration when deploying these materials in environments with fluctuating humidity or exposure to water, as their structural integrity may be affected.
2. Energy absorption applications: The increase in energy absorption upon moisture uptake suggests potential for applications requiring impact resistance or damping properties. However, the concurrent reduction in strength must be accounted for, ensuring that the material's load-bearing capacity remains within acceptable limits for the intended use.
3. Maintenance and recoverability: The ability of the composites to regain their original mechanical properties after drying indicates that moisture-induced degradation is reversible for the studied short term water immersion. This behaviour is advantageous for applications where the material may intermittently encounter moisture, as it allows for restoration of mechanical performance through drying processes, thereby extending the material's service life.

4.4. Summary

This study examined the mechanical properties of wood-PLA composites manufactured via FDM printing, with particular attention to the effects of water absorption. Tensile and SENB tests were conducted and compared with those of pure PLA. The impact of water absorption on mechanical performance was evaluated

through immersion for up to 15 days, followed by a redrying process. The key findings are as follows:

Wood-PLA exhibited significant water absorption owing to the hydrophilic nature of cellulose in the wood fibres. During immersion, water molecules penetrated the polymer matrix and formed hydrogen bonds with the hydroxyl groups in wood fibres and the carbonyl groups in PLA, leading to a reduction in intermolecular interactions and an increase in chain flexibility. As a result, both materials experienced a decline in tensile strength and stiffness but an improvement in elongation at break and energy absorption capacity, with these effects being more pronounced in wood-PLA due to the stronger plasticising action of water on cellulose. The maximum reductions in tensile strength and elastic modulus for wood-PLA were 20% and 10%, respectively, while the maximum increases in elongation at break and energy absorption capacity reached 66% and 48%, respectively.

After drying, both materials largely recovered their original properties, including ultimate tensile strength, elongation at break, Young's modulus, and energy absorption capacity. This recovery is attributed to the role of water as an external plasticiser, with its effects reversed upon removal.

These findings emphasise the influence of environmental conditions on the mechanical behaviour of natural fibre-reinforced FDM composites. The study provides valuable insights for advancing bio-based additive manufacturing. Building on the results from Chapters 3 and 4, which explored the mechanical performance of wood-PLA in both its original and moisture-conditioned states, the observed reduction in tensile strength relative to pure PLA suggests the need to optimise the formulation for better mechanical balance. This serves as the basis for the subsequent investigation into varying wood fibre content, which forms the focus of Chapter 5.

Chapter 5. Influence of wood fibre content on the mechanical properties of FDM-printed wood-PLA composites after water absorption

5.1. Introduction

In recent years, 3D printing has rapidly expanded its footprint across diverse sectors, owing to its high material efficiency, reduced labour costs, and ability to fabricate complex structures directly from digital models [140]. Among the various 3D printing technologies, FDM has become one of the most widely adopted methods due to its technical maturity, cost-effectiveness, and compatibility with a broad range of thermoplastic materials [200]. Its capacity to construct geometrically intricate objects without the limitations of traditional moulding techniques has made it especially suitable for applications in automotive components, biomedical devices, architectural models, and lightweight functional parts [4, 24]. With the growing emphasis on sustainability and environmental impact, natural fibre-reinforced composites have emerged as promising candidates for bio-based FDM printing [15, 22]. These materials integrate biodegradable polymers, such as PLA, with organic reinforcements like wood, flax, or recycled agricultural residues, offering an environmentally friendly alternative to synthetic fibre composites [13, 70]. In particular, wood-PLA composites have garnered attention for their good processability, renewable source origins, and aesthetic appeal, making them suitable for both functional and decorative uses [28, 151, 152].

Despite increasing interest in natural fibre composites, current research efforts have focused on printing parameters and fibre content [62, 64]. Accurately controlling wood fibre content is essential for optimising the mechanical performance of wood-PLA composites in real-world applications [20, 29]. While previous studies have explored wood fibre-reinforced filaments in FDM, there remains a clear research gap in

understanding how different fibre loadings affect the composite's mechanical properties [182]. Most existing research focuses on either single-content filaments or commercial products, lacking comparative analysis across a range of fibre fractions. Moreover, little attention has been paid to how moisture exposure alters the mechanical behaviour of composites with varying fibre contents. As the results from chapter 4, given the hydrophilic nature of wood fibres [67, 183], water absorption can significantly influence strength, stiffness, and ductility through plasticisation or interfacial weakening [164]. However, this influence under different fibre loadings remains underexplored. Such investigations are especially important for applications exposed to humidity or water, such as biodegradable outdoor products or horticultural components [174]. Therefore, this study aims to address these gaps by systematically evaluating the mechanical response of FDM-printed wood-PLA composites with varying fibre contents, under both dry and post-immersion conditions.

This chapter presents a detailed investigation into the mechanical behaviour of wood-PLA composites with different wood fibre contents, specifically 5%, 10%, 15%, and 20% by volume. Custom filaments were prepared through melt mixing and re-extrusion processes, enabling full control over fibre dispersion and volume fraction. This study builds upon the foundational understanding established in Chapter 3 and Chapter 4, which evaluated the mechanical performance and water sensitivity of pure PLA and commercial wood-PLA (40% fibre). Unlike the previous work, the current investigation introduces a systematic variation in fibre content to assess how this parameter influences tensile performance and energy absorption, both before and after environmental conditioning. The insights gained from this chapter aim to advance the understanding of fibre-matrix interactions, identify optimal fibre content ranges, and offer material design strategies for applications that demand both sustainability and mechanical reliability. Section 5.2 details the materials and methods used in this study, including how the filament with different wood content were fabricated, conditioning protocols, and testing. Section 5.3 presents the major findings on the mechanical

properties of the materials with different wood fibre content and conditions. Section 5.4 concludes the key findings of this study.

5.2. Method and materials

To investigate the influence of wood fibre content on the mechanical behaviour of PLA-based composites, customised filaments containing 5%, 10%, 15%, and 20% wood fibre by volume were individually produced.

Two commercial filaments (used in Chapters 3 and 4, as detailed in Section 3.2) were selected as base materials: a pure PLA filament (PLA EF 3D850) and a wood-PLA composite filament comprising 40% pine wood fibre by volume (PLA Wood). These filaments were mechanically shredded using an industrial granulator, producing uniformly sized granules with an average particle size below 1.5 mm, suitable for re-extrusion.

The whole filament production process is shown in Figure 5.1. To obtain intermediate formulations, the granulated materials were blended in defined mass ratios to achieve wood fibre contents of 5%, 10%, 15%, and 20% by volume. In addition to these custom blends, two reference formulations were also prepared: 0% wood fibre (pure PLA) and 40% wood fibre (commercial wood-PLA), both of which were reprocessed using the same extrusion conditions to ensure consistency across all filament samples. All mixtures were processed using a filament extruder (Well-Zoom, China) via melt mixing to ensure homogeneous fibre dispersion within the PLA matrix. During the extrusion, each composition was processed under identical temperature and rotation conditions to minimise batch-to-batch variation. The uniformity of the regenerated filaments was visually checked through continuous filament diameter monitoring, and the extrusion rate was maintained at a stable flow to avoid segregation. This procedure followed the general guidelines of polymer composite filament fabrication reported in previous studies, which are widely recognised as standard

practice for ensuring mixing consistency [201]. The extrusion temperature was maintained at 180 °C, and the screw rotation speed was set to 35 rpm. These parameters were selected based on preliminary trials to ensure sufficient melting of the PLA matrix while preventing thermal degradation of both the polymer and the wood fibres. The moderate screw speed facilitated uniform mixing and stable filament extrusion without inducing excessive shear stress [202, 203]. The extruded filaments were subsequently cooled, spooled, and stored under ambient conditions for later use.

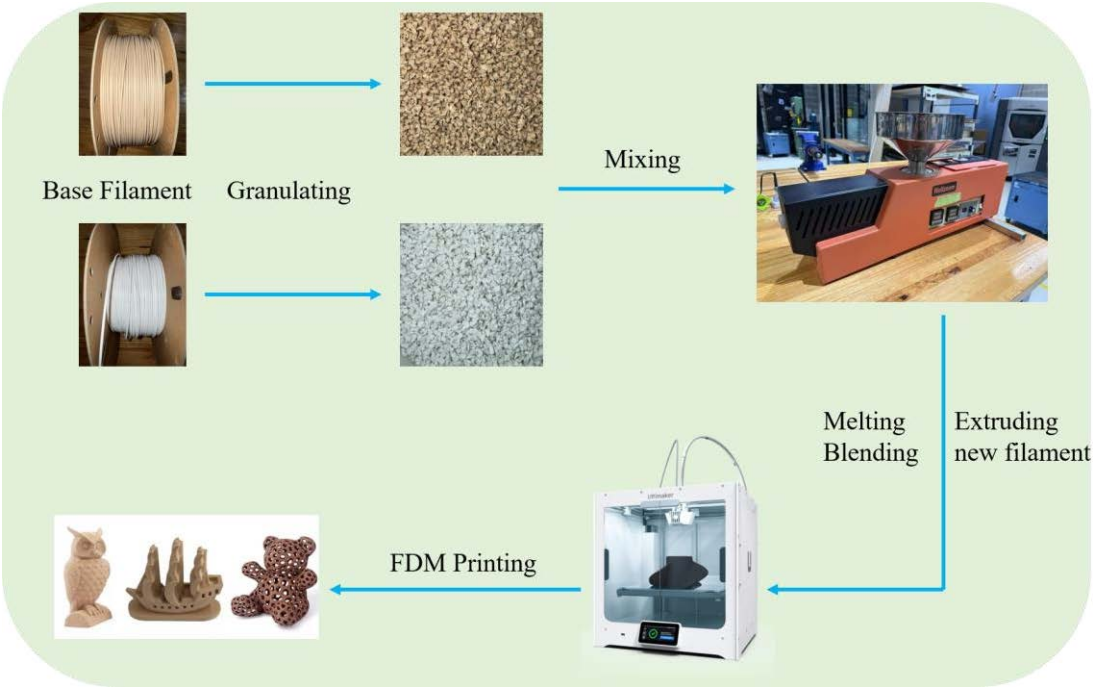

Figure 5.1. The filament manufacturing process.

Tensile specimens were fabricated using the same method described in Chapters 3 and 4 (section 3.2 and Figure 3.1). All samples conformed to the Type IV geometry specified in ASTM D638 [153], with a consistent thickness of 1.6 mm.

This study also examined the tensile property variations of PLA-wood composites with differing wood fibre contents following water absorption, for which dedicated water immersion tests were designed. The samples were classified into three moisture states (Figure 5.2) based on post-processing after printing and laser cutting. The control group comprised non-immersed samples. For water conditioning, all relevant samples

were fully submerged in distilled water for 10 days at room temperature, following the same procedure and environmental conditions described in Chapter 4 (Section 4.2). The water absorption rate was calculated as the percentage mass increase relative to the original state, as defined in Equation (4. 1)).

Tensile tests were conducted on all samples after different conditioning. The testing applied the same parameters and equipment outlined in Chapters 3 and 4. Post-test analysis, including strain energy density calculations and DIC analysis, followed the same procedures in previous chapters to ensure consistency and comparability.

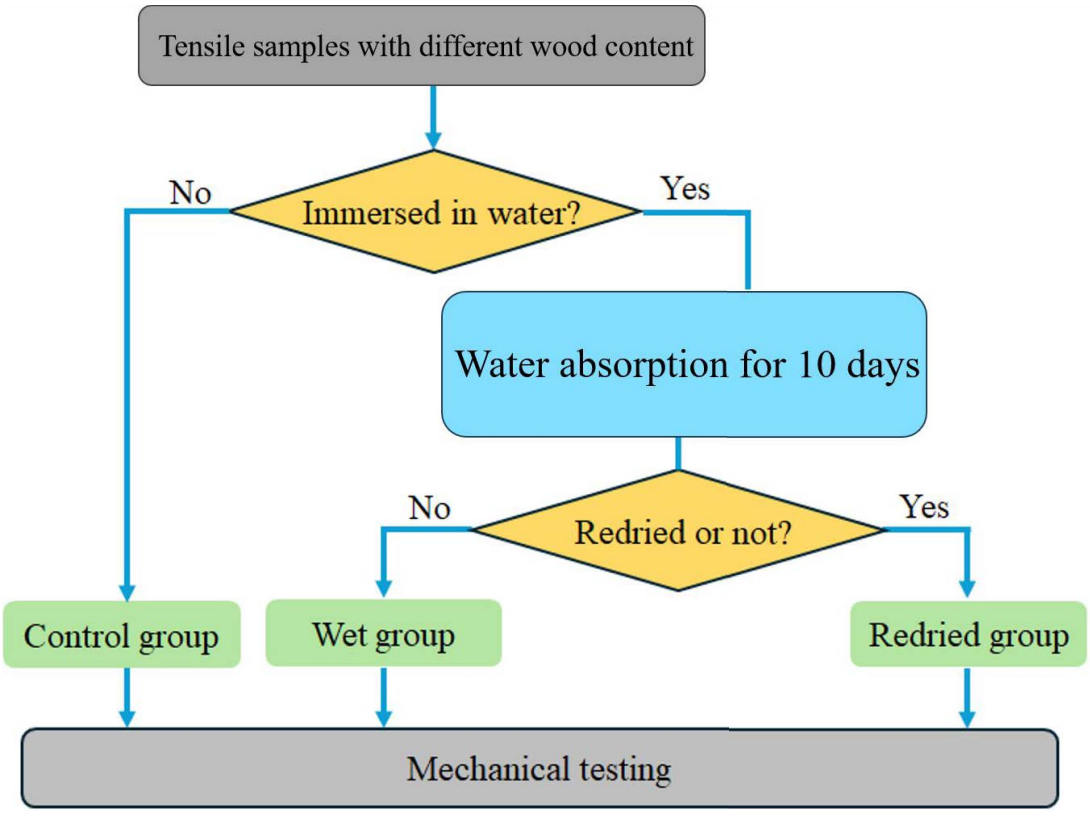

Figure 5.2. Experimental workflow.

5.3. Results and discussion

5.3.1. Mechanical properties of different wood-PLA without water immersion

This section presents the mechanical behaviours of wood-PLA composites with

varying wood fibre contents under the control condition, focusing on their tensile performance. In addition, the printing quality of the two materials was also compared to demonstrate the influence of wood fibre incorporation.

5.3.1.1. Surface property

As shown in Figure 5.3 (a), the surface appearance of FDM-printed PLA composites changes noticeably with increasing wood fibre content. The colour of the samples changed from pure white in the unfilled PLA to increasingly darker, brown-toned shades. At higher magnifications, wood fibres become visible in samples containing between 5% and 20% fibre (marked in red in Figure 5.3 (b)), with a noticeable increase in fibre density as the content rises. Furthermore, the surface of wood-PLA with low wood content (5%) exhibited a relatively smooth and uniform layer-by-layer pattern, characteristic of FDM printing. However, as the wood fibre content increased, this pattern became progressively less distinct. In addition, with the gradual increase in wood fibre content, the surface becomes noticeably rougher and more irregular (Figure 5.3 (b)).

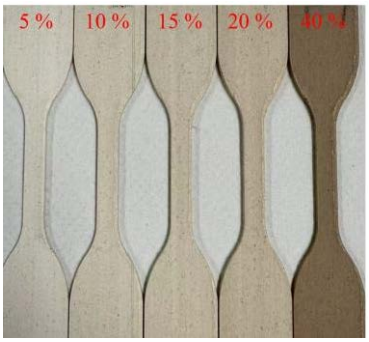

(a)

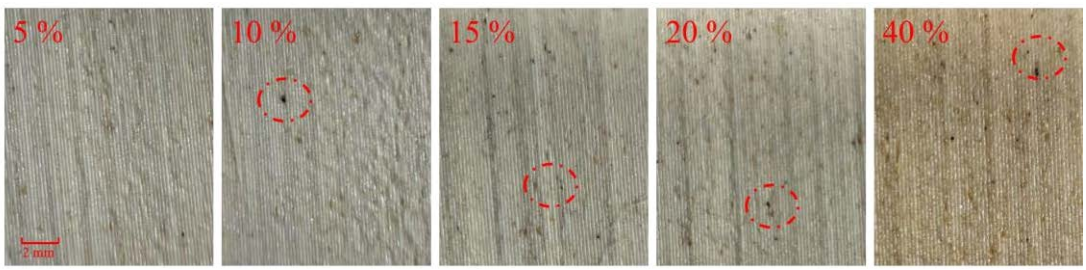

(b)

Figure 5.3. (a) The printed samples with different wood fibre content, (b) the closed view of each sample (visible wood fibres were circled in red).

Additionally, surface defects become increasingly prevalent, characterised by small filaments remaining on the printed surface. The increased surface roughness observed in 3D-printed wood-PLA composites can be largely attributed to the presence of solid wood fibre fillers, which interfere with the uniform flow and extrusion behaviour of the molten polymer during the printing process [182]. These embedded fibres introduce localised flow irregularities and disrupt melt homogeneity [161], leading to inconsistent layer deposition.

5.3.1.2. Tensile property of wood-PLA with different wood content

By comparing the tensile properties of PLA composites with varying wood fibre content, it is evident that both the tensile strength and Young's modulus gradually decrease as the wood fibre content increases. According to Table 5.1, the tensile strength of pure PLA is 54.6 MPa. After the addition of 5% wood fibre, this value decreases to 47.8 MPa. With further increases in wood fibre content, the tensile strength continues to decline, eventually reaching 41.37 MPa. The decline in Young's modulus exhibits a similar pattern, progressively decreasing as the wood fibre content increases. Pure PLA exhibits a Young's modulus of 3074 MPa (Table 5.1), which reduces to 2477 MPa with the incorporation of 5% wood fibre, and continues to decrease to 2051 MPa at 20% wood content, corresponding to an overall reduction of approximately 33%.

The strain energy density, which reflects the energy absorbed per unit volume, shows a rising trend with increasing wood fibre content up to a certain point (Table 5.1). For pure PLA, the strain energy density is 6.39×10^{-7} J/m^3; this increases to 1.081×10^{-6} J/m^3 at 5% and 10% wood fibre content, and peaks at 1.58×10^{-6} J/m^3

with 15% wood fibre, representing a 147% increase compared to pure PLA. Beyond this point, a decline is observed, with the value falling to 8.76 $\times 10^{-7}$ J/m^3 at20% wood fibre content and 6.91 $\times 10^{-7}$ J/m^3 at 40%.

Table 5.1 The tensile results of wood-PLA with different wood fibre content

Fibre Content (%)	0	5	10
Tensile Strength (MPa)	54.6 (2.44)	47.8 (0.54)	44.37 (1.7)
Elastic Modulus (MPa)	3074 (140)	2477 (26)	2254 (78)
Elongation at Break (%)	2 (0.2)	3 (0.7)	3.2 (0.1)
Strain Energy Density (10^{-7} ×J/m^3)	6.39 (0.9)	10.81 (3.6)	10.3 (2.1)

Fibre Content (%)	15	20	40
Tensile Strength (MPa)	42.4 (1.34)	41.37 (1.75)	26.51 (0.86)
Elastic Modulus (MPa)	2246 (83)	2051 (69)	1597 (174)
Elongation at Break (%)	4.4 (0.37)	2.9 (0.19)	3.4 (0.12)
Strain Energy Density (10^{-7} ×J/m^3)	15.8 (1.5)	8.76 (2.1)	6.91 (0.39)

The stress-strain curves of samples with varying wood fibre content are presented in Figure 5.4. By comparing the blue curve (representing pure PLA) with different brown curves (representing wood-PLA composites with different fibre contents), it can be observed that the addition of wood fibre introduces a distinct plastic deformation stage during tensile testing, a feature absents in pure PLA. Pure PLA fractures immediately after reaching its maximum stress, exhibiting a brittle failure behaviour throughout the entire test. In contrast, all wood-PLA composites demonstrate varying degrees of plastic deformation following the peak stress (Figure 5.4). This effect is particularly pronounced in the sample containing 15% wood fibre, which shows the most extended plastic region. Additionally, as the wood fibre content increases from 0%, the peak stress values on the curves gradually decrease, with the most pronounced

reduction occurring between 0% and 5% wood fibre content.

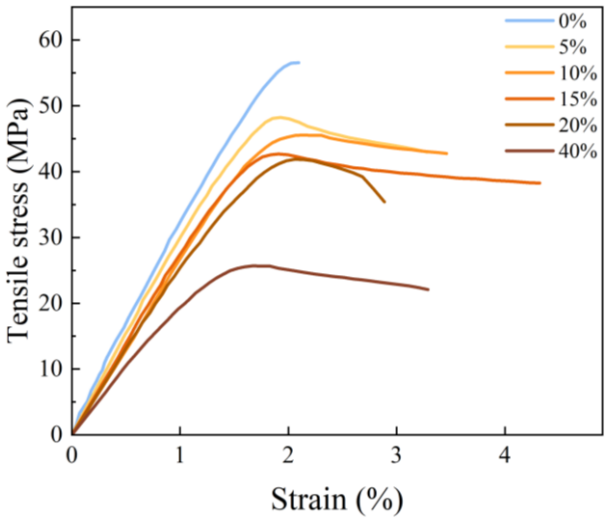

Figure 5.4. The tensile results of wood-PLA samples with different wood fibre content in the control group.

The ε_{yy} strain distribution of the samples at the time of breakage, as analysed using DIC, is illustrated in Figure 5.5. The strain distribution picture of pure PLA reveals a fracture pattern characterised by immediate failure following the formation of a localised strain concentration within the gauge region. However, upon the addition of wood fibre, the magnitude of local strain increases progressively. Notably, the sample with 15% wood fibre content exhibits a wide range of plastic deformation prior to failure, as shown in its strain distribution. In the images corresponding to the 0%, 5%, 10%, 20% and 40% wood fibre composites (Figure 5.5), the strain, indicated in red, is primarily concentrated in a small region at the centre of the gauge section. This localised area is also where fracture subsequently occurs. In contrast, the 15% wood fibre composite exhibits a much more uniform strain distribution, with elevated strain values spread across almost the entire gauge region. This observation provides further evidence that a wood fibre content of 15% enhances the toughness of the composite, resulting in improved toughness under tensile loading.

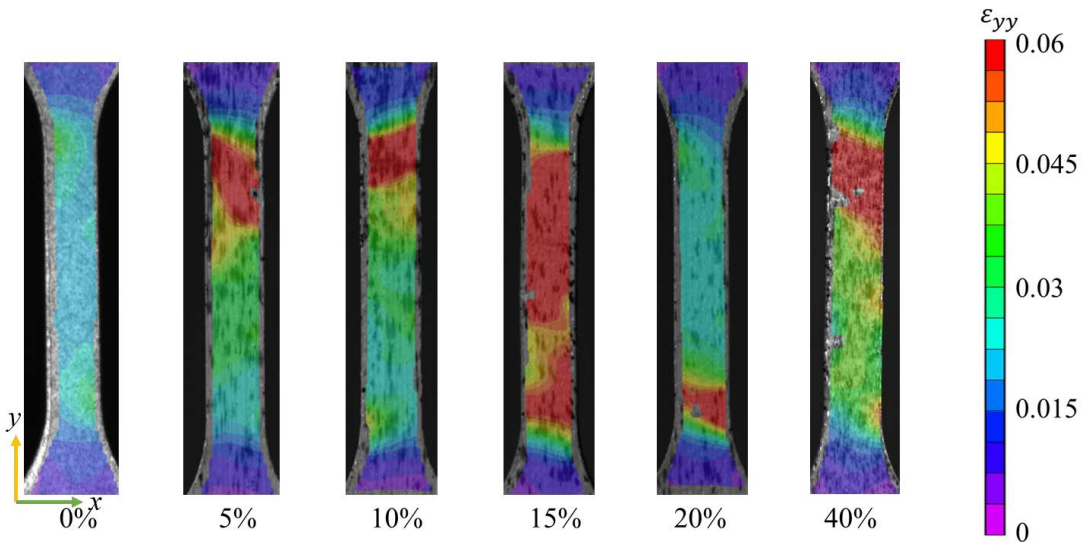

Figure 5.5. ε_{yy} strain contour of the wood-PLA samples with different wood fibre content before breakage.

As wood fibre content increases in PLA composites, the material gradually shows improved toughness and energy absorption ability, while its tensile strength and stiffness decline (mentioned in Table 5.1, Figure 5.4 and Figure 5.5). This trend is caused by the interaction between wood fibres and the PLA matrix. On the one hand, the addition of fibres creates structural discontinuities and weak interfaces between PLA matrix and wood fibres [66, 82]. These defects reduce the material's overall strength [19]. On the other hand, fibres contribute to toughening mechanisms such as changing the fracture pattern and crack bridging [172]. These effects help slow down crack growth and absorb more mechanical energy during deformation [204]. Among all tested samples, the composite with 15% wood fibre content exhibited the highest elongation at break and strain energy density, indicating that 15% is a favourable balance point. This result is consistent with some other similar research results [164, 167]. At this wood fibre content, there are enough fibres to enhance energy absorption, but not so many that they cause fibre agglomeration [205], increased voids [82], and inferior adhesion between PLA matrix and fibre [66]. As a result, the material retains its structural

integrity while gaining additional toughness from the fibre network. This explains why the 15% wood-PLA sample achieved the best mechanical performance in terms of toughness.

5.3.2. Water absorption ability

To assess the hygroscopic behaviour of the composites, the water absorption of wood-PLA samples with varying fibre contents was measured following a 10-day immersion period. Figure 5.6 illustrates the water absorption percentages of wood-PLA composites with varying wood fibre contents after immersion. The horizontal axis represents the wood fibre content by weight (%), while the vertical axis indicates the corresponding water uptake as a percentage of the sample's initial mass. A clear upward trend is observed as wood fibre content increases.

The pure PLA sample (0% wood fibre) exhibits the lowest water absorption, with a recorded value of just 0.5%. Upon the addition of 5% wood fibre, the absorption increases to 0.8%, more than doubling that of the neat PLA. This upward trend continues: the 10% fibre composite reaches 1.1%, and the 15% sample records 1.2%.

At higher fibre contents, the water uptake becomes more substantial. The 20% wood-PLA composite absorbs 1.7% of its mass in water. The most dramatic rise is observed in the 40% composite, which absorbs 7.7%, approximately 15.4 times the amount of the pure PLA. The overall trend suggests progressive increase in water absorption as the wood fibre content rises.

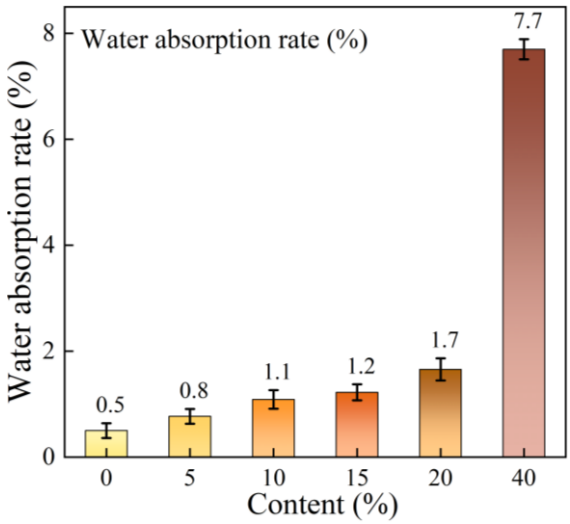

Figure 5.6. Water absorption rate for the samples with different wood fibre content.

The progressive increase in water absorption can be primarily attributed to the presence of wood fibres within the composite. Wood fibres are predominantly composed of cellulose and hemicellulose, both of which are significantly more hydrophilic than PLA chains [67, 206]. In contrast, pure PLA is inherently hydrophobic. As the wood fibre content increases, the overall hydrophilicity of the composite also rises, thereby enhancing its capacity to absorb moisture [67].

In addition, as mentioned in Section 5.3.1.1, increasing the wood fibre content results in a visibly rougher and more uneven surface morphology in the printed samples (Figure 5.3). This increase in surface irregularity facilitates greater contact between the material and water, further contributing to the elevated water uptake observed in composites with higher fibre content.

As previously discussed in Chapter 4, a comparison of water absorption between pure PLA and 40% wood-PLA over 3, 7, 10, and 15 days revealed a significantly higher absorption capacity in the wood-PLA composite (Figure 4.2). In the present chapter, this observation is further validated by the absorption data across a broader range of wood fibre contents (0-40%). The results confirm a clear positive correlation between water absorption capacity and wood fibre content.

Similar conclusions have also been drawn in other studies [206]. Lage-Rivera et al.

investigated the water absorption behaviour of PLA composites filled with coffee grounds as bio-fillers [164]. The findings indicated that the water uptake increased exponentially with rising bio-filler content, particularly when the filler content exceeded 20% [164].

The observed increasing trend in water absorption behaviour can largely be attributed to the presence of wood fibres. These fibres are primarily composed of cellulose, a component known for its strong affinity to water, which substantially enhances the overall moisture uptake of the composite. This is due to the inherently hydrophilic nature of both cellulose and hemicellulose found in wood fibres [206]. In contrast, pure PLA exhibits relatively low water affinity, particularly in its conventionally manufactured form, where the smooth surface limits moisture interaction [67, 78]. Although FDM can improve surface wettability by introducing porosity and irregular surface textures that promote water contact [189], the overall water absorption of FDM-printed pure PLA remains comparatively low.

5.3.3. Tensile properties with water immersion

5.3.3.1. Stress strain curve

Figure 5.7 presents the stress-strain curves of all wood-PLA composites with varying wood fibre content after 10 days of water immersion and subsequent redrying. It includes a comparison with the corresponding curves of samples that were re-dried following each immersion stage. It can be observed that, for each fibre content level, water immersion leads to a reduction in both peak strength and stiffness, accompanied by a noticeable increase in strain at break. However, after re-drying, the tensile properties are largely restored, indicating that the reduction observed was primarily physical and reversible in nature, rather than the result of irreversible chemical degradation.

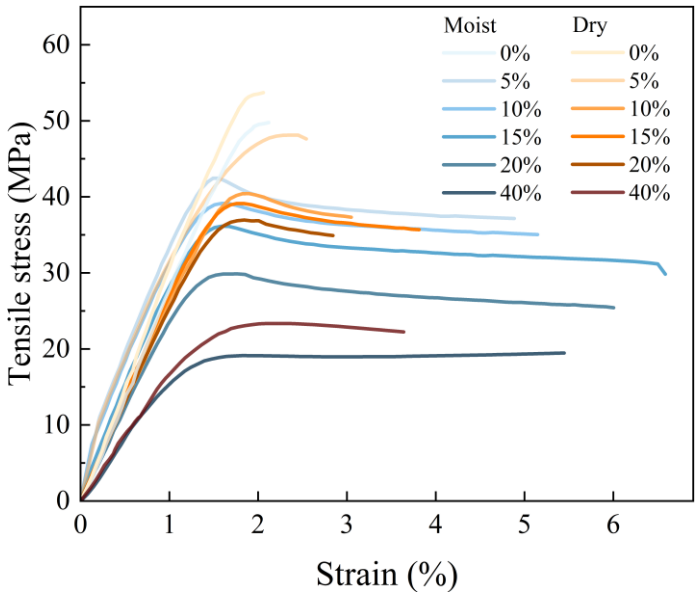

Figure 5.7. The stress strain curve of samples with different wood fibres content and different conditions.

5.3.3.2. Mechanical properties

This section will primarily analyse the tensile strength, elongation at break, Young's modulus, and strain energy density extracted from the stress-strain curves. The data for the original, water-immersed for ten days, and re-dried samples are presented in Figure 5.8. As shown in Figure 5.8 (a), there is a noticeable and significant decrease in tensile strength after 10 days of water immersion. This reduction is particularly pronounced in the samples with higher wood fibre content. For the 5% wood fibre composite, the tensile strength decreases from 47.8 MPa to 42.6 MPa, corresponding to a reduction of 10.9%. In the 20% wood fibre composite, the tensile strength drops dramatically from 41.4 MPa to 29.9 MPa, representing a decline of 27.8%. Similarly, the reduction rate for the 40% wood fibre composite is even more substantial at 29.1% (Figure 5.8 (a)). After re-drying, it is clearly evident that the tensile strength of all samples shows a significant recovery. Regardless of the wood fibre content, the tensile strength largely returns to its original level after the re-drying treatment.

The results of the Young's modulus extraction are presented in Figure 5.8 (b). It is

clearly evident that, after 10 days of water immersion, there is a decrease in Young's modulus, with the reduction being more pronounced at higher wood fibre content. For the 5% wood fibre composite, Young's modulus decreases from 2477 MPa to 2363 MPa, a reduction of 4.6%. In the 20% wood fibre composite, Young's modulus drops from 2051 MPa to 1853 MPa, representing a decline of 9.7%. After re-drying, a noticeable recovery in Young's modulus is observed, with most samples nearly fully recovering their original values. However, the 20% and 40% wood fibre composites still show a slight reduction compared to their original values, although they demonstrate a clear recovery trend.

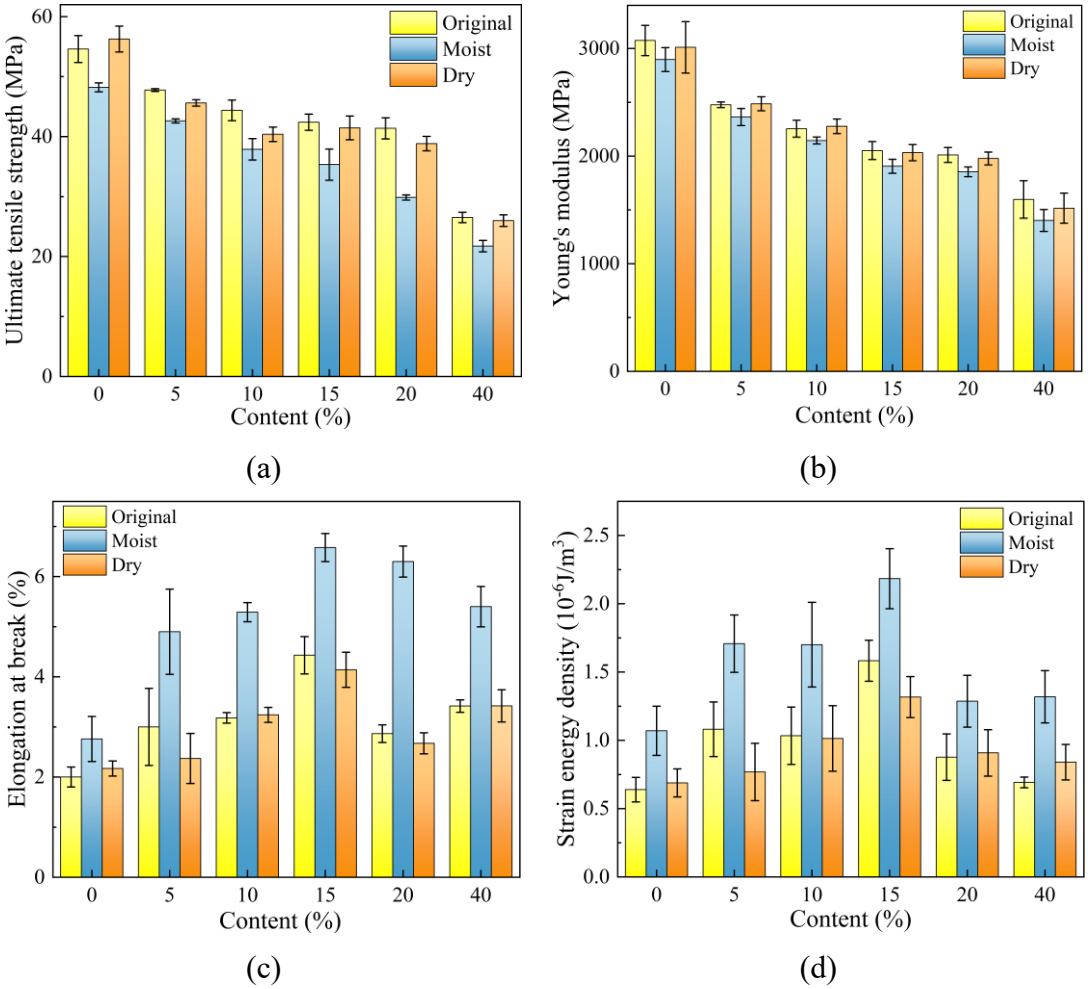

Figure 5.8. Tensile results with different wood fibre content and (wet or redry) conditions, (a) ultimate tensile strength, (b) Young's modulus, (c) elongation at break, (d) strain energy density.

During the 10-day water absorption process, all wood-PLA samples exhibited a significant increase in elongation at break (Figure 5.8 (c)), with the 40% wood fibre composite showing the largest increase, reached 8% after water immersion. After re-drying, the elongation at break of all wood-PLA composites decreased and returned to values that were close to their original levels.

The enhanced elongation at break after full water absorption also significantly increases the strain energy density of the samples. Figure 5.8 (d) illustrates the change in strain energy density of wood-PLA composites with varying wood fibre content after 10 days of water immersion. Notably, the sample with 15% wood fibre content shows the highest strain energy density after water absorption, with a value of 2.18×10^{-6} J/m^3, representing an increase of 38.2% compared to its original value. After re-drying, all samples experience a decrease in strain energy density, returning to values close to their original levels.

5.3.3.3. DIC analysis

Figure 5.9 presents the DIC images of wood-PLA composites with wood fibre contents ranging from 0% to 40% after 10 days of water immersion, captured during tensile testing just prior to fracture. The images display the local strain distribution in the y-direction. A clear increase in local strain can be observed in comparison with the corresponding images in Figure 5.5. Although the red region in the pure PLA sample remains relatively limited, it is still evident that water immersion has led to a noticeable increase in strain (Figure 5.9). In the 40% wood fibre composite, close examination reveals the presence of white surface markings Figure 5.9, commonly referred to as stress whitening. This suggests that significant plastic deformation has occurred without macroscopic fracture, further demonstrating that the enhanced water absorption

introduced by the wood fibres contributes to improved toughness following immersion. A comparison with the corresponding pre-immersion DIC images in Figure 5.5 reveals further insights. While the pure PLA sample continues to exhibit strain localisation within a small region at the point of imminent fracture, the other wood-PLA composites show a more uniform strain distribution across the entire gauge area (Figure 5.9), even though the red region in the 5% fibre sample remains relatively limited. In Figure 5.5, the strain concentration corresponds to a brittle, highly localised fracture pattern, whereas after water immersion (Figure 5.9), the expanded red regions indicate that the deformation became more homogeneous and ductile. This change in failure mode is mainly attributed to the plasticisation effect induced by absorbed water molecules, which form hydrogen bonds with the polymer chains and wood fibres. The detailed analysis of the effect of plasticisation will be presented in next section. This shift in strain behaviour following water immersion suggests that the ductility enhancement imparted by moisture uptake is not confined to a specific region, but rather distributed more evenly throughout the material.

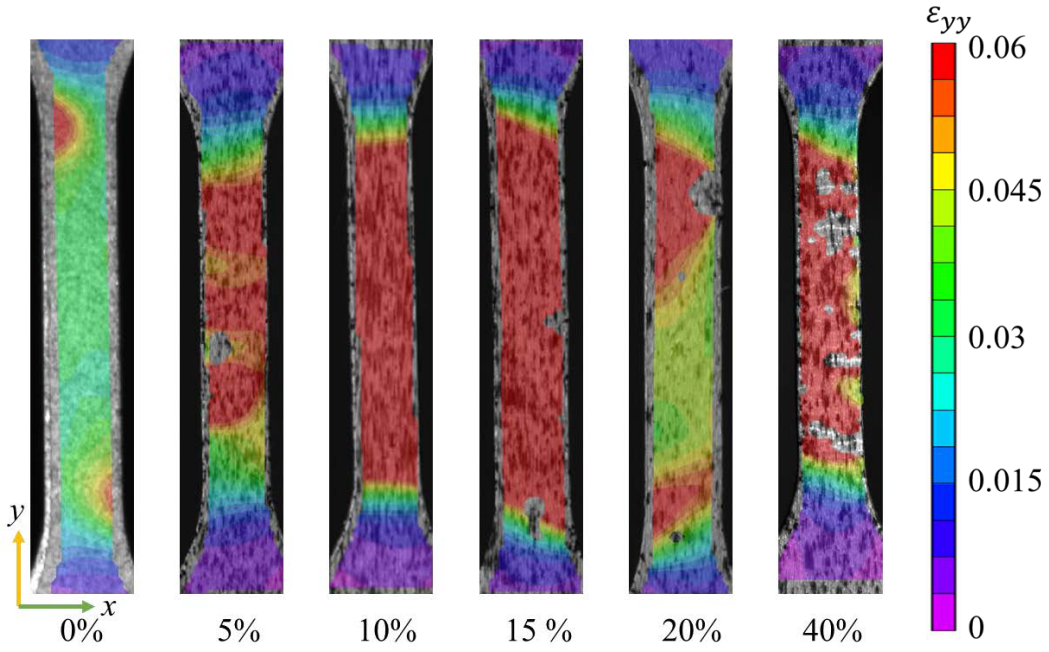

Figure 5.9. ε_{yy} strain contour of the samples with different wood fibre content

after water absorption before breakage.

5.3.4. Discussion on mechanisms and implications

The performance variations observed in wood-PLA composites with different fibre contents after water immersion, as well as the subsequent changes following re-drying, can be primarily attributed to the plasticising effect of water within the material [89]. As mentioned in Chapter 4, water is commonly regarded as an external plasticiser, alongside other typical examples such as glycerol [89, 196]. External plasticisers typically modify the mechanical properties of a material by altering the intermolecular forces, such as hydrogen bonding, between its constituent molecules [164, 167, 197]. This microstructural modification typically manifests macroscopically as softening, with reductions in strength and stiffness, while toughness is noticeably enhanced [207, 208]. Moreover, the main chemical constituents of wood fibres, cellulose and hemicellulose, contain a high density of hydroxyl groups [76, 97], which can form a greater number of hydrogen bonds with water molecules compared to pure PLA [23], making the plasticising effect of water more pronounced in materials with higher wood fibre content. In this process, the interactions between different chains decrease, but the flexibility of each chain increases, thereby plasticising the overall structure to a higher degree.

Another explanation for the observed decrease in strength and modulus, alongside the increase in elongation at break and strain energy density with rising wood fibre content, lies in the enhanced water absorption behaviour discussed in Section 5.3.2. As wood fibre content increases, particularly at higher levels, the composites exhibit significantly greater moisture uptake. This, in turn, leads to a more efficient and pronounced plasticising effect of water, which softens the material matrix and promotes ductile deformation under load.

Following the re-drying process, the tensile properties of the wood-PLA

composites, with varying wood fibre contents, were restored to their respective original levels. This behaviour can be attributed to the nature of water as an external plasticiser during the immersion phase. Rather than forming new, strong chemical bonds, water temporarily alters the intermolecular interactions (hydrogen bonding) between polymer chains [164, 167, 197]. Once the absorbed moisture is fully removed through drying, these weakened intermolecular forces dissipate accordingly [89, 196]. As a result, the mechanical properties observed in tensile testing show a clear recovery, reflecting the reversible nature of this physical plasticisation process.

Based on the findings of this study, two key implications can be drawn regarding the application of wood-PLA composites in environments involving moisture exposure.

First, the reversible plasticising effect of water in wood-PLA composites highlight the potential of these materials in applications where temporary softening and energy absorption are desirable under wet conditions, followed by recovery of stiffness and strength upon drying. This characteristic is particularly beneficial in fields such as packaging or temporary structural components [23], where moisture exposure is intermittent and short-term mechanical resilience is valued.

Second, the effect of plasticisation is strongly influenced by wood fibre content, due to the abundant hydroxyl groups in cellulose and hemicellulose, which facilitate hydrogen bonding with water. This suggests that fibre loading can be strategically tuned to customise the moisture-response behaviour of the composite. For instance, in environments requiring improved toughness or energy dissipation under wet conditions, higher fibre content may be advantageous. This opens up design opportunities for wood-PLA components in reusable, moisture-interactive systems.

5.4. Summary

This study demonstrated the successful fabrication of wood-PLA composite filaments containing 5%, 10%, 15%, and 20% wood fibre by volume. These customised

filaments were produced via melt blending and extrusion, and subsequently employed in FDM printing to manufacture tensile test samples. The mechanical performance of each material was systematically examined, both in the original condition and after exposure to water immersion and redrying processes, providing a comprehensive understanding of how varying wood fibre content influences material behaviour under different environmental conditions.

With increasing wood fibre content, a consistent decline in tensile strength and elastic modulus was observed, beginning from a baseline of 54.6 MPa for pure PLA. In contrast, both elongation at break and strain energy density progressively increased. The 15% wood fibre formulation achieved the highest energy absorption performance, with an elongation at break of 4.4% and a strain energy density of 1.58×10^{-6} J/m^3, representing increases of 120% and 147%, respectively, compared to pure PLA. This enhancement in energy absorption was attributed to the presence of wood fibres, which modified the fracture behaviour of the material. Unlike the brittle failure observed in pure PLA, the wood-PLA composites exhibited a more gradual fracture progression, enabling greater strain accommodation and more effective dissipation of mechanical energy.

Water absorption tests revealed that the hydrophilic nature of cellulose within the wood fibres led to a pronounced increase in moisture uptake with rising fibre content. The overall absorption rate exhibited an approximately exponential growth pattern, particularly in formulations with higher wood fibre concentrations. After 10 days of immersion, all materials experienced a reduction in tensile strength and elastic modulus, while elongation at break and energy absorption capacity increased. These changes reflected the plasticising effect of water within the composite structure.

Following the redrying process, the mechanical properties of the wood-PLA composites largely returned to their original levels across all wood fibre contents. Tensile strength, elastic modulus, elongation at break, and strain energy density showed substantial recovery.

The results highlighted the optimisation of the wood fibre content when utilizing the wood-PLA in real application, and emphasized the sensitivity to the environmental changes, providing new insight to the development of the research of the bio-based composite materials.

Chapter 6. Conclusion and future works

6.1. Conclusion

This thesis presents a comprehensive investigation into the mechanical behaviour and water sensitivity of wood-PLA composites manufactured through FDM. Three interconnected experimental studies were conducted, each designed to deepen the understanding of how wood fibre content influences the performance and applicability of PLA-based materials in additively manufactured components. Together, these studies provide valuable insights into the balance between sustainability, mechanical functionality, and environmental responsiveness in bio-composite 3D printing.

In the first stage of the study, the mechanical behaviour of two commercially available FDM filaments, pure PLA and a wood-PLA composite containing 40% wood fibre by volume, was comparatively analysed. Evaluations included assessments of printing quality, tensile performance, and SENB testing. The results demonstrated that while the wood-PLA composite exhibited lower ultimate tensile strength (23.4 MPa vs. 54.6 MPa for pure PLA), it showed substantially greater elongation at break and strain energy density (8.91×10^{-7} J/m^3 vs 6.39×10^{-7} J/m^3). SENB testing further confirmed this enhanced energy absorption, with wood-PLA samples exhibiting a slower, more progressive fracture mode compared to the brittle failure observed in pure PLA. These findings highlighted the inherent toughness advantage offered by natural fibre reinforcement.

The second stage of the research examined the effects of water immersion and

subsequent redrying on the mechanical performance of the same PLA and wood-PLA materials. Owing to the hydrophilic nature of cellulose and hemicellulose in the wood fibres, the wood-PLA composite exhibited significantly greater moisture uptake. After 10 days of immersion, both materials showed reductions in tensile strength and modulus, accompanied by increases in elongation at break and strain energy density. These changes were more pronounced in the wood-PLA samples. Crucially, the mechanical properties were largely restored following redrying, confirming the reversible nature of the changes. This behaviour reflects the action of water as an external plasticiser, temporarily disrupting intermolecular interactions without inducing permanent chemical degradation. These findings indicate that wood-PLA composites can retain mechanical functionality in moisture-variable environments, supporting their use in applications requiring both energy absorption and environmental responsiveness.

The third study expanded upon these findings by preparing four custom wood-PLA filaments containing 5%, 10%, 15%, and 20% wood fibre by volume. The aim was to investigate how incremental changes in wood fibre content would affect mechanical properties, water uptake, and post-immersion recovery. Custom filaments were produced by mechanically shredding and melt-blending the base PLA and 40% wood-PLA filaments, followed by extrusion into new filament forms. These were printed under consistent FDM parameters, and tensile samples were prepared using laser cutting techniques to ensure dimensional accuracy and reduce stress concentration effects.

The tensile results of the newly developed formulations revealed clear trends: as wood fibre content increased, tensile strength and Young's modulus decreased, while elongation at break and strain energy density increased. Among all formulations, the filament with 15% wood fibre content exhibited the most favourable mechanical profile, achieving the highest values for elongation at break (4.4%) and strain energy density (1.58×10^{-6} J/m^3), representing increases of 120% and 147%, respectively, compared to pure PLA. This optimal balance was attributed to a toughening mechanism known as

crack bridging, where finely dispersed wood fibres hinder crack propagation, allowing for more plastic deformation and improved energy absorption without significant structural failure.

Water absorption testing confirmed a strong positive correlation between wood fibre content and moisture uptake. Particularly in higher fibre formulations (over 20% fibre content), the water absorption increased exponentially. Post-immersion tensile testing again revealed decreases in strength and stiffness, paired with increases in ductility and energy absorption, confirming the plasticising role of water. Crucially, after redrying, all formulations showed a strong tendency to recover their original mechanical characteristics, supporting the conclusion that these changes were physical and reversible.

Overall, the three studies conducted in this thesis have demonstrated the viability and adaptability of wood-PLA composites in FDM-based manufacturing. Key contributions include: (1). Confirming the enhanced toughness and energy absorption capacity of wood-PLA compared to pure PLA; (2). Demonstrating the reversibility of water-induced mechanical changes through redrying; (3). Identifying the 15% wood fibre formulation as the most effective in balancing strength, ductility, and energy performance; (4). Providing foundational insights into the role of fibre content and water interaction in shaping the mechanical response of bio-composite filaments.

These findings highlight the potential of wood-PLA as a sustainable alternative for applications where energy absorption, recoverability, and eco-friendly materials are valued.

6.2. Recommendations for future work

While this study has yielded valuable insights into the mechanical performance and water sensitivity of FDM-fabricated wood–PLA composites, several avenues remain open for further exploration to deepen understanding of this material system.

6.2.1. Long-term water immersion and environmental ageing

While this thesis primarily investigated short-term water immersion effects, it is recommended that future work assess the long-term durability of wood-PLA under sustained exposure to humid environments. In practical applications, especially those involving outdoor or horticultural settings, composite parts may be subjected to extended periods of environmental stress [209]. Evaluating the mechanical property degradation under prolonged immersion, combined with cyclic wetting-drying conditions, would yield a more comprehensive view of material stability. Moreover, analysing the reversibility of plasticisation effects over repeated drying cycles, and the hydrothermal degradation [210], will be essential in determining the long-term feasibility of these materials for functional applications.

6.2.2. Interfacial modification strategies to enhance fibre-matrix bonding

The results of this study suggest that the mechanical properties, particularly stiffness and strength, tend to decrease with increasing wood fibre content. The reason is weak interfacial adhesion between the hydrophilic fibres and the hydrophobic PLA matrix. Therefore, interfacial enhancement strategies represent a crucial direction for future research. Techniques such as fibre surface treatment (e.g., alkali treatment, silane coupling agents [211]), or the use of compatibilisers (e.g., maleic anhydride-grafted PLA [212]) could significantly improve fibre-matrix adhesion. These treatments may help to bridge the mechanical disparity between the two phases and reduce fibre pull-out, leading to higher tensile strength and toughness [213]. Investigating the effects of these modifications at both microscopic (e.g., SEM fracture surface analysis) and macroscopic (e.g., tensile, impact testing) scales will further clarify the role of interfacial bonding in composite performance [211].

Appendix

Approximate calculation of flexural stress in SENB samples

To illustrate the effect of notch length on the crack behaviour, the flexural stress in SENB samples is approximately calculated. In the notched samples in Figure A.1 (a), the sample height is denoted as H= 20 mm, and the notch length is presented as a. When the sample exhibits a deflection of δ, Then flexural stress of the sample above the notch can be approximately calculated based on the simplified schematic shown in Figure A.1 (b).

When the sample in Figure A.1 (b) is subjected to three-point bending, the deflection δ formulas can be applied:

$$\delta = \frac{PL^3}{48EI}, \tag{A1}$$

where P is the central load, L represents the span length, E is Young's modulus, and I denote the second moment of area. The bending moment (M) in the mid-span can be calculated as:

$$M = \frac{PL}{4}. \tag{A2}$$

The maximum flexural stress (σ_B) can be determined by:

$$\sigma_B = \frac{MY}{I}, \tag{A3}$$

where Y is the outermost fibre distance measured from the neutral axis to the edge of the sample. By substituting Equations A1 and A2 into Equation A3, the maximum flexural stress can be rewritten as:

$$\sigma_B = \frac{12\delta EY}{L^2}. \tag{A4}$$

For a specific material, the maximum flexural stress is proportional to the outermost fibre distance. In this study, as the notch length a increases from 4 mm to 10 mm, the value of $Y = (H - a)/2$ decreases from 8 mm to 5 mm, leading to the reduction in the maximum flexural stress at the same deflection. Therefore, the sample

with 10 mm notch length exhibited stronger resistance to flexural fracture.

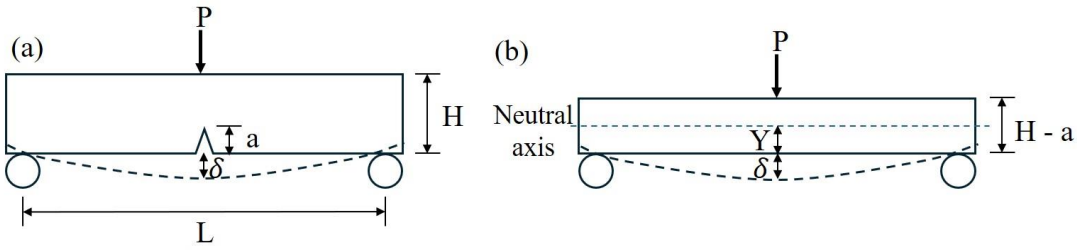

Figure A.1. Approximate calculation diagram of flexural stress in SENB samples.

References

1. Shahrubudin, N., T.C. Lee, and R. Ramlan, *An Overview on 3D Printing Technology: Technological, Materials, and Applications.* Procedia Manufacturing, 2019. **35**: p. 1286-1296.

2. Santo, L., F. Quadrini, A. Accettura, and W. Villadei, *Shape memory composites for self-deployable structures in aerospace applications.* Procedia Engineering, 2014. **88**: p. 42-47.

3. Wu, L., L. Zhao, M. Jian, Y. Mao, M. Yu, and X. Guo, *EHMP-DLP: Multi-projector DLP with energy homogenization for large-size 3D printing.* Rapid Prototyping Journal, 2018. **24**(9): p. 1500-1510.

4. Melocchi, A., N. Inverardi, M. Uboldi, F. Baldi, A. Maroni, S. Pandini, F. Briatico-Vangosa, L. Zema, and A. Gazzaniga, *Retentive device for intravesical drug delivery based on water-induced shape memory response of poly (vinyl alcohol): design concept and 4D printing feasibility.* International journal of pharmaceutics, 2019. **559**: p. 299-311.

5. Yamashita, M. and M. Gotoh, *Impact behavior of honeycomb structures with various cell specifications—numerical simulation and experiment.* International Journal of Impact Engineering, 2005. **32**(1-4): p. 618-630.

6. Tran, J.L., *3D-printed food.* Minn. JL Sci. & Tech., 2016. **17**: p. 855.

7. Rajan, V., B. Sniderman, and P. Baum, *3D opportunity for life: Additive manufacturing takes humanitarian action.* Delight Insight, 2016. **1**(19): p. 1-8.

8. Murariu, M. and P. Dubois, *PLA composites: From production to properties.* Advanced drug delivery reviews, 2016. **107**: p. 17-46.

9. Vishwakarma, S.K., P. Pandey, and N.K. Gupta, *Characterization of ABS material: a review.* Journal of Research in Mechanical Engineering, 2017. **3**(5): p. 13-16.

10. Hsueh, M.-H., C.-J. Lai, S.-H. Wang, Y.-S. Zeng, C.-H. Hsieh, C.-Y. Pan, and W.-C. Huang, *Effect of printing parameters on the thermal and mechanical properties of 3d-printed pla and petg, using fused deposition modeling.* Polymers, 2021. **13**(11): p. 1758.

11. He, Y., Z. Qiao, L. Fan, Z. Xia, J. Ma, X. Zheng, L. Deng, X. Xu, and H. Liu, *Lightweight, ultra-compressed, and environmentally friendly wood/TPU aerogel sensor based on optimized performance of dynamic 3D pore structure.* J Colloid Interface Sci, 2025. **678**(Pt B): p. 188-199.

12. Li, N., Y. Li, and S. Liu, *Rapid prototyping of continuous carbon fiber reinforced polylactic acid composites by 3D printing.* Journal of Materials Processing Technology, 2016. **238**: p. 218-225.

13. Marton, A.M.S., F.M. Monticeli, N.C. Zanini, R.F.S. Barbosa, S.F. Medeiros, D.S. Rosa, and D.R. Mulinari, *Revalorization of Australian royal palm (Archontophoenix alexandrae) waste as reinforcement in acrylonitrile butadiene*

styrene (ABS) for use in 3D printing pen. Journal of Cleaner Production, 2022. **365**.

14. Alfaer, A., Y. Aljabri, A. Alameer, M.A. Illah, H. Thubab, and A. Thubab, *Applications, benefits, and limitations of fiber-reinforced composites in fixed prosthodontics.* Int J Community Med Public Health, 2023. **10**(11): p. 4462-7.

15. Faheed, N.K., *Advantages of natural fiber composites for biomedical applications: a review of recent advances.* Emergent Materials, 2024. **7**(1): p. 63-75.

16. Alarifi, I.M., *A performance evaluation study of 3d printed nylon/glass fiber and nylon/carbon fiber composite materials.* Journal of Materials Research and Technology, 2022. **21**: p. 884-892.

17. Cao, L., J. Xiao, J.K. Kim, and X. Zhang, *Effect of post-process treatments on mechanical properties and surface characteristics of 3D printed short glass fiber reinforced PLA/TPU using the FDM process.* CIRP Journal of Manufacturing Science and Technology, 2023. **41**: p. 135-143.

18. Rijckaert, S., L. Daelemans, L. Cardon, M. Boone, W. Van Paepegem, and K. De Clerck, *Continuous fiber-reinforced aramid/PETG 3D-printed composites with high fiber loading through fused filament fabrication.* Polymers, 2022. **14**(2): p. 298.

19. Akhoundi, B., A.H. Behravesh, and A. Bagheri Saed, *Improving mechanical properties of continuous fiber-reinforced thermoplastic composites produced by FDM 3D printer.* Journal of Reinforced Plastics and Composites, 2018. **38**(3): p. 99-116.

20. Bi, H., Z. Ren, R. Guo, M. Xu, and Y. Song, *Fabrication of flexible wood flour/thermoplastic polyurethane elastomer composites using fused deposition molding.* Industrial crops and products, 2018. **122**: p. 76-84.

21. Di Pompeo, V., A. Forcellese, T. Mancia, M. Simoncini, and A. Vita, *Effect of Geometric Parameters and Moisture Content on the Mechanical Performances of 3D-Printed Isogrid Structures in Short Carbon Fiber-Reinforced Polyamide.* Journal of Materials Engineering and Performance, 2021. **30**(7): p. 5100-5107.

22. Mandala, R., A.P. Bannoth, S. Akella, V.K. Rangari, and D. Kodali, *A short review on fused deposition modeling 3D printing of bio-based polymer nanocomposites.* Journal of Applied Polymer Science, 2021. **139**(14).

23. Siddiqui, M.N., H.H. Redhwi, I. Tsagkalias, E.C. Vouvoudi, and D.S. Achilias, *Development of bio-composites with enhanced antioxidant activity based on poly (lactic acid) with thymol, carvacrol, limonene, or cinnamaldehyde for active food packaging.* Polymers, 2021. **13**(21): p. 3652.

24. Yadav, D.K., R. Srivastava, and S. Dev, *Design & fabrication of ABS part by FDM for automobile application.* Materials Today: Proceedings, 2020. **26**:

p. 2089-2093.

25. Couture, A., G. Lebrun, and L. Laperrière, *Mechanical properties of polylactic acid (PLA) composites reinforced with unidirectional flax and flax-paper layers.* Composite Structures, 2016. **154**: p. 286-295.

26. Antony, S., A. Cherouat, and G. Montay, *Fabrication and Characterization of Hemp Fibre Based 3D Printed Honeycomb Sandwich Structure by FDM Process.* Applied Composite Materials, 2020. **27**(6): p. 935-953.

27. Muller, M., P. Jirku, V. Sleger, R.K. Mishra, M. Hromasova, and J. Novotny, *Effect of Infill Density in FDM 3D Printing on Low-Cycle Stress of Bamboo-Filled PLA-Based Material.* Polymers (Basel), 2022. **14**(22).

28. Krapez Tomec, D. and M. Kariz, *Use of Wood in Additive Manufacturing: Review and Future Prospects.* Polymers (Basel), 2022. **14**(6).

29. Bhayana, M., J. Singh, A. Sharma, and M. Gupta, *A review on optimized FDM 3D printed Wood/PLA bio composite material characteristics.* Materials Today: Proceedings, 2023.

30. Rajak, D.K., P.H. Wagh, and E. Linul, *Manufacturing technologies of carbon/glass fiber-reinforced polymer composites and their properties: A review.* Polymers, 2021. **13**(21): p. 3721.

31. Wang, P., B. Zou, S. Ding, L. Li, and C. Huang, *Effects of FDM-3D printing parameters on mechanical properties and microstructure of CF/PEEK and GF/PEEK.* Chinese Journal of Aeronautics, 2021. **34**(9): p. 236-246.

32. Anwer, M.A.S. and H.E. Naguib, *Study on the morphological, dynamic mechanical and thermal properties of PLA carbon nanofibre composites.* Composites Part B: Engineering, 2016. **91**: p. 631-639.

33. Tian, X., T. Liu, Q. Wang, A. Dilmurat, D. Li, and G. Ziegmann, *Recycling and remanufacturing of 3D printed continuous carbon fiber reinforced PLA composites.* Journal of Cleaner Production, 2017. **142**: p. 1609-1618.

34. Ksouri, I., N. Guermazi, N. Haddar, and H.F. Ayedi, *Effects of processing steps and hygrothermal ageing on mechanical performance of PA6GF30 composite: Interfacial shear strength.* Polymer Composites, 2016. **39**(2): p. 504-512.

35. Sathishkumar, T., S. Satheeshkumar, and J. Naveen, *Glass fiber-reinforced polymer composites–a review.* Journal of reinforced plastics and composites, 2014. **33**(13): p. 1258-1275.

36. Li, H., C. Richards, and J. Watson, *High-performance glass fiber development for composite applications.* International Journal of Applied Glass Science, 2014. **5**(1): p. 65-81.

37. Gkartzou, E., E.P. Koumoulos, and C.A. Charitidis, *Production and 3D printing processing of bio-based thermoplastic filament.* Manufacturing Review, 2017. **4**.

38. Jiang, L., X. Peng, and D. Walczyk, *3D printing of biofiber-reinforced composites and their mechanical properties: a review.* Rapid Prototyping Journal, 2020. **26**(6): p. 1113-1129.

39. Zhang, H., Y. Guo, K. Jiang, D.L. Bourell, D. Zhao, Y. Yu, P. Wang, and Z. Li, *A review of selective laser sintering of wood-plastic composites.* 2016.

40. Ferreira, R.T.L., I.C. Amatte, T.A. Dutra, and D. Bürger, *Experimental characterization and micrography of 3D printed PLA and PLA reinforced with short carbon fibers.* Composites Part B: Engineering, 2017. **124**: p. 88-100.

41. Melenka, G.W., B.K.O. Cheung, J.S. Schofield, M.R. Dawson, and J.P. Carey, *Evaluation and prediction of the tensile properties of continuous fiber-reinforced 3D printed structures.* Composite Structures, 2016. **153**: p. 866-875.

42. Srinidhi, M.S., R. Soundararajan, K.S. Satishkumar, and S. Suresh, *Enhancing the FDM infill pattern outcomes of mechanical behavior for as-built and annealed PETG and CFPETG composites parts.* Materials Today: Proceedings, 2021. **45**: p. 7208-7212.

43. Bodaghi, M., A. Sadooghi, M. Bakhshi, S.J. Hashemi, K. Rahmani, and M. Keshavarz Motamedi, *Glass Fiber Reinforced Acrylonitrile Butadiene Styrene Composite Gears by FDM 3D Printing.* Advanced Materials Interfaces, 2023. **10**(27).

44. Sodeifian, G., S. Ghaseminejad, and A.A. Yousefi, *Preparation of polypropylene/short glass fiber composite as Fused Deposition Modeling (FDM) filament.* Results in Physics, 2019. **12**: p. 205-222.

45. Rana, R. and R. Purohit, *A Review on mechanical property of sisal glass fiber reinforced polymer composites.* Materials Today: Proceedings, 2017. **4**(2): p. 3466-3476.

46. Hashemi, S.J., A. Sadooghi, K. Rahmani, and S. Akbari, *Experimental study of the effect of temperature and velocity in channel forming of polyvinyl chloride composite reinforced by 3D-fiberglass with an aluminum middle layer.* SN Applied Sciences, 2022. **4**(3): p. 66.

47. Rahmanian, S., A. Suraya, B. Roshanravan, R. Othman, A. Nasser, R. Zahari, and E. Zainudin, *The influence of multiscale fillers on the rheological and mechanical properties of carbon-nanotube–silica-reinforced epoxy composite.* Materials & Design, 2015. **88**: p. 227-235.

48. Wang, P., B. Zou, and S. Ding, *Modeling of surface roughness based on heat transfer considering diffusion among deposition filaments for FDM 3D printing heat-resistant resin.* Applied Thermal Engineering, 2019. **161**: p. 114064.

49. Xie, Y., C.A. Hill, Z. Xiao, H. Militz, and C. Mai, *Silane coupling agents used for natural fiber/polymer composites: A review.* Composites Part A: Applied Science and Manufacturing, 2010. **41**(7): p. 806-819.

50. Wang, P., B. Zou, H. Xiao, S. Ding, and C. Huang, *Effects of printing parameters of fused deposition modeling on mechanical properties, surface quality, and microstructure of PEEK.* Journal of Materials Processing Technology, 2019. **271**: p. 62-74.

51. Ning, F., W. Cong, J. Qiu, J. Wei, and S. Wang, *Additive manufacturing of carbon fiber reinforced thermoplastic composites using fused deposition modeling.* Composites Part B: Engineering, 2015. **80**: p. 369-378.

52. Andrew, J.J. and H. Dhakal, *Sustainable biobased composites for advanced applications: recent trends and future opportunities–A critical review.* Composites Part C: Open Access, 2022. **7**: p. 100220.

53. Mohanty, A.K., M. Misra, and L. Drzal, *Sustainable bio-composites from renewable resources: opportunities and challenges in the green materials world.* Journal of Polymers and the Environment, 2002. **10**: p. 19-26.

54. Wu, Y., C. Xia, L. Cai, A.C. Garcia, and S.Q. Shi, *Development of natural fiber-reinforced composite with comparable mechanical properties and reduced energy consumption and environmental impacts for replacing automotive glass-fiber sheet molding compound.* Journal of Cleaner Production, 2018. **184**: p. 92-100.

55. Supian, A., M. Asyraf, A. Syamsir, Q. Ma, K. Hazrati, M. Azlin, M. Mubarak Ali, A. Ghani, L.S. Hua, and S. SaifulAzry, *Kenaf/glass fiber-reinforced polymer composites: Pioneering sustainable materials with enhanced mechanical and tribological properties.* Polymer Composites, 2024.

56. Cakir Yigit, N. and I. Karagoz, *A review of recent advances in bio-based polymer composite filaments for 3D printing.* Polymer-Plastics Technology and Materials, 2023. **62**(9): p. 1077-1095.

57. Avella, M., A. Buzarovska, M.E. Errico, G. Gentile, and A. Grozdanov, *Eco-Challenges of Bio-Based Polymer Composites.* Materials, 2009. **2**(3): p. 911-925.

58. Calì, M., G. Pascoletti, M. Gaeta, G. Milazzo, and R. Ambu, *New filaments with natural fillers for FDM 3D printing and their applications in biomedical field.* Procedia Manufacturing, 2020. **51**: p. 698-703.

59. Tokoro, R., D.M. Vu, K. Okubo, T. Tanaka, T. Fujii, and T. Fujiura, *How to improve mechanical properties of polylactic acid with bamboo fibers.* Journal of Materials Science, 2007. **43**(2): p. 775-787.

60. Travieso-Rodriguez, J.A., M.D. Zandi, R. Jerez-Mesa, and J. Lluma-Fuentes, *Fatigue behavior of PLA-wood composite manufactured by fused filament fabrication.* Journal of Materials Research and Technology, 2020. **9**(4): p. 8507-8516.

61. Aliotta, L., A. Vannozzi, D. Bonacchi, M.B. Coltelli, and A. Lazzeri, *Analysis, Development, and Scaling-Up of Poly(lactic acid) (PLA) Biocomposites with Hazelnuts Shell Powder (HSP).* Polymers (Basel), 2021. **13**(23).

62. Kariz, M., M. Sernek, M. Obućina, and M.K. Kuzman, *Effect of wood content in FDM filament on properties of 3D printed parts.* Materials Today Communications, 2018. **14**: p. 135-140.

63. Pandey, K., R. Antil, S. Saha, J. Jacob, and B. Balavairavan, *Poly(lactic acid)/thermoplastic polyurethane/wood flour composites: evaluation of morphology, thermal, mechanical and biodegradation properties.* Materials Research Express, 2019. **6**(12).

64. Yang, T.-C. and C.-H. Yeh, *Morphology and mechanical properties of 3D printed wood fiber/polylactic acid composite parts using fused deposition modeling (FDM): the effects of printing speed.* Polymers, 2020. **12**(6): p. 1334.

65. Le Duigou, A., M. Castro, R. Bevan, and N. Martin, *3D printing of wood fibre biocomposites: From mechanical to actuation functionality.* Materials & Design, 2016. **96**: p. 106-114.

66. Tao, Y., H. Wang, Z. Li, P. Li, and S.Q. Shi, *Development and application of wood flour-filled polylactic acid composite filament for 3D printing.* Materials, 2017. **10**(4): p. 339.

67. Haryńska, A., H. Janik, M. Sienkiewicz, B. Mikolaszek, and J. Kucińska-Lipka, *PLA–Potato Thermoplastic Starch Filament as a Sustainable Alternative to the Conventional PLA Filament: Processing, Characterization, and FFF 3D Printing.* ACS Sustainable Chemistry & Engineering, 2021. **9**(20): p. 6923-6938.

68. Liu, H., H. He, X. Peng, B. Huang, and J. Li, *Three-dimensional printing of poly(lactic acid) bio-based composites with sugarcane bagasse fiber: Effect of printing orientation on tensile performance.* Polymers for Advanced Technologies, 2019. **30**(4): p. 910-922.

69. Costa, I.L.M., P.H.F. Pereira, A.M. Claro, N.C.d. Amaral, H.d.S. Barud, R.B. Ribeiro, and D.R. Mulinari, *3D-printing pen from valorization of pine cone residues as reinforcement in acrylonitrile butadiene styrene (ABS): Microstructure and thermal properties.* Journal of Thermoplastic Composite Materials, 2021. **36**(2): p. 535-554.

70. Bajwa, D., M. Eichers, J. Shojaeiarani, and A. Kallmeyer, *Influence of biobased plasticizers on 3D printed polylactic acid composites filled with sustainable biofiller.* Industrial Crops and Products, 2021. **173**.

71. Taborda-Ríos, J.A., O. López-Botello, P. Zambrano-Robledo, L.A. Reyes-Osorio, and C. Garza, *Mechanical characterisation of a bamboo fibre/polylactic acid composite produced by fused deposition modelling.* Journal of Reinforced Plastics and Composites, 2020. **39**(23-24): p. 932-944.

72. Long, H., Z. Wu, Q. Dong, Y. Shen, W. Zhou, Y. Luo, C. Zhang, and X. Dong, *Mechanical and thermal properties of bamboo fiber reinforced polypropylene/polylactic acid composites for 3D printing.* Polymer Engineering & Science, 2018. **59**(s2).

73. Hua, L., X. Wang, L. Ding, S. Zeng, J. Liu, and Z. Wu, *Effects of fabrication parameters on the mechanical properties of short basalt-fiber-reinforced thermoplastic composites for fused deposition modeling-based 3D printing.* Polymer Composites, 2023. **44**(6): p. 3341-3357.

74. Esmaeili, M., G. Pircheraghi, R. Bagheri, and V. Altstädt, *Poly (lactic acid)/coplasticized thermoplastic starch blend: Effect of plasticizer migration on rheological and mechanical properties.* Polymers for Advanced Technologies, 2019. **30**(4): p. 839-851.

75. Diestel, S. and A. Krause, *Wood-based composites with thermoplastic polyurethane as matrix polymer.* Journal of Applied Polymer Science, 2018. **135**(25).

76. Bergenstråhle, M., J. Wohlert, M.E. Himmel, and J.W. Brady, *Simulation studies of the insolubility of cellulose.* Carbohydrate research, 2010. **345**(14): p. 2060-2066.

77. Tanabe, I., *Double-ECO model technologies for an environmentally-friendly manufacturing.* Procedia CIRP, 2016. **48**: p. 495-501.

78. Ecker, J.V., A. Haider, I. Burzic, A. Huber, G. Eder, and S. Hild, *Mechanical properties and water absorption behaviour of PLA and PLA/wood composites prepared by 3D printing and injection moulding.* Rapid Prototyping Journal, 2019. **25**(4): p. 672-678.

79. Depuydt, D., M. Balthazar, K. Hendrickx, W. Six, E. Ferraris, F. Desplentere, J. Ivens, and A.W. Van Vuure, *Production and characterization of bamboo and flax fiber reinforced polylactic acid filaments for fused deposition modeling (FDM).* Polymer Composites, 2018. **40**(5): p. 1951-1963.

80. Yu, S., Y.H. Hwang, J.Y. Hwang, and S.H. Hong, *Analytical study on the 3D-printed structure and mechanical properties of basalt fiber-reinforced PLA composites using X-ray microscopy.* Composites Science and Technology, 2019. **175**: p. 18-27.

81. Ergene, B., Y.E. İnci, B. Çetintaş, and B. Daysal, *An experimental study on the wear performance of 3D printed polylactic acid and carbon fiber reinforced polylactic acid parts: Effect of infill rate and water absorption time.* Polymer Composites, 2024.

82. Liu, Z., Q. Lei, and S. Xing, *Mechanical characteristics of wood, ceramic, metal and carbon fiber-based PLA composites fabricated by FDM.* Journal of Materials Research and Technology, 2019. **8**(5): p. 3741-3751.

83. Zhang, Z., *The effects of moisture conditioning on the mechanical properties of the fused deposition modeling (FDM) printed carbon fiber reinforced composites*. 2023.

84. Guo, A., C. Liu, S. Li, X. Zhou, J. Wang, S. Wang, P. Qu, and Y. Hu, *Water absorption rates and mechanical properties of material extrusion-printed continuous carbon fiber-reinforced nylon composites.* Journal of Materials

Research and Technology, 2022. **21**: p. 3098-3112.

85. Hassan, A., N.A. Rahman, and R. Yahya, *Moisture absorption effect on thermal, dynamic mechanical and mechanical properties of injection-molded short glass-fiber/polyamide 6,6 composites.* Fibers and Polymers, 2012. **13**(7): p. 899-906.

86. Hadi, A., A. Kadauw, and H. Zeidler, *The effect of printing temperature and moisture on tensile properties of 3D printed glass fiber reinforced nylon 6.* Materials Today: Proceedings, 2023. **91**: p. 48-55.

87. Ostberg, G.M. and J.C. Seferis, *Annealing effects on the crystallinity of polyetheretherketone (PEEK) and its carbon fiber composite.* Journal of Applied Polymer Science, 1987. **33**(1): p. 29-39.

88. Batista, N.L., P. Olivier, G. Bernhart, M.C. Rezende, and E.C. Botelho, *Correlation between degree of crystallinity, morphology and mechanical properties of PPS/carbon fiber laminates.* Materials Research, 2016. **19**(1): p. 195-201.

89. Wong, C.Y., W.Y. Wong, K.S. Loh, and A.B. Mohamad, *Study of the plasticising effect on polymer and its development in fuel cell application.* Renewable and Sustainable Energy Reviews, 2017. **79**: p. 794-805.

90. Gao, H., Y. Sun, M. Wang, Z. Wang, G. Han, L. Jin, P. Lin, Y. Xia, and K. Zhang, *Mechanically robust and reprocessable acrylate vitrimers with hydrogen-bond-integrated networks for photo-3D printing.* ACS Applied Materials & Interfaces, 2020. **13**(1): p. 1581-1591.

91. Mulakkal, M.C., R.S. Trask, V.P. Ting, and A.M. Seddon, *Responsive cellulose-hydrogel composite ink for 4D printing.* Materials & Design, 2018. **160**: p. 108-118.

92. Kamau-Devers, K., Z. Kortum, and S.A. Miller, *Hydrothermal aging of bio-based poly (lactic acid)(PLA) wood polymer composites: Studies on sorption behavior, morphology, and heat conductance.* Construction and Building Materials, 2019. **214**: p. 290-302.

93. Sydney Gladman, A., E.A. Matsumoto, R.G. Nuzzo, L. Mahadevan, and J.A. Lewis, *Biomimetic 4D printing.* Nature materials, 2016. **15**(4): p. 413-418.

94. Burgert, I. and P. Fratzl, *Actuation systems in plants as prototypes for bioinspired devices.* Philosophical Transactions of the Royal Society A: Mathematical, Physical and Engineering Sciences, 2009. **367**(1893): p. 1541-1557.

95. Correa, D., A. Papadopoulou, C. Guberan, N. Jhaveri, S. Reichert, A. Menges, and S. Tibbits, *3D-Printed Wood: Programming Hygroscopic Material Transformations.* 3D Printing and Additive Manufacturing, 2015. **2**(3): p. 106-116.

96. Ayrilmis, N., R. Nagarajan, and M.K. Kuzman, *Effects of the Face/Core*

Layer Ratio on the Mechanical Properties of 3D Printed Wood/Polylactic Acid (PLA) Green Biocomposite Panels with a Gyroid Core. Polymers (Basel), 2020. **12**(12).

97. Wohlert, M., T. Benselfelt, L. Wågberg, I. Furó, L.A. Berglund, and J. Wohlert, *Cellulose and the role of hydrogen bonds: not in charge of everything.* Cellulose, 2022: p. 1-23.

98. Singh, G. and A. Verma, *A Brief Review on injection moulding manufacturing process.* Materials Today: Proceedings, 2017. **4**(2): p. 1423-1433.

99. Farooque, R., M. Asjad, and S. Rizvi, *A current state of art applied to injection moulding manufacturing process–a review.* Materials Today: Proceedings, 2021. **43**: p. 441-446.

100. Ecker, J.V., C. Fürst, C. Unterweger, B. Plank, and A. Haider. *3D computed tomography as quality control tool in advanced composite manufacturing*. in *Proceedings of the 8th Conference on Industrial Computed Tomography, Wels, Austria*. 2018.

101. Huda, M., L. Drzal, M. Misra, and A. Mohanty, *Wood-fiber-reinforced poly (lactic acid) composites: evaluation of the physicomechanical and morphological properties.* Journal of applied polymer science, 2006. **102**(5): p. 4856-4869.

102. Yew, G., A.M. Yusof, Z.M. Ishak, and U. Ishiaku, *Water absorption and enzymatic degradation of poly (lactic acid)/rice starch composites.* Polymer Degradation and stability, 2005. **90**(3): p. 488-500.

103. Krapez Tomec, D., A. Straze, A. Haider, and M. Kariz, *Hygromorphic Response Dynamics of 3D-Printed Wood-PLA Composite Bilayer Actuators.* Polymers (Basel), 2021. **13**(19).

104. Bai, J. and G. Bu, *Progress in 4D printing technology.* J. Adv. Manuf. Sci. Technol, 2022. **2**(1): p. 2022001-2022001.

105. Aghajani, S., C. Wu, Q. Li, and J. Fang, *Additively manufactured composite lattices: A state-of-the-art review on fabrications, architectures, constituent materials, mechanical properties, and future directions.* Thin-Walled Structures, 2023: p. 111539.

106. Zeng, C., L. Liu, W. Bian, J. Leng, and Y. Liu, *Compression behavior and energy absorption of 3D printed continuous fiber reinforced composite honeycomb structures with shape memory effects.* Additive Manufacturing, 2021. **38**.

107. Jackowski, J., P. Posuniak, K. Zielonka, and R. Jurecki, *Experimental Testing of Energy-Absorbing Structures Used to Enhance the Crashworthiness of the Vehicles.* Energies, 2023. **16**(5): p. 2183.

108. de Andrade, F.M. and C.A. Magalhães, *Evolutionary structural optimization in energy absorption structures.* Advances in Engineering Software, 2022. **169**: p. 103145.

109. Quan, C., B. Han, Z. Hou, Q. Zhang, X. Tian, and T.J. Lu, *3d printed continuous fiber reinforced composite auxetic honeycomb structures.* Composites Part B: Engineering, 2020. **187**.

110. Damanpack, A., A. Sousa, and M. Bodaghi, *Porous PLAs with controllable density by FDM 3D printing and chemical foaming agent.* Micromachines, 2021. **12**(8): p. 866.

111. Li, Y., Z. Feng, L. Hao, L. Huang, C. Xin, Y. Wang, E. Bilotti, K. Essa, H. Zhang, and Z. Li, *A review on functionally graded materials and structures via additive manufacturing: from multi-scale design to versatile functional properties.* Advanced Materials Technologies, 2020. **5**(6): p. 1900981.

112. Chen, K., F. Yang, C. Yao, T. Liu, and H. Jiang, *Single material FDM printed nacre-like composite structure with high fracture resistance: Utilizing interface as soft phase.* Composites Communications, 2023. **42**: p. 101682.

113. Santiago, R., H. Ramos, S. AlMahri, O. Banabila, H. Alabdouli, D.-W. Lee, A. Aziz, N. Rajput, M. Alves, and Z. Guan, *Modelling and optimisation of TPMS-based lattices subjected to high strain-rate impact loadings.* International Journal of Impact Engineering, 2023. **177**: p. 104592.

114. Bezazi, A., C. Remillat, P. Innocenti, and F. Scarpa, *In-plane mechanical and thermal conductivity properties of a rectangular–hexagonal honeycomb structure.* Composite Structures, 2008. **84**(3): p. 248-255.

115. Dou, H., W. Ye, D. Zhang, Y. Cheng, and C. Wu, *Comparative study on in-plane compression properties of 3D printed continuous carbon fiber reinforced composite honeycomb and aluminum alloy honeycomb.* Thin-Walled Structures, 2022. **176**.

116. Cheng, Y., J. Li, X. Qian, and S. Rudykh, *3D printed recoverable honeycomb composites reinforced by continuous carbon fibers.* Composite Structures, 2021. **268**.

117. Bates, S.R.G., I.R. Farrow, and R.S. Trask, *3D printed polyurethane honeycombs for repeated tailored energy absorption.* Materials & Design, 2016. **112**: p. 172-183.

118. Bezazi, A. and F. Scarpa, *Mechanical behaviour of conventional and negative Poisson's ratio thermoplastic polyurethane foams under compressive cyclic loading.* International Journal of fatigue, 2007. **29**(5): p. 922-930.

119. Scarpa, F., P. Pastorino, A. Garelli, S. Patsias, and M. Ruzzene, *Auxetic compliant flexible PU foams: static and dynamic properties.* physica status solidi (b), 2005. **242**(3): p. 681-694.

120. Kim, D.H., S. Kim, S.R. Park, N.X. Fang, and Y.T. Cho, *Shape-Deformed Mushroom-like Reentrant Structures for Robust Liquid-Repellent Surfaces.* ACS Appl Mater Interfaces, 2021. **13**(28): p. 33618-33626.

121. Liu, W., N. Wang, T. Luo, and Z. Lin, *In-plane dynamic crushing of*

re-entrant auxetic cellular structure. Materials & Design, 2016. **100**: p. 84-91.

122. Dong, K., M. Panahi-Sarmad, Z. Cui, X. Huang, and X. Xiao, *Electro-induced shape memory effect of 4D printed auxetic composite using PLA/TPU/CNT filament embedded synergistically with continuous carbon fiber: A theoretical & experimental analysis.* Composites Part B: Engineering, 2021. **220**.

123. Essassi, K., J.-l. Rebiere, A. El Mahi, M.A. Ben Souf, A. Bouguecha, and M. Haddar, *Experimental and analytical investigation of the bending behaviour of 3D-printed bio-based sandwich structures composites with auxetic core under cyclic fatigue tests.* Composites Part A: Applied Science and Manufacturing, 2020. **131**.

124. Mines, R., S. Tsopanos, Y. Shen, R. Hasan, and S. McKown, *Drop weight impact behaviour of sandwich panels with metallic micro lattice cores.* International Journal of Impact Engineering, 2013. **60**: p. 120-132.

125. Taherkhani, B., M.B. Azizkhani, J. Kadkhodapour, A.P. Anaraki, and S. Rastgordani, *Highly sensitive, piezoresistive, silicone/carbon fiber-based auxetic sensor for low strain values.* Sensors and Actuators A: Physical, 2020. **305**.

126. Moetazedian, A., A. Gleadall, X. Han, and V.V. Silberschmidt, *Effect of environment on mechanical properties of 3D printed polylactide for biomedical applications.* Journal of the mechanical behavior of biomedical materials, 2020. **102**: p. 103510.

127. Yu, S., J. Sun, and J. Bai, *Investigation of functionally graded TPMS structures fabricated by additive manufacturing.* Materials & Design, 2019. **182**: p. 108021.

128. Lal Lazar, P.J., J. Subramanian, E. Natarajan, K. Markandan, and S. Ramesh, *Anisotropic structure-property relations of FDM printed short glass fiber reinforced polyamide TPMS structures under quasi-static compression.* Journal of Materials Research and Technology, 2023. **24**: p. 9562-9579.

129. Saleh, M., S. Anwar, A.M. Al-Ahmari, and A. Alfaify, *Compression Performance and Failure Analysis of 3D-Printed Carbon Fiber/PLA Composite TPMS Lattice Structures.* Polymers (Basel), 2022. **14**(21).

130. He, P., J. Zhao, J. Zhang, B. Li, Z. Gou, M. Gou, and X. Li, *Bioprinting of skin constructs for wound healing.* Burns & trauma, 2018. **6**.

131. Dong, Z. and X. Zhao, *Application of TPMS structure in bone regeneration.* Engineered Regeneration, 2021. **2**: p. 154-162.

132. Zhong, M., W. Zhou, H. Xi, Y. Liang, and Z. Wu, *Double-level energy absorption of 3d printed tpms cellular structures via wall thickness gradient design.* Materials, 2021. **14**(21): p. 6262.

133. Zheng, X., F. Duan, Z. Song, H. Mo, Z. Li, Y. Song, Y. Su, and X. Wang, *A TMPS-designed personalized mandibular scaffolds with optimized SLA parameters and mechanical properties.* Frontiers in Materials, 2022. **9**: p.

966031.

134. Shi, X., W. Liao, P. Li, C. Zhang, T. Liu, C. Wang, and J. Wu, *Comparison of compression performance and energy absorption of lattice structures fabricated by selective laser melting.* Advanced Engineering Materials, 2020. **22**(11): p. 2000453.

135. AlMahri, S., R. Santiago, D.-W. Lee, H. Ramos, H. Alabdouli, M. Alteneiji, Z. Guan, W. Cantwell, and M. Alves, *Evaluation of the dynamic response of triply periodic minimal surfaces subjected to high strain-rate compression.* Additive Manufacturing, 2021. **46**: p. 102220.

136. Wright, W.J., H. Koerner, D. Rapking, A. Abbott, and E. Celik, *Rapid fiber alignment quantification in direct write printing of short fiber reinforced composites.* Composites Part B: Engineering, 2022. **236**: p. 109814.

137. Mandava, P.K., R. Joyce, J.B. Day, and R. Salary. *Investigation of the Mechanical Properties of Additively Manufactured Bone Tissue Scaffolds, Composed of Polyamide, Polyolefin, and Cellulose Fibers*. in *International Manufacturing Science and Engineering Conference*. 2022. American Society of Mechanical Engineers.

138. Veeman, D., S. Palaniyappan, G.J. Surendhar, and R. Shanmugam, *Process optimization of compressive property and dimensional error on wood polylactic acid gyroid-structured polymer composite.* Journal of Reinforced Plastics and Composites, 2022.

139. KV, S., J. Baskar, and P. Paul, *Overview on L9 taguchi optimizational method.* International Journal of Advanced Research in Engineering and Technology, 2019. **10**(2).

140. Levy, G.N., R. Schindel, and J.-P. Kruth, *Rapid manufacturing and rapid tooling with layer manufacturing (LM) technologies, state of the art and future perspectives.* CIRP annals, 2003. **52**(2): p. 589-609.

141. Brooks, H. and S. Molony, *Design and evaluation of additively manufactured parts with three dimensional continuous fibre reinforcement.* Materials & Design, 2016. **90**: p. 276-283.

142. Turner, B.N., R. Strong, and S.A. Gold, *A review of melt extrusion additive manufacturing processes: I. Process design and modeling.* Rapid prototyping journal, 2014. **20**(3): p. 192-204.

143. Anitha, R., S. Arunachalam, and P. Radhakrishnan, *Critical parameters influencing the quality of prototypes in fused deposition modelling.* Journal of Materials Processing Technology, 2001. **118**(1-3): p. 385-388.

144. Chakraborty, S. and M.C. Biswas, *3D printing technology of polymer-fiber composites in textile and fashion industry: A potential roadmap of concept to consumer.* Composite Structures, 2020. **248**: p. 112562.

145. Zaneldin, E., W. Ahmed, A. Mansour, and A.E. Hassan, *Dimensional stability of 3D printed objects made from plastic waste using FDM: Potential*

construction applications. Buildings, 2021. **11**(11): p. 516.

146. Muthe, L.P., K. Pickering, and C. Gauss, *A review of 3D/4D printing of poly-lactic acid composites with bio-derived reinforcements.* Composites Part C: Open Access, 2022. **8**: p. 100271.

147. Heidari-Rarani, M., M. Rafiee-Afarani, and A. Zahedi, *Mechanical characterization of FDM 3D printing of continuous carbon fiber reinforced PLA composites.* Composites Part B: Engineering, 2019. **175**: p. 107147.

148. Zeng, C., L. Liu, W. Bian, J. Leng, and Y. Liu, *Bending performance and failure behavior of 3D printed continuous fiber reinforced composite corrugated sandwich structures with shape memory capability.* Composite Structures, 2021. **262**: p. 113626.

149. Gama, N., A. Ferreira, A. Barros-Timmons, and D. Evtuguin, *Polyamide 6/modified pine bark particle composites for additive manufacturing.* Journal of Materials Science, 2021. **56**: p. 19093-19105.

150. La Mantia, F. and M. Morreale, *Green composites: A brief review.* Composites Part A: Applied Science and Manufacturing, 2011. **42**(6): p. 579-588.

151. Tao, Y., L. Pan, D. Liu, and P. Li, *A case study: Mechanical modeling optimization of cellular structure fabricated using wood flour-filled polylactic acid composites with fused deposition modeling.* Composite Structures, 2019. **216**: p. 360-365.

152. Huang, Y., S. Löschke, and G. Proust, *In the mix: The effect of wood composition on the 3D printability and mechanical performance of wood-plastic composites.* Composites Part C: Open Access, 2021. **5**: p. 100140.

153. International, A., *Standard Test Method for Tensile Properties of Plastics*. 2022.

154. Li, M., Y. Xu, and J. Fang, *Orthotropic mechanical properties of PLA materials fabricated by fused deposition modeling.* Thin-Walled Structures, 2024. **199**: p. 111800.

155. Linforth, S., T. Ngo, P. Tran, D. Ruan, and R. Odish, *Investigation of the auxetic oval structure for energy absorption through quasi-static and dynamic experiments.* International journal of impact engineering, 2021. **147**: p. 103741.

156. Dizon, J.R.C., A.H. Espera Jr, Q. Chen, and R.C. Advincula, *Mechanical characterization of 3D-printed polymers.* Additive manufacturing, 2018. **20**: p. 44-67.

157. International, A., *Standard Test Method for Measurement of Fracture Toughness*. 2021.

158. International, A., *Standard Test Methods for Plane-Strain Fracture Toughness and Crack Propagation of Plastics*. 2021.

159. Li, T., Y. Chen, and L. Wang, *Enhanced fracture toughness in architected interpenetrating phase composites by 3D printing.* Composites Science and Technology, 2018. **167**: p. 251-259.

160. Lampron, O., A. Lingua, D. Therriault, and M. Lévesque, *Characterization of the non-isotropic tensile and fracture behavior of unidirectional polylactic acid parts manufactured by material extrusion.* Additive Manufacturing, 2023. **61**: p. 103369.

161. Kotsilkova, R. and S. Tabakova, *Exploring effects of graphene and carbon nanotubes on rheology and flow instability for designing printable polymer nanocomposites.* Nanomaterials, 2023. **13**(5): p. 835.

162. Martínez-Sánchez, J.A., P.E. Romero, F. Comino, E. Molero, and M. Ruiz de Adana, *Effect of Material Extrusion Process Parameters to Enhance Water Vapour Adsorption Capacity of PLA/Wood Composite Printed Parts.* Polymers, 2024. **16**(20): p. 2934.

163. Balla, V.K., K.H. Kate, J. Satyavolu, P. Singh, and J.G.D. Tadimeti, *Additive manufacturing of natural fiber reinforced polymer composites: Processing and prospects.* Composites Part B: Engineering, 2019. **174**: p. 106956.

164. Lage-Rivera, S., A. Ares-Pernas, M.S. Dopico-García, J. Covas, and M.J. Abad, *Comparing lignin and spent coffee grounds as bio-fillers in PLA 3D-printable filaments.* Polymer Composites, 2024. **45**(16): p. 14566-14579.

165. Siddiqui, V.U., J. Yusuf, S. Sapuan, M.Z. Hasan, M.M. Mudah Bistari, and Z.G. Mohammadsalih, *Mechanical properties and flammability analysis of wood fiber filled polylactic acid (PLA) composites using additive manufacturing.* Journal of Natural Fibers, 2024. **21**(1): p. 2409868.

166. Mazur, K.E., A. Borucka, P. Kaczor, S. Gądek, R. Bogucki, D. Mirzewiński, and S. Kuciel, *Mechanical, thermal and microstructural characteristic of 3D printed polylactide composites with natural fibers: wood, bamboo and cork.* Journal of Polymers and the Environment, 2022. **30**(6): p. 2341-2354.

167. Yu, I.K., O.Y. Chan, Q. Zhang, L. Wang, K.-H. Wong, and D.C. Tsang, *Upcycling of spent tea leaves and spent coffee grounds into sustainable 3D-printing materials: natural plasticization and low-energy fabrication.* ACS Sustainable Chemistry & Engineering, 2023. **11**(16): p. 6230-6240.

168. PP, M.S., J. Pitchaimani, and M. Doddamani, *A short banana fiber—PLA filament for 3D printing: Development and characterization.* Polymer Composites, 2025. **46**(6): p. 4863-4880.

169. Zhao, P., C. Rao, F. Gu, N. Sharmin, and J. Fu, *Close-looped recycling of polylactic acid used in 3D printing: An experimental investigation and life cycle assessment.* Journal of Cleaner Production, 2018. **197**: p. 1046-1055.

170. Beltrán, F., V. Lorenzo, J. Acosta, M. De La Orden, and J.M. Urreaga, *Effect of simulated mechanical recycling processes on the structure and properties of poly (lactic acid).* Journal of environmental management, 2018. **216**: p. 25-31.

171. Beltrán, F., V. Lorenzo, M. De la Orden, and J. Martínez-Urreaga, *Effect*

of different mechanical recycling processes on the hydrolytic degradation of poly (l-lactic acid). Polymer Degradation and Stability, 2016. **133**: p. 339-348.

172. Gao, Y., B. Li, J. Wang, and X.-Q. Feng, *Fracture toughness analysis of helical fiber-reinforced biocomposites.* Journal of the Mechanics and Physics of Solids, 2021. **146**: p. 104206.

173. Zhang, M., F. Yue, and B. Chen, *Optimizing toughness and cost-effectiveness in one-part geopolymers via fiber reinforcement: a comprehensive investigation of PVA, PE, and glass fibers.* Construction and Building Materials, 2024. **437**: p. 136999.

174. Aniskevich, A., O. Bulderberga, and L. Stankevics, *Moisture sorption and degradation of polymer filaments used in 3D printing.* Polymers, 2023. **15**(12): p. 2600.

175. Mohammed, M., A.J.a.M. Jawad, A.M. Mohammed, J.K. Oleiwi, T. Adam, A.F. Osman, O.S. Dahham, B.O. Betar, S.C. Gopinath, and M. Jaafar, *Challenges and advancement in water absorption of natural fiber-reinforced polymer composites.* Polymer Testing, 2023. **124**: p. 108083.

176. Nicolau, A., M.A. Pop, and C. Coșereanu, *3D printing application in wood furniture components assembling.* Materials, 2022. **15**(8): p. 2907.

177. Estakhrianhaghighi, E., A. Mirabolghasemi, Y. Zhang, L. Lessard, and A. Akbarzadeh, *3D-printed wood-fiber reinforced architected cellular composites.* Advanced Engineering Materials, 2020. **22**(11): p. 2000565.

178. Kariz, M., M. Sernek, and M.K. Kuzman, *Effect of humidity on 3D-printed specimens from wood-PLA filaments.* Wood Res, 2018. **63**(5): p. 917-922.

179. Ainin, F.N., M. Azaman, M. Abdul Majid, and M. Ridzuan, *The influence of water absorption on the mechanical performance of 3D-printed sandwich composite structures made from PLA-based materials under quasi-static loading conditions.* Polymer Composites, 2025. **46**(7): p. 6221-6240.

180. Oliver-Ortega, H., Q. Tarrés, P. Mutjé, M. Delgado-Aguilar, J.A. Méndez, and F.X. Espinach, *Impact strength and water uptake behavior of bleached kraft softwood-reinforced PLA composites as alternative to PP-based materials.* Polymers, 2020. **12**(9): p. 2144.

181. Ayrilmis, N., M. Kariz, J.H. Kwon, and M. Kitek Kuzman, *Effect of printing layer thickness on water absorption and mechanical properties of 3D-printed wood/PLA composite materials.* The International Journal of Advanced Manufacturing Technology, 2019. **102**: p. 2195-2200.

182. Ayrilmis, N., M. Kariž, and M. Kitek Kuzman, *Effect of wood flour content on surface properties of 3D printed materials produced from wood flour/PLA filament.* International Journal of Polymer Analysis and Characterization, 2019. **24**(7): p. 659-666.

183. Azka, M.A., S. Sapuan, H. Abral, E. Zainudin, and F.A. Aziz, *An*

examination of recent research of water absorption behavior of natural fiber reinforced polylactic acid (PLA) composites: A review. International Journal of Biological Macromolecules, 2024: p. 131845.

184. Zandvliet, C., N. Bandyopadhyay, and D. Ray, *Water absorption of jute/polylactic acid composite intended for an interior application and comparison with wood-based panels.* Journal of The Institution of Engineers (India): Series D, 2014. **95**: p. 49-55.

185. International, A., *ASTM D570-22: Standard Test Method for Water Absorption of Plastics*. 2022, ASTM International: West Conshohocken, PA.

186. Mamand, D.M., J.M. Hadi, R.A. Omer, and S.B. Aziz. *FTIR, UV-VIS, and DFT Approach to Study the Structural, Optical and Thermal Properties of Chitosan Biopolymer*. in *Doklady Physical Chemistry*. 2024. Springer.

187. Cuiffo, M.A., J. Snyder, A.M. Elliott, N. Romero, S. Kannan, and G.P. Halada, *Impact of the fused deposition (FDM) printing process on polylactic acid (PLA) chemistry and structure.* Applied Sciences, 2017. **7**(6): p. 579.

188. Grigsby, W.J., M. Gaugler, and D. Torayno, *Understanding the PLA–Wood Adhesion Interface for the Development of PLA-Bonded Softwood Laminates.* Fibers, 2022. **10**(6): p. 51.

189. Tronvoll, S.A., T. Welo, and C.W. Elverum, *The effects of voids on structural properties of fused deposition modelled parts: A probabilistic approach.* The International Journal of Advanced Manufacturing Technology, 2018. **97**: p. 3607-3618.

190. Al Aita, A., M. Aslam, and F. Smarandache, *Jonckheere Trend Test under Indeterminacy with Applications*. 2024: Infinite Study.

191. Avci, A., A.A. Eker, M.S. Bodur, and Z. Candan, *Water absorption characterization of boron compounds-reinforced PLA/flax fiber sustainable composite.* International journal of biological macromolecules, 2023. **233**: p. 123546.

192. Langer, E., K. Bortel, S. Waskiewicz, and M. Lenartowicz-Klik, *Assessment of traditional plasticizers.* Plastics Design Library, Plasticizers Derived from Post-Consumer PET, William Andrew Publishing, 2020: p. 1-11.

193. Lim, H. and S.W. Hoag, *Plasticizer effects on physical–mechanical properties of solvent cast Soluplus® films.* Aaps Pharmscitech, 2013. **14**: p. 903-910.

194. Souissi, S., W. Bennour, R. Khammassi, and A. Elloumi, *Mechanical properties of 3D printed parts: effect of ultraviolet PLA filaments ageing and water absorption.* Journal of Elastomers & Plastics, 2023. **55**(2): p. 184-200.

195. Erbil, Y.H., *Vinyl acetate emulsion polymerization and copolymerization with acrylic monomers*. 2000: CRC press.

196. Zareh, M.M., *Plasticizers and their role in membrane selective electrodes.* Recent Advances in Plasticizers, 2012: p. 113-124.

197. Eyerer, P., M. Weller, and C. Hübner, *Polymers-Opportunities and Risks II: sustainability, product design and processing*. Vol. 12. 2010: Springer Science & Business Media.

198. Vieira, M.G.A., M.A. Da Silva, L.O. Dos Santos, and M.M. Beppu, *Natural-based plasticizers and biopolymer films: A review.* European polymer journal, 2011. **47**(3): p. 254-263.

199. Modi, C., *Effect of components (polymer, plasticizer and solvent) as a variable in fabrication of diclofenac transdermal patch.* Journal of Pharmacy and Bioallied Sciences, 2012. **4**(Suppl 1): p. S57-S59.

200. Syrlybayev, D., B. Zharylkassyn, A. Seisekulova, M. Akhmetov, A. Perveen, and D. Talamona, *Optimisation of strength properties of FDM printed parts—A critical review.* Polymers, 2021. **13**(10): p. 1587.

201. Ror, C.K., S. Negi, and V. Mishra, *Development and characterization of sustainable 3D printing filaments using post-consumer recycled PET: processing and characterization.* Journal of Polymer Research, 2023. **30**(9): p. 350.

202. Bhagia, S., R.R. Lowden, D. Erdman III, M. Rodriguez Jr, B.A. Haga, I.R.M. Solano, N.C. Gallego, Y. Pu, W. Muchero, and V. Kunc, *Tensile properties of 3D-printed wood-filled PLA materials using poplar trees.* Applied Materials Today, 2020. **21**: p. 100832.

203. Koffi, A., L. Toubal, M. Jin, D. Koffi, F. Döpper, H.W. Schmidt, and C. Neuber, *Extrusion-based 3D printing with high-density polyethylene Birch-fiber composites.* Journal of Applied Polymer Science, 2022. **139**(15): p. 51937.

204. Wang, H., Z. Wu, J. Tao, B. Wang, and C. He, *Bamboo-Inspired Crack-Face Bridging Fiber Reinforced Composites Simultaneously Attain High Strength and Toughness.* Advanced Science, 2024. **11**(10): p. 2308070.

205. Filgueira, D., S. Holmen, J.K. Melbø, D. Moldes, A.T. Echtermeyer, and G. Chinga-Carrasco, *Enzymatic-assisted modification of thermomechanical pulp fibers to improve the interfacial adhesion with poly (lactic acid) for 3D printing.* ACS Sustainable Chemistry & Engineering, 2017. **5**(10): p. 9338-9346.

206. Pouzet, M., M. Dubois, K. Charlet, and A. Béakou, *From hydrophilic to hydrophobic wood using direct fluorination: A localized treatment.* Comptes Rendus. Chimie, 2018. **21**(8): p. 800-807.

207. Langer, E., K. Bortel, M. Lenartowicz-Klik, and S. Waskiewicz, *Plasticizers derived from post-consumer PET: Research trends and potential applications.* 2019.

208. Suaduang, N., S. Ross, G. Ross, S. Pratumshat, and S. Mahasaranon, *Effect of spent coffee grounds filler on the physical and mechanical properties of poly (lactic acid) bio-composite films.* Materials Today: Proceedings, 2019. **17**: p. 2104-2110.

209. Sun, Y., D. Li, Y. Shi, Z. Wang, S.I. Okeke, L. Yang, W. Zhang, Z. Zhang, Y. Shi, and L. Xiao, *Application of 3d printing technology in sensor*

development for water quality monitoring. Sensors, 2023. **23**(5): p. 2366.

210. Bergaliyeva, S., D.L. Sales, F.J. Delgado, S. Bolegenova, and S.I. Molina, *Effect of thermal and hydrothermal accelerated aging on 3D printed polylactic acid.* Polymers, 2022. **14**(23): p. 5256.

211. Yang, Z. and K. Sun, *Enhanced characterization of wheat straw-PLA composites with silane coupling agent and alkali pretreatment.* Ecotoxicology and Environmental Safety, 2025. **290**: p. 117612.

212. Miao, Z., L. Li, Y.-h. Xie, D. Feng, F. Wu, D. Xie, Y. Liu, and Y. Mei, *Revisiting maleic anhydride-grafted biopolymers for improved compatibility and toughening of PLA/PBAT blends: Effects of molecular weight and grafting ratio.* Polymer, 2025. **320**: p. 128055.

213. Pornwannachai, W., A.R. Horrocks, and B.K. Kandola, *Surface modification of commingled flax/PP and flax/PLA Fibres by Silane or atmospheric argon plasma exposure to improve fibre–matrix adhesion in composites.* Fibers, 2021. **10**(1): p. 2.